

Flavor singlet phenomena in lattice QCD

Stephan Güsken

Physics Department, University of Wuppertal, D-42097 Wuppertal, Germany

Abstract

Flavor singlet combinations of quark operators $\mathcal{O}_S^\Gamma = \bar{u}\Gamma u + \bar{d}\Gamma d + \bar{s}\Gamma s$ contribute to many important physical observables in the low energy region of QCD. Experimentally one finds the values of some of these observables to be in sharp contrast to the naive (perturbative) theoretical expectations. This indicates that non perturbative vacuum properties might play a major role in the comprehension of these phenomena. An example of such a vacuum contribution is the axial anomaly, which appears in the divergence of the flavor singlet axial current and which is connected to the topological properties of QCD.

From a field theoretical point of view flavor singlet matrix elements differ from non singlet amplitudes in the occurrence of so called disconnected insertions. These are correlations of hadron propagators with quark-antiquark loops or correlations between quark-antiquark loops, which are mediated by vacuum fluctuations. According to their respective flavor composition, the disconnected insertions cancel largely in non singlet processes, but add in flavor singlet amplitudes.

The lattice approach provides an ideal tool to study flavor singlet phenomena. Being a first principle method it should be capable to uncover non perturbative vacuum contributions and to yield, on the long run, reliable results for the size of such contributions in QCD.

The present article reviews the status of flavor singlet matrix element calculations in lattice QCD with respect to methods, results and reliability. Special emphasis is paid to the discussion of state of the art calculations of the pion nucleon sigma term $\sigma_{\pi N}$, the flavor singlet axial coupling of the proton G_A^1 , and the η' mass.

Contents:

1	Introduction	3
1.1	The Subject	4
1.2	The Method	6
2	The Pion-Nucleon-Sigma Term	10
2.1	Operators and Correlation Functions	12
2.2	What has to be computed	15
2.3	Lattice Results	19
2.3.1	Quenched QCD	19
2.3.2	Full QCD	23
2.4	Discussion	28
3	The Flavor Singlet Axial Coupling of the Proton	30
3.1	Preparation	31
3.2	Direct Method	35
3.2.1	Renormalization	37
3.3	Topological Method	39
3.4	Lattice Results	43
3.4.1	Quenched QCD	43
3.4.2	Full QCD	47
3.5	Summary	51
4	The Mass of the η' Meson and the $U(1)$ Problem	52
4.1	The Problem	52
4.2	Lattice Technique	54
4.3	Lattice Results	57
4.4	Outlook	63
5	Final Remarks	65

1 Introduction

Quantum field theories are today by far the most successful candidates in describing the fundamental forces of nature, and there is still no evidence that the standard model – a Lorentz and gauge invariant quantum field theory with gauge group $SU(3)_c \times SU(2)_w \times U(1)_Y$ – fails in the description of electroweak and strong phenomena.

One of the most fascinating consequences of such theories is that the physical vacuum is not vacuous. It rather behaves like a Lorentz invariant medium, which is made up from ground state fluctuations of quantum fields. This property, which is absent in classical field theories and also in quantum theory, implies a tremendous spectrum of new and partly curious physics phenomena, whose range has still not been fully explored yet.

A particle brought into such a vacuum, interacts with it. Excitation, polarization and anti-polarization effects occur and give rise to quite singular phenomena such as the decay of particles into classically forbidden channels, e.g. the decay $\Phi \rightarrow 3\pi$, the running of the classically constant coupling with the distance of two particles or the property of confinement of strongly interacting particles [1].

Due to its internal dynamics, the vacuum itself may exhibit a non-trivial structure. Symmetries, which are present on the classical level, can be destroyed by quantum fluctuations.

A qualitatively well understood consequence of such a spontaneous symmetry breaking is the appearance of massless (Nambu-Goldstone) bosons in case of a broken global symmetry [2, 3], and of (massive) gauge bosons [4–7] in case of a broken (local) gauge symmetry. The former mechanism, applied to the chiral $SU(3)$ symmetry, explains the smallness of the masses of the pseudo scalar meson octet members. The latter allows to include massive W and Z gauge bosons into the theory of electroweak interactions.

A third and much more hidden way of symmetry breaking occurs, if the quantum fluctuations form an anomaly, i.e. if the conservation of a classical current gets spoiled by vacuum effects. In the standard model, this is known to happen to the axial vector current [8, 9]. On the one hand the implications of such symmetry breaking can be disastrous, if the anomalous current couples to a gauge field. In that case the renormalizability of the theory, and thus its physics content, gets lost [10] unless the gauge properties and the particle content of the theory are arranged such that the anomalous contributions cancel each other. Fortunately, the standard model is constructed in this way. On the other hand, if the anomalous current does not couple to a gauge field, this ‘dynamical’ symmetry breaking supplies a new handle to understand quite a number of physics phenomena. Besides the successful calculation of the decay $\pi_0 \rightarrow \gamma\gamma$, [9], it has been shown [11] that the anomaly of the flavor singlet axial vector current is related to a non-trivial topological structure of the vacuum, which in turn can be used to explain qualitatively the large mass of the η' meson [12, 13]. Moreover, the unexpectedly small value of the flavor singlet axial vector coupling of the proton G_A^1 , which lead to the so called proton spin crisis, is also closely connected to the influence of this anomaly [14–16].

We do not attempt to discuss all the implications of the quantum vacuum here. We rather want to concentrate on a certain class of phenomena in the deeply non-perturbative

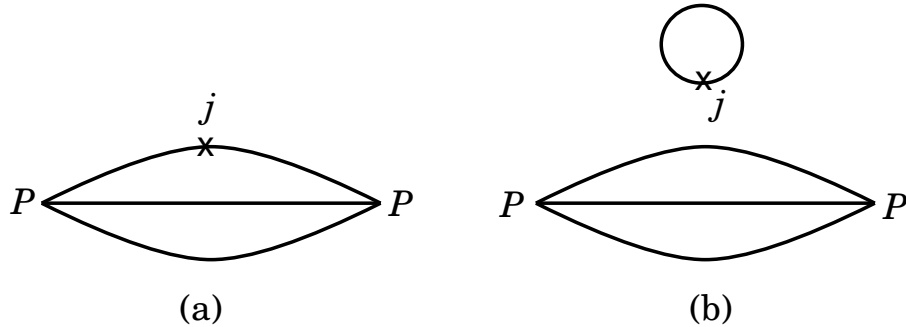


Figure 1: *Connected (a) and disconnected (b) insertions of a proton interacting with a current j . Please note that all quark lines, including the quark loop, are connected by infinitely many gluon lines and virtual quark loops.*

regime of the quantum field theory of strong interactions (QCD), which are expected to be determined to a large extent by vacuum properties: The flavor singlet phenomena.

1.1 The Subject

Suppose a (composite) particle, say a proton, interacts with a current j . Then quantum field theory tells us that, in addition to the direct coupling, a second process contributes, which is the interaction of the current j with a vacuum quark-antiquark loop in the field of the proton. Both contributions, the connected (direct) and the disconnected¹ (vacuum) insertion, are shown schematically in fig.1.

One would expect however, that the disconnected insertion is small compared to the connected one if the current j has a flavor non-singlet structure. Consider for example the flavor triplet and flavor octet currents

$$j_3 = \bar{u}\Gamma u - \bar{d}\Gamma d, \quad j_8 = \bar{u}\Gamma u + \bar{d}\Gamma d - 2\bar{s}\Gamma s, \quad (1)$$

where Γ denotes a combination of Dirac matrices, and the electromagnetic current

$$j_{em}^\mu = 2/3\bar{u}\gamma^\mu u - 1/3\bar{d}\gamma^\mu d - 1/3\bar{s}\gamma^\mu s. \quad (2)$$

Assuming an approximate flavor symmetry of the vacuum, the contributions from each quark flavor u, d, s to the disconnected insertion would largely cancel each other.

The situation changes drastically if we choose j to be a flavor singlet current

$$j_1 = \bar{u}\Gamma u + \bar{d}\Gamma d + \bar{s}\Gamma s. \quad (3)$$

In this case, the single quark contributions simply add up, and there is no a priori reason why the disconnected part should be small any more. Thus, flavor singlet processes are promising candidates to study vacuum polarization and vacuum structure effects.

¹Note that these ‘disconnected’ insertions are still connected in the field theoretical sense. There are however no valence quark lines which connect the quark-loop and the Proton propagator.

So far we have introduced flavor singlet phenomena solely as generic constructs. Of course, to be able to extract physics information from such processes one has to know to which physical situations they are related, whether they can be characterized by observables which are accessible to experiment and, last not least, how the diagrams in fig.1 can be calculated reliably in QCD. Only then, by comparison of the theoretical expectation with the experimental measurement, flavor singlet phenomena can help to scrutinize the quantum field theoretical picture of the vacuum.

The question of how and to what precision flavor singlet matrix elements can be calculated is one of the major issues of this review. As mentioned above, we will concentrate on flavor singlet phenomena in the deeply non-perturbative regime of QCD, i.e. at momentum transfers below $O(\Lambda_{QCD})$. The only known technique, which allows to solve QCD in this regime without additional assumptions is the method of lattice QCD. Thus we will use this method here.

Flavor singlet processes contribute to many physical observables, the most important ones being related to the chiral structure of the strong interaction. A scalar current ($j_1(\Gamma = 1)$), multiplied by a (quark) mass has the structure of a mass term in the QCD Lagrange density. Indeed, it turns out that $j_1(\Gamma = 1)$, when inserted between hadron ground states, just measures the explicit breaking of the chiral symmetry in QCD. The quantity $m_q \langle N | \bar{u}u + \bar{d}d | N \rangle$ is known as the pion-nucleon-sigma term $\sigma_{\pi N}$. Its value can be extracted from πN scattering data [17], although the analysis is rather indirect and requires much theoretical input [18].

A very interesting situation arises if we choose j_1 to be a axial vector current ($\Gamma = \gamma_\mu \gamma_5$). The conservation of this current is spoiled by the axial anomaly, and one would expect to track the effect of this anomaly in the disconnected insertion of fig.1. In fact, the corresponding amplitude, connected + disconnected, just defines the axial flavor singlet coupling of the proton G_A^1 , which is extracted from the first moment of the spin dependent proton structure function g_1^P . Naively, G_A^1 can be interpreted as the fraction of the the proton spin carried by quarks. It was first measured from polarized muon proton scattering by EMC [19]. The result, which has been consolidated by several succeeding experiments [20–24] revealed a much smaller singlet coupling than expected [25]. One might wonder of course whether this result can be derived directly from QCD by a calculation of the diagrams in fig.1.

The flavor singlet tensor charge of a nucleon, $Q_T = \langle N | j_1(\Gamma = \sigma_{\mu\nu} \gamma_5) | N \rangle$ can be extracted from the first moment of the chirality violating structure function h_1 of a nucleon. Since the chiral anomaly is absent here, one would not expect an anomalous result as found for G_A^1 . Although experimental measurements of Q_T are not available yet, it is interesting to investigate by a QCD calculation whether this expectation is justified.

Closely related to the axial vector current is the pseudo scalar current ($\Gamma = \gamma_5$), as the divergence of the former is connected to the latter by the axial Ward identity. Thus we expect to perceive the influence of the axial anomaly also if we choose j_1 to be a pseudo scalar current. The prominent application of this choice is the $U(1)$ problem of

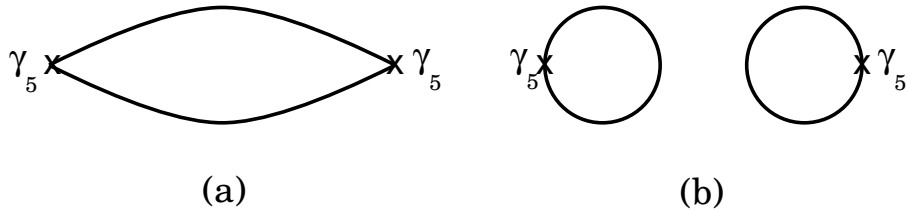


Figure 2: *Connected (a) and disconnected (b) contributions to the η' propagator.*

QCD, i.e. large mass of the ‘would be’ Goldstone boson η' . We mentioned above that a deep qualitative understanding in terms of the axial anomaly in conjunction with a topological structure of the vacuum has been achieved already, but of course one would like to calculate the η' mass directly from QCD. The graphs which have to be evaluated for this purpose are slightly different from those given in fig.1. As can be seen from fig.2, the connected contribution is simply the standard propagator of a pseudo scalar particle. The disconnected part, which contributes in case of the flavor singlet combination, consists of the correlation of two (pseudo scalar) vacuum loops. Clearly, one expects that the contribution of this correlation gives rise to the large η' mass.

To summarize, flavor singlet phenomena are closely connected with the quantum structure of the vacuum. Thus, a strong motivation to study these processes is to learn about this structure, and to contribute to our knowledge about whether and how the standard model concept of the quantum vacuum is realized in nature.

In the following chapters we will discuss the application of lattice QCD to the determination of $\sigma_{\pi N}$, G_A^1 , and to the $U(1)$ problem².

1.2 The Method

Although there has been tremendous progress in the qualitative understanding of vacuum properties over the last 30 years, a precise quantitative matching of experimental results with theoretical calculations is still missing in many cases. The reason is mainly not a lack of experimental results, but rather lies in the fact that most of the QCD vacuum phenomena cannot be treated within the framework of standard perturbation theory. The only method known today which is capable to treat non-perturbative phenomena from first principles, i.e. from the definition of the theory itself, is the method of lattice gauge theory [27]. We describe here only some important properties of lattice gauge theory which will enable the reader to follow the line of presentation of this review, and to develop a feeling for the reliability of the results.

Lattice QCD was invented by K. Wilson [28] about 3 decades ago. The basic intention was to setup a gauge invariant and non perturbative regularization scheme for QCD. This can be achieved if one puts the path functional [29], which in principle contains all

²The results of a pioneering lattice calculation of the tensor charge Q_T can be found in ref. [26].

information of a given quantum field theory, on a space-time grid with a lattice constant a and a lattice extension $L \times a$. The reduction from continuous to discrete space-time instantly introduces an ultraviolet cutoff, which removes possible singularities due to high momentum limits. Since the action density can be formulated gauge invariantly on that grid, this procedure defines a gauge invariant regularization scheme.

The second important ingredient, which makes quantum field theory look like statistical mechanics and which opens the door to a numerical treatment is the Wick rotation, i.e. the change from Minkowski metric of the space-time grid to Euclidian metric by a rotation of 90 degrees of the time axis in the complex plane. Fortunately all (time independent) properties of the theory remain untouched by this manipulation. The great advantage is, that the time dependence of n-point correlation functions is changed from an oscillatory to an exponential behavior. This enables for the numerical evaluation of the path integral.

With these settings, n-point functions of (arbitrary) operators $O_1, O_2, \dots O_n$ can be expressed by

$$\langle O_1(x_1)O_2(x_2) \dots O_n(x_n) \rangle = \tag{4}$$

$$Z^{-1} \int d[U]d[\psi]d[\bar{\psi}] \left\{ O_1(x_1)O_2(x_2) \dots O_n(x_n) e^{-S_f(U,\psi,\bar{\psi},M,g_0)-S_g(U,g_0)} \right\} ,$$

where

$$Z^{-1} = \int d[U]d[\psi]d[\bar{\psi}] e^{-S_f - S_g} . \tag{5}$$

The fermion fields ψ and $\bar{\psi}$ are anti-commuting Grassmann variables. The gluonic degrees of freedom are represented by the gauge-links $U_\mu(x)$. Those are $SU(3)$ color matrices, defined as the parallel transporters, which gauge-invariantly connect the fermion fields at lattice point x with the fermion fields at the neighboring point in the direction μ . $S_f(U, \psi, \bar{\psi}, M, g_0)$ and $S_g(U, g_0)$ denote the fermionic and gluonic parts of the (lattice discretized) QCD action.

Note that there are only two free parameters in eq.(4), the bare coupling g_0 and the bare quark mass³ M . All dimensionful quantities are given in units of the lattice spacing a . We emphasize that a is not a free parameter: At a given choice of g_0 , M can be tuned such that the lattice value of a dimensionless quantity, say the ratio M_π/M_ρ , corresponds to its physical value. The size of a is then determined by the matching condition⁴ $M_\rho = m_\rho a$.

The first step in the evaluation of the path integral can be done analytically. Since S_f has the generic form

$$S_f = \bar{\psi}M(U)\psi , \tag{6}$$

³For clarity we consider here only one (light) quark mass. Although the extension to more (non-degenerate) quark masses is in principle straightforward, one faces severe problems in the implementation of the Monte Carlo process. Most (unquenched) lattice calculations are therefore done with (two or four) degenerate quarks.

⁴Lattice values are indicated by capital letters, physical values by small letters.

the fermionic degrees of freedom can be integrated out [33]. Eq.(4) then reads

$$\langle O_1(x_1)O_2(x_2)\dots O_n(x_n)\rangle = Z^{-1} \int d[U] \det(M)F(U, M^{-1}(U))e^{-S_g}. \quad (7)$$

F is a known function, which depends on the choice of the operators O_i . It can be expressed in terms of the inverse fermionic matrix M^{-1} and the gauge links U . For example, for the quark propagator, $O_1(x_1)O_2(x_2) = \psi(x_1, a, \alpha)\bar{\psi}(x_2, a', \alpha')$, F is given by $M_{x_1, b, \beta; x_2, b', \beta'}^{-1}$, where b, b', β, β' denote color and Dirac indices.

To proceed further in the evaluation of eq.(7) one relies on numerical importance sampling methods [34, 35], which generate ‘gauge configurations’ $[U]$ with a probability

$$P[U] \propto \det(M[U]) \times \exp(-S_g[U]). \quad (8)$$

The expectation value $\langle O_1(x_1)O_2(x_2)\dots O_n(x_n)\rangle$ then is just the average of $F[U]$ over all gauge configurations $[U]$. Note that all results achieved with such a Monte Carlo procedure pick up a statistical uncertainty, since one is always limited to a finite sample of gauge configurations. Of course, this uncertainty can be reduced systematically by increasing the size of the statistical sample.

The most computer time consuming part of this stochastic approach is the generation of a statistically representative sample of configurations. Especially the calculation of $\det(M[U])$, which is a highly non local quantity, slows down the Monte Carlo process considerably, and it is only in these days that computers become powerful enough to create statistically significant ensembles of $[U]$ on acceptably large lattices. Therefore, in the past, the bulk of lattice results has been achieved in the quenched approximation, i.e. by setting the fermion determinant to the fixed value $\det(M) = 1$. In terms of physics, ‘quenched’ corresponds to a neglect of fermionic vacuum loops in the process of generating gauge configurations.

Naively one might expect that most of the quenching effects can be accounted for by a redefinition of the coupling g_0 . However, this expectation could be misleading when one studies flavor singlet phenomena. As explained above, fermionic vacuum loops play a crucial role in this case. Allowing for such loops in the construction of n point functions, but neglecting them in the creation of vacuum configurations could induce a systematic bias. The size of this bias can only be estimated by a comparison of quenched and unquenched results. This will be one important topic of this review.

We did not yet discuss the explicit forms of S_f and S_g . Clearly there is a lot a freedom in the definition of these quantities, as they have to coincide with the QCD action only in the continuum limit, i.e. at $a \rightarrow 0$ and $L \rightarrow \infty$. Of course one tries to construct the discretized action density such that as many continuum symmetries as possible are preserved and discretization errors are kept as small as possible. However, due to the so called fermion doubling problem [30–32], this turned out to be a highly non-trivial task. Two different prescriptions, one proposed by Wilson [28, 36] and one by Kogut and

Susskind [37], have been mainly used for S_f over the recent years. With the Wilson action, discretization errors occur, together with an explicit breaking of the chiral symmetry, at $O(a)$ in the lattice spacing. The Kogut-Susskind method preserves the $U(1)$ chiral symmetry, but mixes internal (spin) and external (space) degrees of freedom. In that scheme discretization errors contribute at $O(a^2)$.

Much effort has been invested to reduce the discretization errors of the Wilson action from $O(a)$ to $O(a^2)$. The most promising candidates to achieve this goal are by now the semi-perturbatively [39] and the non-perturbatively [38] improved versions of the Sheikholeslami-Wohlert action [40].

The lattice definition of S_g is much less problematic. The Wilson prescription [28], which exhibits discretization errors at $O(a^2)$ is still mostly used, but improved versions [41] ($O(a^4)$) are also available.

In order to make contact with continuum physics, the parameters g_0 and M have to be tuned such that the cutoff a^{-1} is removed while keeping the quark-mass m at its physical value. In QCD this means that, because of asymptotic freedom, one has to take the limits $g_0 \rightarrow 0$, $M = m a \rightarrow 0$. Of course, to keep the physical size $L a$ of the lattice finite, one has to increase $L \propto 1/a$ in this procedure.

In practice, one takes these limits by an extrapolation of the results from several sets of parameters (g_0, M, L) to the continuum.

The question of how close to the continuum limit these sets of parameters *can* be chosen, is, after all, a question of computer power. In terms of statistical physics, the continuum limit is located at a phase transition point of second (or higher) order. Close to this point all correlation lengths of the system start to grow exponentially and the Monte Carlo process of generating decorrelated configurations slows down more and more.

Current resources have enabled for Monte Carlo simulations with lattice specifications $a \approx 0.05 \text{ fm}$, $L/a \approx 3 \text{ fm}$, $m \approx 1/2 m_{\text{strange}}$ in the quenched case, and $a \approx 0.1 \text{ fm}$, $L/a \approx 2 \text{ fm}$, $m \approx m_{\text{strange}}$ for full QCD [42].

The question of how close to the continuum limit the parameter sets *have to be* chosen to allow for a reliable extrapolation, is difficult to answer in general. Although the functional dependence of the lattice results on M and a is well known close to their respective limits⁵ it is not a priori clear, at which values of M and a the asymptotic behavior sets in. Therefore one has to check the onset of asymptotics carefully with the lattice data in each case. Clearly, the reliability of the continuum extrapolation improves successively as more and more lattice results become available.

⁵Close to the continuum limit the M dependence can then be calculated by chiral perturbation theory [43–45] and the a dependence is proportional to the order in a at which discretization errors occur.

2 The Pion-Nucleon-Sigma Term

The Pion-Nucleon-Sigma term $\sigma_{\pi N}$ is defined as the double commutator of the axial charge with the Hamilton density, sandwiched between nucleon states at momentum zero:

$$\sigma_{\pi N} = \frac{1}{2M} \langle N | [Q^5(0), [Q^5(0), \mathcal{H}(0)] | N \rangle, \quad (9)$$

where M is the nucleon mass and \mathcal{H} is the QCD Hamilton density. The axial charge is given by

$$Q^5(x_0) = \int A^0(x_0, \vec{x}) d^3x, \quad \text{with } A^0 = \bar{q} \gamma_0 \frac{\lambda_3}{2} q, \quad \text{and } q = (u, d, s). \quad (10)$$

Since $\sigma_{\pi N}$ contains the time derivative $\dot{Q}^5 = [Q^5, \mathcal{H}]$ of the axial charge, it supplies a direct measure of the explicit chiral symmetry breaking of QCD. If the chiral symmetry would be conserved, the axial charge would be also conserved ($\dot{Q}^5 = 0$) and $\sigma_{\pi N}$ would vanish.

In order to exploit eq.(9) one uses the assumption that the chiral symmetry breaking term of the Hamilton density is given by [46, 47]

$$\mathcal{H}' = m_u \bar{u}u + m_d \bar{d}d + m_s \bar{s}s. \quad (11)$$

Neglecting, in addition, $SU(2)$ flavor symmetry breaking effects, i.e. assuming $m_u = m_d$, eq.(9) takes the form

$$\sigma_{\pi N} = \frac{1}{2M} \frac{m_u + m_d}{2} \langle N | \bar{u}u + \bar{d}d | N \rangle. \quad (12)$$

Note that the matrix element on the r.h.s. exhibits a ($SU(2)$) flavor singlet structure, as discussed in the previous section.

The determination of the physical value of $\sigma_{\pi N}$ from πN scattering experiments requires a lot of theoretical input. The isospin even πN scattering amplitude ⁶ \bar{D}^+ is related to $\sigma_{\pi N}$ at the (unphysical) Cheng-Dashen point⁷ by [48]

$$\Sigma = F_\pi^2 \bar{D}^+(2m_\pi^2), \quad \Sigma \rightarrow \sigma_{\pi N} \quad \text{for } m_u, m_d \rightarrow 0. \quad (13)$$

Since $\sigma_{\pi N}$ is defined at pion momentum transfer $t = 0$, a number of successive extrapolations is necessary to extract its value from the experimental data: One first has to extrapolate \bar{D}^+ from the physical region $t \leq 0$ to the Cheng-Dashen point [49]. The most recent analysis of experimental data leads to $\sigma_{\pi N}(2m_\pi^2) \simeq 60 \text{ MeV}$ [18], where a (small) correction term $\Delta_R = \Sigma - \sigma_{\pi N}(2m_\pi^2)$ due to the non vanishing quark masses has been included.

The second step is to calculate the shift $\Delta_\sigma = \sigma_{\pi N}(2m_\pi^2) - \sigma_{\pi N}(0)$ of $\sigma_{\pi N}$ when going from the Cheng-Dashen point to $t = 0$. Gasser, Leutwyler and Sainio [18] have performed

⁶ \bar{D}^+ is the scattering amplitude with the born term removed.

⁷The Cheng-Dashen point is defined by $q^2 = q'^2 = 2m_\pi^2$, $t = 2m_\pi^2$, $\nu = \nu_B = 0$. q, q' are the momenta of the incoming and outgoing pion, t, ν, ν_b are given by $t = (q_\mu - q'_\mu)^2$, $\nu = \frac{PQ}{M}$, $\nu_B = \frac{t - q^2 - q'^2}{4M}$. Q_μ and P_μ denote the pion and nucleon momentum sums: $Q_\mu = \frac{1}{2}(q_\mu - q'_\mu)$ and $P_\mu = \frac{1}{2}(p_\mu - p'_\mu)$.

a careful analysis of this shift by means of dispersive relations and chiral perturbation theory. They find $\Delta_\sigma \simeq 15\text{MeV}$, and, correspondingly

$$\sigma_{\pi N} \simeq 45\text{MeV} . \quad (14)$$

A similar analysis has been done in the framework of heavy baryon chiral perturbation theory by the authors of ref. [50]. They find $\sigma_{\pi N} = 48 \pm 10\text{MeV}$, which is consistent with eq.14.

Additional information about $\sigma_{\pi N}$ can be extracted from the baryon octet mass splittings. On the one hand, the octet quantity

$$\sigma_0 = \frac{m_u + m_d}{2} \langle N | \bar{u}u + \bar{d}d - 2\bar{s}s | N \rangle \quad (15)$$

is related to $\sigma_{\pi N}$ by

$$\sigma_{\pi N} = \frac{\sigma_0}{1 - y} , \quad y = \frac{2 \langle N | \bar{s}s | N \rangle}{\langle N | \bar{u}u + \bar{d}d | N \rangle} . \quad (16)$$

Thus, under the assumption that the strange quark contribution to the nucleon mass is small, $\langle N | \bar{s}s | N \rangle \simeq 0$, one would expect $\sigma_{\pi N} \simeq \sigma_0$.

On the other hand, σ_0 is directly related to the nucleon mass shift caused by explicit $SU(3)$ flavor symmetry breaking. To first order in $m_s - 1/2(m_u + m_d)$ one finds

$$\Delta M_N = \frac{1}{3} \left(\frac{m_u + m_d}{2} - m_s \right) \langle N | \bar{u}u + \bar{d}d - 2\bar{s}s | N \rangle , \quad (17)$$

or, for the baryon octet mass splittings in general

$$\Delta M_B = \langle B | c_8 u_8 | B \rangle = \alpha \text{tr}(\bar{B} u_8 B) + \beta \text{tr}(\bar{B} B u_8) . \quad (18)$$

B on the r.h.s. denotes the baryon matrix, and the octet quantities c_8 and u_8 are defined as

$$c_8 = \frac{1}{\sqrt{3}} \left(\frac{m_u + m_d}{2} - m_s \right) , \quad u_8 = \frac{1}{\sqrt{3}} (\bar{u}u + \bar{d}d - 2\bar{s}s) . \quad (19)$$

From the analysis of the mass splittings one naively extracts $\sigma_0 \simeq 25\text{MeV}$. It has been pointed out however [51], that the corrections due to terms $\propto (m_s - 1/2(m_u + m_d))^2$ enhance this value on a (20 – 30)% level. Including these terms one finds [52]

$$\sigma_0 = 35 \pm 5\text{MeV} . \quad (20)$$

Comparing eq.(14) with these findings one concludes that

$$y \simeq 0.2 - 0.4 . \quad (21)$$

Let us try to interpret this result in terms of connected and disconnected insertions. The term $\langle N | \bar{s}s | P \rangle$ receives a contribution only from the disconnected part of fig. 1, since the nucleon does not contain a valence strange quark. Thus, the result $y \neq 0$ is direct evidence, that disconnected diagrams really contribute to $\sigma_{\pi N}$.

To get an idea of what eq.(21) can tell about connected and disconnected insertions, we reformulate y in terms of the ratio of disconnected to connected contributions

$$R_{dc} = \frac{\langle N|\bar{u}u + \bar{d}d|N\rangle_{disc}}{\langle N|\bar{u}u + \bar{d}d|N\rangle_{con}} \quad (22)$$

and of the flavor symmetry breaking parameter α_{sb} of the disconnected insertions

$$\alpha_{sb} = \frac{\langle N|\bar{s}s|N\rangle}{\langle N|\bar{q}_l q_l|N\rangle_{disc}}, \quad (23)$$

where q_l denotes a light quark. This yields

$$y = \alpha_{sb} \left(\frac{R_{dc}}{1 + R_{dc}} \right). \quad (24)$$

Thus, naively assuming flavor symmetry of the disconnected (vacuum) parts ($\alpha_{sb} = 1$), one would need $R_{dc} \simeq 0.5$ to achieve $y \simeq 0.3$, i.e. the connected contribution to $\sigma_{\pi N}$ should dominate by a factor of 2. On the other hand, if one would assume connected and disconnected parts to contribute equally to $\sigma_{\pi N}$, one would need a strong symmetry breaking, $\alpha_{sb} \simeq 0.6$, to explain the experimental estimate of eq.(21).

Of course, these assumptions are speculative and an accurate determination of the matrix elements in eq's.(22,23) is highly needed. It will be interesting to see, to what extent state of the art lattice calculations can contribute to this task.

2.1 Operators and Correlation Functions

We are interested in a computation of matrix elements $\langle N|\bar{q}q|N\rangle$. The path integral approach, c.f. eq. (4), tells us how to determine correlation functions of operators. In this paragraph we explain which correlation functions are needed and how they can be combined to obtain the required information.

Consider the correlation functions

$$G_{NN}(x_0) = \sum_{\vec{x}} \langle N(\vec{0}, 0)^\dagger N(\vec{x}, x_0) \rangle \quad (25)$$

and

$$G_{NqN}(x_0) = \sum_{\vec{x}} \sum_{\vec{y}, y_0} \langle N^\dagger(\vec{0}, 0) \bar{q}(\vec{y}, y_0) q(\vec{y}, y_0) N(\vec{x}, x_0) \rangle. \quad (26)$$

Here, N denotes the creation operator of a nucleon-like particle, i.e. a particle with the nucleon quantum numbers, which is however not necessarily in its ground state. Such an operator is most easily expressed in terms of the fermion fields⁸ u and d [53]⁹

$$N_\gamma = \sum_{a,b,c} (u^a C \gamma_5 d^b) u_\gamma^c \epsilon^{a,b,c}. \quad (27)$$

⁸We write down here the expression for the proton. For the neutron, u and d have to be interchanged.

⁹For the time being explicit forms of operators and correlation functions in terms of fermion fields and fermion propagators will be valid only for the Wilson quark action.

C is the charge conjugation operator, Greek letters denote Dirac indices, and small Latin letters are used for color indices. The time (x_0) dependence of the momentum zero nucleon propagator G_{NN} is well known. It has the form¹⁰

$$G_{NN}(x_0) = \sum_n |\langle 0|N^\dagger|n\rangle|^2 e^{-M_n x_0} \xrightarrow{x_0 \rightarrow \infty} |\langle 0|N^\dagger|N\rangle|^2 e^{-M_N x_0} . \quad (28)$$

Thus, although G_{NN} contains all (radial) excitations of the nucleon, the ground state is isolated in the limit of large x_0 .

We now turn to the time dependence of the ‘insertion propagator’ G_{NqN} . Since the term $m_q \bar{q}q$ is contained in the QCD action, G_{NqN} can be constructed by deriving G_{NN} with respect to the quark mass. Because of

$$\langle N^\dagger(\vec{0}, 0)N(\vec{x}, x_0) \rangle = Z^{-1} \int d[U]d[\psi]d[\bar{\psi}] N^\dagger(\vec{0}, 0)N(\vec{x}, x_0) e^{-S_f(m_q \bar{q}q) - S_g} \quad (29)$$

it follows that

$$\begin{aligned} \langle N^\dagger(\vec{0}, 0) \sum_{\vec{y}, y_0} (\bar{q}q)(\vec{y}, y_0) N(\vec{x}, x_0) \rangle_c \\ &= G_{NqN}(x_0) - \langle N^\dagger(\vec{0}, 0)N(\vec{x}, x_0) \rangle \langle \sum_{\vec{y}, y_0} (\bar{q}q)(\vec{y}, y_0) \rangle \\ &= -\frac{\partial}{\partial m_q} \left\{ Z^{-1} \int d[U]d[\psi]d[\bar{\psi}] N^\dagger(\vec{0}, 0)N(\vec{x}, x_0) e^{-S_f - S_g} \right\} \\ &= -\frac{\partial}{\partial m_q} \langle N^\dagger(\vec{0}, 0)N(\vec{x}, x_0) \rangle . \end{aligned} \quad (30)$$

Using eq. (28) one finally gets in the limit of large x_0 ¹¹

$$R^{SUM}(x_0) \equiv \frac{G_{NqN}(x_0)}{G_{NN}(x_0)} - \langle \sum_{\vec{y}, y_0} (\bar{q}q)(\vec{y}, y_0) \rangle = A + \frac{\partial M_N}{\partial m_q} x_0 , \quad (31)$$

with $A = -\partial/\partial m_q (\ln |\langle 0|N^\dagger|N\rangle|^2)$. Note that it is the connected correlation function, in the field theoretical meaning

$$\langle N(\bar{q}q)N^\dagger \rangle_c = \langle N(\bar{q}q)N^\dagger \rangle - \langle NN^\dagger \rangle \langle \bar{q}q \rangle , \quad (32)$$

which contributes to eq. (31). Thus, the lattice value of chiral condensate $\langle \bar{q}q \rangle$ is explicitly subtracted¹².

¹⁰For the sake of clarity we will always assume a lattice with infinitely large extension in time. The corrections due to finite time extension are well known, but they will not be discussed here.

¹¹This summation method has been introduced by Maiani et al. [54].

¹²As the latter diverges cubically with the cutoff a^{-1} [55], this could lead to numerical problems for lattice simulations close to the continuum limit.

The next step is to determine the derivative $\partial M_N/\partial m_q$ in terms of the matrix element $\langle N|\bar{q}q|N\rangle$. The Feynman-Hellmann theorem [56] states that

$$\frac{\partial E}{\partial \lambda} = \left\langle \frac{\partial \mathcal{H}}{\partial \lambda} \right\rangle, \quad (33)$$

for any parameter λ on which the Hamiltonian \mathcal{H} depends. Thus, since the explicitly quark mass dependent part of \mathcal{H} is given by $m_q\bar{q}q$ one finds

$$\frac{\partial M_N}{\partial m_q} = \langle N|\bar{q}q|N\rangle. \quad (34)$$

One procedure to determine the relevant matrix element is therefore to calculate the correlation functions G_{NN} and G_{NqN} by solving the corresponding (lattice) path integrals, and then to extract the slope of the ratio R^{SUM} . We call this technique *summation method*.

Clearly, according to eq. (34), one can determine $\langle N|\bar{q}q|N\rangle$ also by a direct lattice calculation of $M_N(m_q)$ at several quark masses m_q . However, this would require to derive $M_N(m_q)$ numerically with respect to m_q , which in practice leads to a significant loss of statistical accuracy. We will come back to this point later on. Note that this method does not discriminate between connected and disconnected insertions, and it cannot be used to calculate the y parameter, eq. (16). Applied in the quenched approximation, it yields only the connected part of $\sigma_{\pi N}$.

One could argue, that the requirement of the nucleon being in its ground state might not be strictly fulfilled for the 3-point correlator G_{NqN} . Although x_0 can be made large, there are always short (time) distance contributions from the correlation of the scalar insertion $(\bar{q}q)(y_0)$ with the proton, since G_{NqN} contains the sum over y_0 . To check on the influence of such contributions we sketch here briefly a third method to compute $\langle N|\bar{q}q|N\rangle$. This method, which we call *plateau method*, uses the correlation function

$$C_{NqN}(x_0, y_0) = \sum_{\vec{x}} \sum_{\vec{y}} \langle N^\dagger(\vec{0}, 0) \bar{q}(\vec{y}, y_0) q(\vec{y}, y_0) N(\vec{x}, x_0) \rangle, \quad (35)$$

in which we do not sum over y_0 . The connection to the matrix element $\langle N|\bar{q}q|N\rangle$ can be most easily obtained in the (Euclidian) continuum¹³. The prescriptions for shifts of operators \mathcal{O} in space and time are given by

$$\mathcal{O}(\vec{0}, x_0) = e^{i\vec{P}\vec{x}} \mathcal{O}(\vec{x}, x_0) e^{-i\vec{P}\vec{x}} \quad \text{and} \quad \mathcal{O}(\vec{x}, 0) = e^{-\mathcal{H}x_0} \mathcal{O}(\vec{x}, x_0) e^{\mathcal{H}x_0}. \quad (36)$$

\mathcal{P} and \mathcal{H} denote the momentum and Hamilton operators. Inserting complete sets of energy eigenstates $|n\rangle$

$$\sum_n |n\rangle \langle n| = 1 \quad (37)$$

¹³The corresponding calculation on the lattice would have to be performed in the somewhat cumbersome transfer matrix formalism [27]. The result is however identical if we assume an infinitely extended lattice in time.

to the right and to the left of $\bar{q}(\vec{y}, y_0)q(\vec{y}, y_0)$ in C_{NqN} , shifting all operators to $(\vec{0}, 0)$, and carrying out the spatial sums one finally gets for the (field theoretically connected) part

$$\begin{aligned} C_{NqN}(x_0, y_0) - G_{NN} \langle \sum_{\vec{y}} \bar{q}q(\vec{y}, y_0) \rangle \\ = \sum_{n, n'} \langle 0|N^\dagger|n \rangle \langle n|\bar{u}u|n' \rangle \langle n'|N|0 \rangle e^{-E_n y_0} e^{-E_{n'}(x_0 - y_0)}. \end{aligned} \quad (38)$$

The ground state $|n\rangle = |n'\rangle = |N\rangle$ is isolated only if both time separations, $(x_0 - y_0)$ and y_0 , become large.

Note that eq. (38) is independent of y_0 in the large (time) distance limit. In this region, the ratio

$$R^{PLA}(x_0, y_0) = \frac{C_{NqN}}{G_{NN}} - \langle \sum_{\vec{y}} \bar{q}q(\vec{y}, y_0) \rangle = \langle N|\bar{q}q|N \rangle \quad (39)$$

is just the matrix element of interest. Thus, instead of looking at a linear slope, one has to identify a plateau region in (x_0, y_0) .

The *plateau method* is clearly superior to the *summation method* with respect to a reliable ground state identification. However, the ratio R^{PLA} might be more noisy than R^{SUM} , as one refrains from accumulating statistics by summing over y_0 . We will see below, that statistical fluctuations are indeed a major problem in the determination of disconnected contributions. In this case, even the *summation method* might fail, since contributions from the region $y_0 \gg x_0$ occur, which do not add to the signal but largely enhance the noise.

The *plateau accumulation method* (*PAM*) tries to avoid the drawbacks of the methods described above. It is defined by

$$R^{PAM}(x_0, \Delta x_0, \Delta x'_0) = \sum_{y_0 = \Delta x_0}^{x_0 - \Delta x'_0} R^{PLA}(x_0, y_0), \quad (40)$$

with $1 \leq \Delta x_0, \Delta x'_0 \leq x_0$. The asymptotic time dependence is given by

$$R^{PAM}(x_0, \Delta x_0, \Delta x'_0) = A + \langle N|\bar{q}q|N \rangle (x_0 - \Delta x'_0 - \Delta x_0). \quad (41)$$

With *PAM* the summation is restricted to the region in y_0 where ground state behavior of the 3-point correlator can be expected. Clearly, to ensure ground state behavior, one has to vary $\Delta x_0, \Delta x'_0$, and to compare the results.

In the next paragraph we will briefly explain how the correlations functions G_{NN} , G_{NqN} and C_{NqN} can be determined on the lattice.

2.2 What has to be computed

Assume that we would have been able to create a statistically significant set of gauge configurations [U] by some fancy Monte Carlo algorithm. Then, to evaluate the path integral according to eq. (7), one ‘simply’ determines the function $F(U, M^{-1}(U))$ for each of the

correlation functions G_{NN} , G_{NqN} and C_{NqN} , calculates its values on each gauge configuration, and finally averages over all configurations. The purpose of this paragraph is to construct F for the above correlations functions, and to explain how it can be calculated numerically on each gauge configuration.

The key quantity, from which all our correlation functions can be constructed, is the propagator Δ_q of a quark q , created at (\vec{x}, x_0) and annihilated at (\vec{y}, y_0)

$$\Delta_q(\vec{x}, x_0; \vec{y}, y_0) = \bar{q}(\vec{x}, x_0)q(\vec{y}, y_0) . \quad (42)$$

Once we know the corresponding function F_{Δ_q} , it is just a matter of combinatorics to determine $F_{G_{NN}}$, $F_{G_{NqN}}$ and $F_{C_{NqN}}$.

F_{Δ_q} can be most easily obtained in the generating functional formalism [27, 33]. One finds

$$F_{\Delta_q}(\vec{x}, x_0; \vec{y}, y_0) = M^{-1}(\vec{y}, y_0; \vec{x}, x_0) , \quad (43)$$

where M is the fermion matrix, c.f. eq. (6). If we insert the nucleon operator, eq. (27), into eq's. (25), (26), and (35) and contract \bar{q} and q in all possible ways, we can express $F_{G_{NN}}$, $F_{G_{NqN}}$ and $F_{C_{NqN}}$ in terms of M^{-1} . Note that \bar{q} and q are anti-commuting Grassmann variables

$$\{\bar{q}(x), \bar{q}(y)\} = \{q(x), q(y)\} = \{q(x), \bar{q}(y)\} = 0 . \quad (44)$$

We do not give here the explicit expressions for all these functions as those are quite lengthy. We merely want to discuss their structure in order to reveal how the different parts can be computed.

The propagator of a nucleon that travels from the source $(\vec{0}, 0)$ to the sink (\vec{x}, x_0) contains the product of three quark propagators

$$\begin{aligned} G_{NN}^{\gamma, \gamma'}(0; x) &= \langle F_{G_{NN}}^{\gamma, \gamma'}(0; x) \rangle \\ &= \langle (M_u^{-1})^{\gamma, \gamma'}(x; 0) [C\gamma_5 M_d^{-1}(x; 0) C\gamma_5]^{\alpha, \alpha'} (M_u^{-1})^{\alpha, \alpha'}(x; 0) \\ &\quad + (M_u^{-1})^{\gamma, \alpha'}(x; 0) [C\gamma_5 M_d^{-1}(x; 0) C\gamma_5]^{\alpha, \alpha'} (M_u^{-1})^{\alpha, \gamma'}(x; 0) \rangle . \end{aligned} \quad (45)$$

Here we have suppressed the color structure on the r.h.s.. With the source point $(\vec{0}, 0)$ being fixed, the computational problem in exploiting this equation is just to determine one row¹⁴ of the inverse of the fermion matrix, i.e. to solve

$$M_{x; x'} F_{\Delta_q}(0; x') = \delta_{x, 0} . \quad (46)$$

Although M is a huge matrix of size $(N_s^3 \times N_t \times 3 \times 4 \times 2)^2$, the solution of this equation is not a severe problem¹⁵ if one uses fast iterative inverters [57–59].

¹⁴In fact, as each fermion has 3 color and 4 Dirac degrees of freedom, one has to compute 12 rows of M^{-1} .

¹⁵This is true for typical lattice sizes and quark masses used in current simulations.

We now turn to the calculation of G_{NqN} . The application of the contraction procedure reveals two important differences to eq. (45). First of all, there is an additional term $F_{G_{NN}}(0; x) \sum_y \text{Tr}(M^{-1}(y; y))$. This term can be identified immediately with the disconnected contribution to G_{NqN} , since $M^{-1}(y, y)$ describes just the quark propagation from $y \rightarrow y$. Thus,

$$G_{NqN}^{disc} = \langle F_{G_{NN}}(0; x) \sum_y \text{Tr}(M^{-1}(y; y)) \rangle. \quad (47)$$

In our graphical language, G_{NqN}^{disc} is represented by fig. 1(b). The computational expense to calculate this contribution is huge. We will come back to this point below.

The second difference concerns the connected part of G_{NqN} . Since we have inserted the operator $\sum_y (\bar{q}q)(y)$, one of the nucleon valence quarks, started at the source 0, will always meet the ‘inserted’ quark at y , where the (scalar) interaction is located, and then travel to its destination at x . Thus, the propagator of this quark is modified

$$M_q^{-1}(x, 0) \rightarrow \tilde{M}_q^{-1}(x, 0) = \sum_y M_q^{-1}(x, y) M_q^{-1}(y, 0). \quad (48)$$

Graphically, such a modified quark propagator is represented by the upper quark line of fig.1(a).

Therefore, G_{NqN} can be written in the form of eq. (45), but with one quark propagator replaced by a modified propagator. Choosing the notation $G_{NN} = \mathcal{F}(M_u^{-1}, M_d^{-1}, M_u^{-1})$ one gets in the case of an u -quark insertion

$$G_{NqN}^{con}(u) = \mathcal{F}(\tilde{M}_u^{-1}, M_d^{-1}, M_u^{-1}) + \mathcal{F}(M_u^{-1}, M_d^{-1}, \tilde{M}_u^{-1}), \quad (49)$$

and for the d -quark insertion

$$G_{NqN}^{con}(d) = \mathcal{F}(M_u^{-1}, \tilde{M}_d^{-1}, M_u^{-1}). \quad (50)$$

Clearly, there is no such contribution for the s -quark.

The numerical computation of \tilde{M}^{-1} can be done in a two step procedure [54]. One first determines $M^{-1}(x, 0)$ according to eq. (46). Then, because of

$$M(x, x') \tilde{M}^{-1}(x', 0) = M(x, x') M^{-1}(x', y) M^{-1}(y, 0) = M^{-1}(x, 0), \quad (51)$$

one replaces the r.h.s. of eq. (46) by $M^{-1}(x, 0)$ and solves this equation with the standard method. Thus, the computational effort to determine $\tilde{M}^{-1}(x, 0)$ is just twice the effort for the quark propagator.

We didn’t comment yet on the structure of C_{NqN} in terms of quark propagators. As the difference to G_{NqN} is only that the sum over y_0 is missing, we could write down the connected and disconnected parts of C_{NqN} exactly in the form of eq’s. (49), (50), and (47), albeit omitting the sum over y_0 . We could also use the two step procedure outlined above for the connected part. However, in doing so one would have to apply the second step of this procedure for each time slice separately, increasing the numerical effort linearly with

the number of time slices. In order to avoid this increase one can use alternatively the ‘insertion’ procedure invented by Martinelli and Sachrajda [60]. This method allows for an arbitrary variation of y_0 without additional inversions.

We have seen already, that \tilde{M}^{-1} can be easily obtained from the solution of eq. (46) if the the source, i.e. it’s r.h.s., is suitably modified. This concept can be extended to even more involved effective propagators. Martinelli and Sachrajda use the main part of the proton propagator as a source. Schematically, one has

$$\mathbf{M}\left\{ P(0) \begin{array}{c} \xrightarrow{\quad y \quad} \\ \xrightarrow{\quad \mathbf{x} \quad} \\ \xrightarrow{\quad \quad \quad} \end{array} P(x) \right\} = P(0) \begin{array}{c} \xrightarrow{\quad \quad \quad} \\ \xrightarrow{\quad \quad \quad} \end{array} P(x) . \quad (52)$$

The r.h.s. of this equation is given by a combination of quark propagators. Note that the timeslice x_0 of the nucleon sink is fixed. C_{NqN} is obtained from the product of the solution to eq. (52), $\tilde{C}(y, 0)$, and $M^{-1}(y; 0)$, for arbitrary y_0 . The expected ground state behavior, eq. (39), can be identified as follows: One first chooses a large value of x_0 . Then one varies y_0 between 0 and x_0 to obtain the plateau region.

The disconnected parts of G_{NqN} and C_{NqN} have quite simple structures. All we need to know is the nucleon propagator and the ‘quark loop’, $\sum_y Tr M^{-1}(y, y)$. However, if one would use eq. (46) to determine the trace, the computational effort would be $N_s^3 \times N_t$ times the cost for the calculation of a single quark propagator, a prohibitively large amount of computer time.

The key to reduce this amount drastically can again be found in a suitable modification of the source term of eq. (46). Suppose we would insert the source I , with $I_y = 1$, to the r.h.s. . Then, the solution \tilde{M}^{-1} to this equation is given by

$$\tilde{M}^{-1} = \sum_y M^{-1}(x, y) I_y = \sum_y M^{-1}(x, y) . \quad (53)$$

Summation over x yields

$$\sum_x \sum_y M^{-1}(x, y) = \sum_y Tr M^{-1}(y, y) + \sum_{x, y; x \neq y} M^{-1}(x, y) . \quad (54)$$

As the second term on the r.h.s. is not gauge invariant, one expects it to cancel out in the process of averaging over all gauge configurations. Note however, that this cancellation is mingled with the ‘normal’ statistical fluctuations of $\sum_y Tr M^{-1}(y, y)$. Since one is in practice always limited to a finite sample of gauge configurations, a systematic bias due to a non-cancellation of the second term could be easily overlooked. Furthermore, one would expect an increase of the statistical uncertainty, since the noise of this term adds to the noise of $\sum_y Tr M^{-1}(y, y)$.

Thus, it is highly desirable to modify this ‘volume source’ method [61] such that it allows to remove $\sum_{x, y; x \neq y} M^{-1}(x, y)$ on each single gauge configuration. This is achieved by the ‘stochastic estimator’ methods [62, 63], which we will now explain briefly.

The major difference between the ‘volume source’ method and the stochastic estimator technique is that the volume source vector I is replaced by a random vector η , which has the properties

$$\langle \eta_i \rangle = 0 \quad \text{and} \quad \langle \eta_i \eta_j \rangle = \delta_{i,j}. \quad (55)$$

Note that the brackets denote the average over the distribution of random numbers on each gauge configuration. For each choice s of a random source η^s one gets

$$\tilde{M}^{-1} \eta^s = \sum_y M^{-1}(x, y) \eta_y^s \quad (56)$$

as a solution to the modified eq. (46). The average over N_E random sources then yields

$$\frac{1}{N_E} \sum_{s=1}^{N_E} \sum_{x,y} \eta_x^s M^{-1}(x, y) \eta_y^s = \frac{1}{N_E} \sum_{s=1}^{N_E} \left[\sum_y \eta_y^s M^{-1}(y, y) \eta_y^s + \sum_{x,y;x \neq y} \eta_x^s M^{-1}(x, y) \eta_y^s \right]. \quad (57)$$

For large N_E the second term on the r.h.s. cancels according to eq. (55), and the first term reduces to the desired result $Tr M^{-1}$ on each single gauge configuration. The onset of asymptotics and the statistical accuracy of $Tr M^{-1}$ can be monitored within the course of sampling estimates. We emphasize that both these properties depend on the choice of the random number distribution. It has been shown in ref’s. [64, 74] that a (complex) Z_2 distribution [63] is superior to a Gaussian distribution [62]. Unfortunately it turns out that even then the number of estimates N_E has to be chosen of $O(300)$ for current lattice sizes.

We mention finally that the stochastic estimator technique allows to compute single matrix elements of M^{-1} . For example, using Z_2 noise¹⁶, the combination

$$\frac{1}{N_E} \sum_{s=1}^{N_E} \sum_y \eta_{z_0}^s M^{-1}(x_0, y) \eta_y^s = \frac{1}{N_E} \sum_{s=1}^{N_E} \left[M^{-1}(x_0, z_0) + \sum_{y \neq z_0} \eta_{z_0}^s M^{-1}(x, y) \eta_y^s \right], \quad (58)$$

yields $M^{-1}(x_0, z_0)$ in the limit $N_E \rightarrow \infty$.

2.3 Lattice Results

2.3.1 Quenched QCD

The numerical determination of disconnected contributions by application of the methods outlined above requires both, high statistics of gauge configurations and, at least if one uses stochastic estimator techniques, a multiple of compute power ($O(300)$) compared to standard propagator calculations. Early, exploratory lattice simulations [54, 60, 65] were therefore restricted to the calculation of the connected part of $\sigma_{\pi N}$ in the quenched approximation. As a result, an astonishingly small value, $\sigma_{\pi N}^{con} \simeq 15 \text{MeV}$, was found in these calculations, suggesting that the disconnected contribution to the full pion-nucleon-sigma term should be approximately twice this number.

¹⁶For Z_2 noise, the property of the average $\langle \eta_i \eta_i \rangle = 1$ holds for each estimate, i.e. $\eta_i \eta_i = 1$.

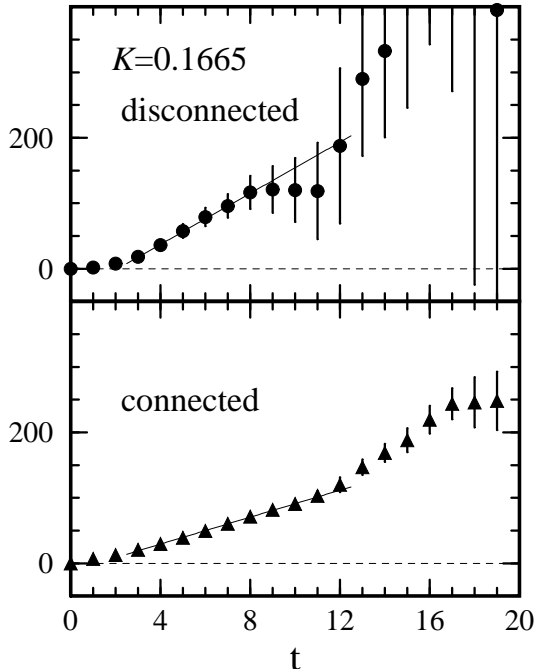


Figure 3: Ref. [66]: The ratio $R^{SUM}(t)$ for the connected and disconnected contributions ($u+d$ insertion) to the scalar density amplitude of a proton $\langle P|\bar{u}u + \bar{d}d|P\rangle$, at a quark mass corresponding to $m_\pi/m_\rho = 0.604$.

Due to the advances in computer speed and algorithms, it is nowadays possible to investigate connected and disconnected parts in some detail. A high statistics simulation (300-400 gauge configurations, depending on the quark mass) has been performed by Fukugita et al. [66] at a lattice cutoff of $a^{-1} \simeq 1.5\text{GeV}$. They used a slightly modified wall source technique for the disconnected contributions and analyzed all signals with the summation method, eq. (31).

To illustrate the statistical quality of their data we show in fig. 3 the ratio $R^{SUM}(t)$ both for the connected and the disconnected contributions to $\sigma_{\pi N}$. Note that, although the errors to the disconnected data are large, the expected linear rise of the signal can nevertheless be identified in both cases.

A similar analysis, although with a significantly smaller statistical sample (24 gauge configurations for the connected and 50 for the disconnected part) has been done by Dong et al. [67] at a larger cutoff, $a^{-1} \simeq 2\text{GeV}$. They have applied the stochastic estimator technique, eq. (57), with (complex) Z_2 noise and 300 estimates per configuration.

In fig.4 we show the results of both simulations as a function of $(m_\pi/m_\rho)^2$.

The data for the connected insertion is consistent within statistical errors, whereas the estimates of ref. [67] for the disconnected contribution appear to be significantly lower than those of [66]. This might indicate a finite cutoff effect, but in view of the very limited sample of gauge configurations used in ref. [67] it is likely that the statistical errors have been underestimated substantially.

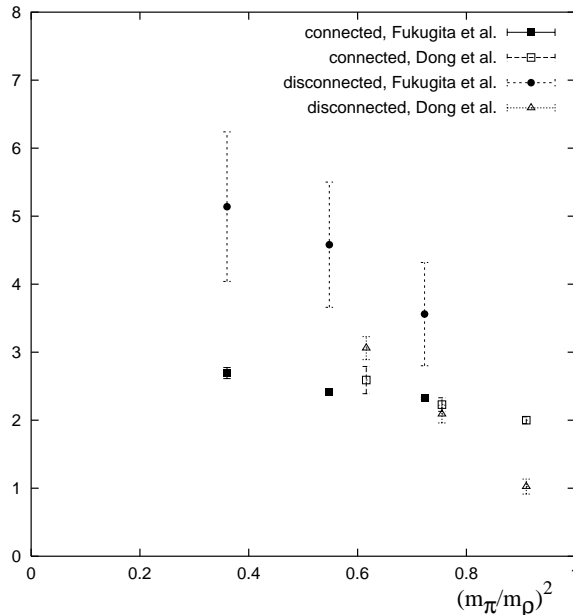


Figure 4: *Connected and disconnected contributions to the scalar density amplitude of a proton, $\langle P|\bar{u}u + \bar{d}d|P\rangle$. The data has been taken from Fukugita et al. [66] and from Dong et al. [67]. To compare the results of different simulations we have renormalized the amplitudes consistently with the tadpole improved renormalization factor Z_s [39].*

Obviously, the mass dependence of the connected and the disconnected part is quite different. The disconnected part grows significantly with decreasing quark mass whereas the connected part is basically unaffected by the variation of mass.

An extrapolation (see below) to the light quark mass, $(m_\pi/m_\rho)_{phys}^2 = 0.033$, consolidates the presumption from the results of the early quenched calculations. One finds

$$R_{dc}^{quen} = \frac{\langle P|\bar{u}u + \bar{d}d|P\rangle_{disc}}{\langle P|\bar{u}u + \bar{d}d|P\rangle_{con}} = \begin{cases} 2.23(52) & \text{ref. [66]} \\ 1.8(1) & \text{ref. [67]} \end{cases}, \quad (59)$$

and

$$\sigma_{\pi N}^{quenched} = \begin{cases} 43(7)\text{MeV} & \text{ref. [66]} \\ 50(3)\text{MeV} & \text{ref. [67]} \end{cases}. \quad (60)$$

Within errors the quenched findings of $\sigma_{\pi N}$ are consistent with the estimates extracted from experiment. The disconnected contribution appears to be much larger than the connected one. Thus, according to eq. (24), one needs a strong breaking of flavor symmetry for the disconnected part to achieve a low value of y .

Note that $\sigma_{\pi N}$ is a renormalization group invariant quantity. Thus, the lattice result, multiplied by the lattice scale yields directly the physical result.

The matrix element and the quark mass individually are connected to their respective physical values by renormalization factors $Z_s = 1/Z_m$, which depend on the bare coupling

g_0 and the lattice quark mass

$$\langle P|\bar{u}u + \bar{d}d|P\rangle^{phys} = Z_s \langle P|\bar{u}u + \bar{d}d|P\rangle^{latt} \quad , \quad m_q^{phys} = Z_m m_q^{latt} \quad . \quad (61)$$

We will discuss the methods to determine these factors in the next chapter. Here, we mention however, that the lattice result for the light quark mass used to obtain $\sigma_{\pi N}$ corresponds to a physical mass $m_l(2\text{GeV})_{\overline{MS}} \simeq 5\text{MeV}$.

We did not comment yet on the ansatz used for the extrapolation of the matrix elements to the light quark mass. Since both simulations have only three data points at their disposal, and in view of the fact that the statistical errors to the disconnected parts are large, one would not expect to be able to resolve reliably contributions from higher orders in the quark mass. Correspondingly, ref. [66] uses a linear ansatz.

Inspired by chiral perturbation theory, ref. [67] extrapolates with a non-linear, non-analytic ansatz of the form $C + D\sqrt{m_q}$. This, of course, leads to an enhancement of the results at the light quark mass. However, even in high precision calculations of the hadron spectrum [68], with $O(800)$ gauge configurations and quark masses corresponding to $(m_\pi/m_\rho)^2 = 0.16$, one does not find numerical evidence for the presence of such non-analytic contributions.

We have seen above, that the ratio of disconnected to connected contributions to $\sigma_{\pi N}$ is astonishingly large in the quenched approximation. Assuming an approximate flavor symmetry of the disconnected parts, one would conclude that the y parameter, defined in eq. (16), takes the value $y = 2/3$. This is much higher than the phenomenological expectation, $y \simeq 0.2 - 0.4$, and it would indicate that the strange quark contribution to the nucleon mass, $m_s \langle N|\bar{s}s|N\rangle$ is as large as ~ 400 MeV [18].

To determine y and to check the assumption of flavor symmetry, one has to calculate the (purely disconnected) strange density matrix element of the proton. In the quenched approximation, this is done in two steps.

First, one adjusts the lattice quark mass such that the physical strange meson spectrum (K, K^*, Φ) is reproduced¹⁷. This determines the strange quark mass. In the second step one extrapolates the matrix element as a function of the valence quark mass of the proton to the light quark mass, while keeping the loop quark fixed at the strange mass. This then yields the lattice value of $\langle N|\bar{s}s|N\rangle$.

Using this procedure, ref. [66] finds

$$y = 0.66(15) \quad , \quad (62)$$

which is almost exactly the value one expects from the assumption of flavor symmetry of the disconnected contributions. The result appears plausible, since the quenched QCD vacuum is not sensitive to quark mass and quark flavor.

¹⁷The value for the strange quark mass depends ($O(10\%)$) on the physical quantity (m_K or m_{K^*}, m_Φ) used to define it [42]. This however does not influence the results discussed below.

Note that y depends on the ratio $Z_s(m_s)/Z_s(m_l)$. Since the change of Z_s with the lattice quark mass is expected to be small in the light and strange quark region, this ratio should be close to 1. Using the tadpole improved perturbative renormalization scheme [39], which has been applied in ref. [66], one finds $Z_s(m_s)/Z_s(m_l) \simeq 1.06$.

It has been suggested by Lagaë and Liu [69] that the lattice quark mass dependent part of the renormalization factor would be quite different for connected and disconnected amplitudes. Use of their result would induce a strong symmetry breaking in the disconnected sector. The authors of ref. [67] have applied this modified renormalization procedure to their raw data. On top of this they have used the non-analytic ansatz for the chiral extrapolation discussed above. Both manipulations lower the value of y , and they find $y = 0.36(3)$.

We do however not agree with the suggestion of Lagaë and Liu, at least in the case of scalar quark loops, for the following reason: Since the combination $m_q \langle P | \bar{q}q | P \rangle$ is a renormalization group invariant quantity, both parts of the amplitude, connected and disconnected, will be renormalized by the same factor $Z_S = 1/Z_m$, where Z_m renormalizes the quark mass. Choosing different factors, $Z_S^{con} \neq Z_S^{disc}$ would violate the renormalization group invariance.

In summary, quenched lattice simulations find $\sigma_{\pi N}$ to be consistent with the phenomenological expectation. It turns out that the ratio of disconnected to connected contributions is close to 2 and that the flavor symmetry of the disconnected part is nearly unbroken. This leads to a large value of the y parameter. It is therefore of utmost interest to study these aspects in full QCD lattice calculations.

2.3.2 Full QCD

We have seen above, c.f. fig. 4, that quenched simulations with a statistics of $O(300)$ configurations find statistical errors on disconnected contributions of $\sim 30\%$. This is bad news if one plans to determine such contributions in full QCD, for two reasons. First, the creation of gauge configurations in full QCD enhances the computational demands by a factor of $O(1000)$. Thus, one needs a ‘high end’ supercomputer to generate statistical samples with comparable size. Secondly, a comparison of quenched and full QCD spectrum results at equal statistics revealed [70], that the statistical fluctuations on full QCD configurations might be much larger than in quenched QCD. Early, exploratory full QCD simulations [71, 72] have therefore not been able to extract possible unquenching effects on $\sigma_{\pi N}$ and y .

Recently, the SESAM collaboration has generated 4 samples of 200 statistically independent gauge configurations with $n_f = 2$ mass degenerate Wilson quarks, on a $n_s^3 \times n_t = 16^3 \times 32$ lattice, and a lattice cutoff $a_\rho^{-1} \simeq 2.3\text{GeV}$. The samples correspond to different sea quark masses, with $m_\pi/m_\rho = 0.833(3), 0.809(15), 0.758(11)$ and $0.686(11)$ [70].

The analysis [73, 74] of these configurations indeed showed that the standard procedures, i.e. *summation method* combined with the wall source or the stochastic estimator technique

– fail in producing a reasonable signal for the disconnected contribution to $\sigma_{\pi N}$. The situation can be significantly improved however, if one uses *PAM*, together with a stochastic estimator technique with (complex) Z_2 noise.

We illustrate this result in figs. 5 and 6, where we compare the signals for the ratio R^{PAM} , created using the Z_2 stochastic estimator method with those for R^{SUM} , generated with the *wall source* and, alternatively, with Z_2 stochastic estimator technique.

Obviously, the former combination (R^{PAM} + Z_2 stochastic estimator) is superior with respect to the statistical quality of the signal. However, the errors are even then of $O(30\%)$.

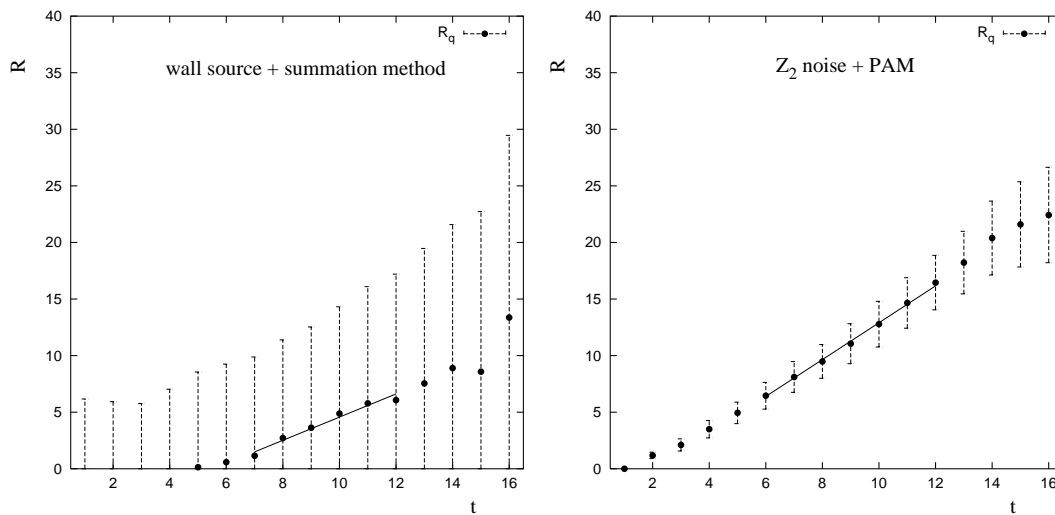


Figure 5: Disconnected contribution to $\sigma_{\pi N}$. Comparison of wall source + summation method with Z_2 stochastic estimator + PAM at a sea quark mass corresponding to $m_\pi/m_\rho = 0.833$. The solid lines indicate the region of ground state behavior of the signal.

Using the *plateau method* for the connected contributions and *PAM* + stochastic Z_2 noise for the disconnected part, the authors of ref. [73] have determined the scalar amplitudes of the proton at the 4 SESAM quark masses. The results are shown in fig. 7, together with the linear extrapolations to the light quark mass.

At first sight the full QCD results look quite similar to those of the quenched analysis, c.f. fig. 4. To see this in some more detail we compare in tab. 1 the $n_f = 2$ results at the light quark mass with the findings of ref. [66].

It turns out that, although the amplitudes are consistent within errors, the relative weight of disconnected and connected amplitudes is quite different. One finds

$$R_{dc}^{full} = 1.26(57), \quad (63)$$

compared to $R_{dc}^{quen} = 2.23(52)$. This might give a first indication for the influence of sea

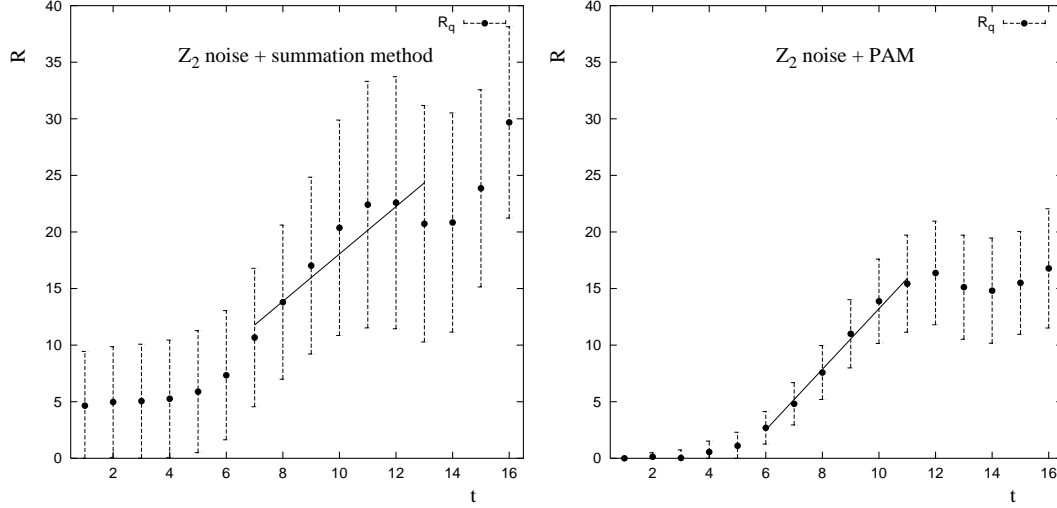


Figure 6: Disconnected contribution to $\sigma_{\pi N}$. Summation method with PAM at a sea quark mass corresponding to $m_{\pi}/m_{\rho} = 0.686$. In both methods, the stochastic estimator technique with complex Z_2 noise has been used. The solid lines indicate the region of ground state behavior of the signal.

	$Z_S(C_u + C_d)$	$Z_S(2D_q)$	sum	$Z_S^{-1}m_l a^{-1}[\text{MeV}]$	$a^{-1}[\text{GeV}]$
ref. [66] quenched	2.62(6)	5.8(1.4)	8.6(1.4)	5.0(2)	1.45(2)
ref. [73] $n_f = 2$	3.11(25)	3.9(1.8)	7.0(2.0)	2.7(2) [75]	2.30(6)

Table 1: Results at the light quark mass. For comparison all data has been renormalized by the tadpole improved perturbative renormalization factors Z_S , Z_M [39].

quarks on scalar density nucleon matrix elements¹⁸. As we mentioned above, the ratio R_{dc} is one of the two quantities which fix the value of the y -parameter.

A consistency check to the sum of amplitudes can be done in full QCD by use of the Feynman-Hellmann theorem, eq. (34). From a quadratic fit to the proton mass data, the

¹⁸Some caution in the interpretation of this difference is in order since the results have been obtained at unequal lattice cutoffs.

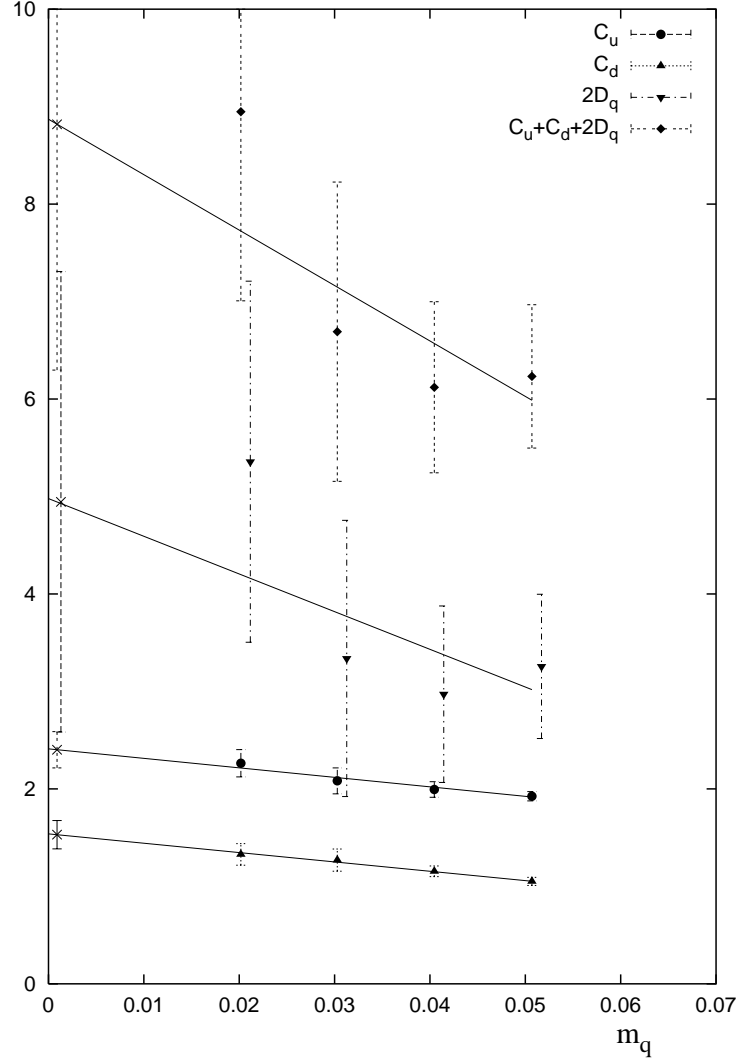


Figure 7: *Full QCD: Linear extrapolation of connected and disconnected amplitudes to the light quark mass, from ref. [73]. Bursts indicate the results of the extrapolation. C_q denotes the connected, and D_q the disconnected contributions to $\sigma_{\pi N}$.*

authors of ref. [73] find

$$Z_S \frac{\partial M_N}{\partial m_q}(m_l) = 9.2(3.9) . \quad (64)$$

This is in agreement with the result of the direct determination. Note, that the statistical error in eq. (64) is larger.

From tab. 1 one extracts a rather small value of the pion-nucleon-sigma term

$$\sigma_{\pi N} = 18(5)\text{MeV} . \quad (65)$$

Clearly, this is almost exclusively due to the weight of the light quark, which is lower by nearly a factor 2 in the $n_f = 2$ case compared to the quenched result. We emphasize, that in both cases the standard lattice definition¹⁹ of quark masses [76] has been used.

It has been argued by R. Gupta [76] that the perturbative renormalization would be inappropriate in full QCD, and that non-perturbative contributions due to the presence of sea quarks would enhance Z_m by approximately a factor of 2. This however does not affect the result for $\sigma_{\pi N}$, as this is a renormalization group invariant quantity.

Another explanation could come from the lattice definition of the quark mass. Due to finite cutoff effects, different definitions of physical quantities can lead to different answers on the lattice. Of course, the results have to agree in the continuum limit.

It is known from quenched simulations, that the standard definition of the lattice quark mass, which is extracted from the discretized Hamilton density, and the PCAC definition, which uses the axial Ward identity [76], do not agree at finite lattice cutoff. At $a^{-1} \simeq 2\text{GeV}$, the (perturbatively renormalized) quark masses differ by about 30%. A scaling analysis revealed [77] that the cutoff dependence of the quark mass in the standard definition is much weaker than in the PCAC definition, thus favoring the former.

The situation could be different in full QCD simulations. Indeed, the (preliminary) results of the CP-PACS collaboration [77] indicate a stronger cutoff dependence of the quark mass in the standard definition. For a definite conclusion on that issue however more data at different cutoffs are needed.

We now turn to the determination of the y parameter in full QCD. In principle, since one needs a strange quark loop contribution in this context, a fully consistent QCD lattice calculation would require both, light and strange quarks to be present in the quark sea. Such a $n_f \geq 3$ simulation with non-degenerate quarks will surely be one of the next large projects in lattice QCD, but it has not been performed yet.

Within the framework of QCD simulations with degenerate light sea quarks, one has to rely on a *semi-quenched* analysis, where the strange quark has no counterpart in the sea of quarks. This at least accounts for the light quark mass dependence of the vacuum and is therefore more appropriate than a pure quenched analysis of y .

The *semi-quenched* method is technically very similar to the quenched procedure outlined above. The physical difference is that the mass of the light valence quark is always identified with the sea quark mass.

Using this procedure, the SESAM collaboration finds [73]

$$Z_S \langle P | 2\bar{s}s | P \rangle = 4.1(1.5) , \quad (66)$$

¹⁹The standard definition of the bare quark mass is given in terms of hopping parameters κ by $m_q a = 1/2(1/\kappa - 1/\kappa_c)$. The critical parameter κ_c is determined such that the pion mass vanishes for this choice of κ .

which is in accordance with the result from the light quark region, given in tab.1. This indicates, that the flavor symmetry of the disconnected contributions to the scalar proton amplitude is still intact, even in the presence of light sea quarks.

Thus, only R_{dc} serves to reduce the value of the y parameter. Correspondingly, the result

$$y^{n_f=2} = 0.59(13) \tag{67}$$

differs only slightly from the quenched value.

2.4 Discussion

Let us shortly comprise the physics information that evolves from lattice QCD simulations discussed above. Taking the results at face value, the following picture arises: In quenched QCD, $\sigma_{\pi N}$ is consistent with the ‘experimental’ value. However, the major contribution (2/3) comes from the vacuum polarization (disconnected) part of the amplitude. As those parts turn out to be flavor invariant, the y parameter picks up a rather large value (2/3), in sharp contrast to the phenomenological expectation.

In full QCD, with two degenerate sea quarks, the connected part is slightly enhanced whereas the disconnected amplitude is decreased. The sum of both contributions is still close to the quenched result. Because the light quark mass is found to be quite small, the full QCD lattice result differs from the ‘experimental’ value by about a factor of two. The flavor symmetry of the disconnected parts seems not to be hampered by the presence of light sea quarks. Thus, the y parameter decreases only slightly.

Let us now discuss what could be done to consolidate this picture. First of all, the statistical errors to the disconnected contributions are too large. Although the stochastic estimator technique with complex Z_2 noise in combination with *PAM* reduces these errors considerably, one is still confronted with uncertainties of $O(30\%)$, on gauge configuration samples of $O(200)$.

In the case of quenched QCD it should be no major problem to reduce these errors by a factor of 10, simply by exploiting the computational power of currently available parallel supercomputers.

For full QCD calculations the situation looks less promising. One can expect however, that the signal to noise ratio will improve on larger lattices, due to self averaging effects.

Once one has succeeded in reducing the statistical errors to a few percent, a scaling analysis of $\sigma_{\pi N}$ and y can be done. This will remove possible cutoff effects and lead to reliable continuum values for $\sigma_{\pi N}$. Since the y parameter depends on (a ratio of) renormalization factors it will be advantageous to use non-perturbative renormalization techniques [78, 79] instead of the standard (tadpole improved) perturbative methods. This might weaken the cutoff dependence of y considerably.

The last step in a full QCD determination of y will be to include sea quarks of different masses into the generation of vacuum configurations. A lattice simulation with two degenerate light and two degenerate strange quarks should be feasible even with cur-

rent algorithmic and computational facilities, as it avoids the sign problem of the fermion determinant [80].

3 The Flavor Singlet Axial Coupling of the Proton

About a decade ago the European Muon Collaboration (EMC) [19] announced measurements of the first moment of the polarized proton structure function g_1^p , which implied an unexpectedly low value for the flavor singlet axial coupling of the proton $G_A^1 \simeq 0$, defined by

$$s_\mu G_A^1 = \langle p, s | A_\mu^0(q) | p, s \rangle_{q^2=0} . \quad (68)$$

s_μ is the proton spin vector, and A_μ^0 is the flavor singlet axial current

$$A_\mu^0 = Z_A^S \sum_{q=u,d,s} \bar{q} \gamma_\mu \gamma_5 q . \quad (69)$$

Z_A^S denotes the renormalization constant of the singlet current in the continuum.

In the simple parton model, G_A^1 can be interpreted as the fraction of the proton spin carried by the quarks. Thus, on first sight, the EMC result indicated that the quarks would not contribute substantially to the proton spin: The confusion which followed from this naive interpretation was called the ‘proton spin crisis’.

On top of this, the EMC result stands in contradiction to the Ellis-Jaffe sum rule [25], which can be derived in the OZI (Zweig rule) limit of QCD. This indicated already that the proton spin problem might be deeply connected to the quantum field theoretical properties of QCD.

Since then, in a tremendous effort, both on the experimental [20–24] and on the theoretical side [81], the EMC result has been refined and a clear qualitative understanding of the phenomenon could be achieved.

The latest analysis of experimental results [23], including all proton, deuteron and neutron data, yields²⁰

$$G_A^1 = 0.29 \pm 0.06 , \quad (70)$$

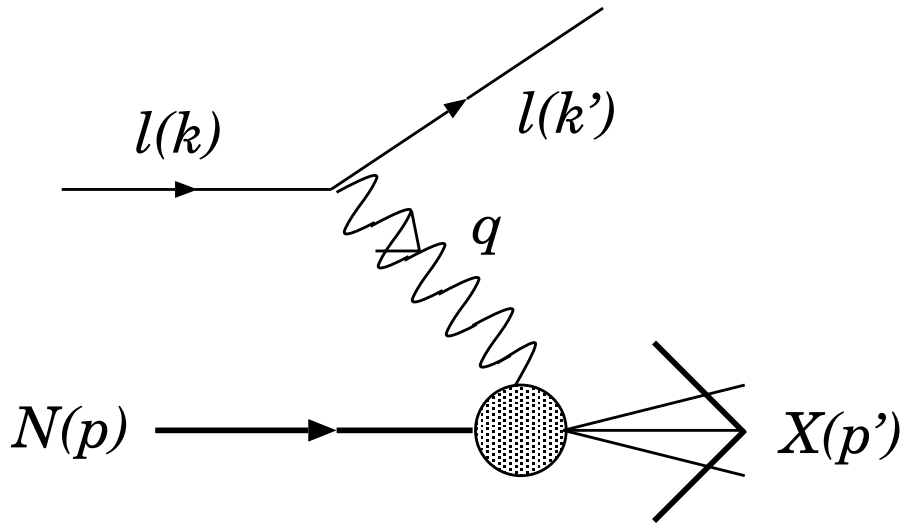
which is significantly below the Ellis-Jaffe prediction of $(G_A^1)^{EJ} = 0.58$.

From the theoretical investigations it appears that it is the influence of the $U(1)$ axial anomaly, which leads to the small value of G_A^1 . This immediately removes the ‘proton spin crisis’, as an interpretation in terms of the simple parton model is no longer valid. We mentioned in the introduction that the axial anomaly is closely connected to the topological properties of the QCD vacuum. Thus, the anomalous value of G_A^1 is one of the rare opportunities for a quantitative study of topological aspects.

The lattice approach provides (at least) two different methods for the calculation of G_A^1 .

The first one, which we will call the *direct method*, is to evaluate the r.h.s. of eq. (68). Since this is a flavor singlet matrix element, one expects contributions from both

²⁰This is at a renormalization scale of $Q_0^2 = 5\text{GeV}^2$.

Figure 8: *Inclusive polarized DIS scattering.*

the connected and the disconnected parts, depicted in fig. 1. If it turns out, that the smallness of G_A^1 originates from sizeable (negative) disconnected contributions, one could immediately clarify why and to what extent the Ellis-Jaffe sum rule fails: Disconnected diagrams are excluded in the OZI limit of QCD.

The second method, which we will denote as the *topological method*, focuses on the topological aspects – charge and susceptibility – of QCD. Here, one calculates the correlation of the proton propagator and the topological charge density. A success of this approach with respect to a small value of G_A^1 would encourage for a detailed, quantitative investigation of the connection between the axial anomaly, QCD topology and instantons.

Both methods will be explained below in detail.

3.1 Preparation

Let us briefly recall how G_A^1 is connected to the polarized deep inelastic scattering (DIS) of leptons and protons, shown schematically in fig.8.

The differential cross section for lepton proton DIS in the laboratory frame is given by

$$\frac{d^2\sigma}{d\Omega dE'} = \frac{1}{2M} \frac{\alpha^2}{q^4} \frac{E}{E'} L_{\mu\nu} W^{\mu\nu}, \quad (71)$$

where M is the proton mass, E and E' are the energies of the incoming and outgoing lepton, and $L_{\mu\nu}$ and $W_{\mu\nu}$ denote the leptonic and hadronic tensors, respectively. $W_{\mu\nu}$ can be parameterized by two spin independent structure functions, F_1 and F_2 , and by two spin sensitive functions, g_1^p and g_2^p

$$\begin{aligned}
W_{\mu\nu} &= F_1 \left(-g_{\mu\nu} + \frac{q_\mu q_\nu}{q^2} \right) + F_2 \left(p_\mu - \frac{pq}{q^2} q_\mu \right) \left(p_\nu - \frac{pq}{q^2} q_\nu \right) / (pq) \\
&+ i \frac{M}{pq} \epsilon_{\mu\nu\rho\sigma} q^\rho \left\{ s^\sigma g_1^p + \left[s^\sigma - \frac{sq}{pq} p^\sigma \right] g_2^p \right\}.
\end{aligned} \tag{72}$$

s denotes the polarization vector of the proton.

The polarized structure functions g_1^p and g_2^p can be extracted experimentally from the measurement of the asymmetries

$$A_{\parallel} = \frac{d\sigma^{\uparrow\downarrow} - d\sigma^{\uparrow\uparrow}}{d\sigma^{\uparrow\downarrow} + d\sigma^{\uparrow\uparrow}}, \quad A_{\perp} = \frac{d\sigma^{\downarrow\rightarrow} - d\sigma^{\uparrow\rightarrow}}{d\sigma^{\downarrow\rightarrow} + d\sigma^{\uparrow\rightarrow}}, \tag{73}$$

where the arrows indicate the polarizations of the lepton (first arrow) and the proton (second arrow): up and down arrows stand for longitudinal polarizations, and the right arrow denotes a proton spin direction transverse to the lepton momentum and towards the direction of the scattered lepton.

On the theoretical side, g_1^p is given by the proton matrix element of two electromagnetic currents carrying large space like momentum. Its first moment

$$\Gamma_1^p(Q^2) \equiv \int_0^1 dx g_1^p(x, Q^2), \quad Q^2 = -q^2, \quad x = \frac{Q^2}{2pq} \tag{74}$$

can be derived using the operator product expansion (OPE) [82]. Including terms up to twist two one obtains

$$J^\rho(q) J^\sigma(-q) \stackrel{Q^2 \rightarrow \infty}{\sim} 2\epsilon^{\rho\sigma\nu\mu} \frac{q_\nu}{Q^2} \left[C_1^{NS}(\alpha_s) \left(A_\mu^3 + \frac{1}{\sqrt{3}} A_\mu^8 \right) + \frac{2}{3} C_1^S(\alpha_s) A_\mu^0 \right], \tag{75}$$

and correspondingly

$$\Gamma_1^p(Q^2) = \frac{1}{12} C_1^{NS} \left(G_A^3 + \frac{1}{3} G_A^8 \right) + \frac{1}{9} C_1^S G_A^1. \tag{76}$$

The Wilson coefficients C_1^{NS} and C_1^S are both known to $O(\alpha_s^3)$ [83]. The non-singlet form factors G_A^3 , G_A^8 and the singlet coupling G_A^1 are given by the forward proton matrix elements of the (renormalized) axial currents

$$\langle p, s | A_\mu^3 | p, s \rangle = s_\mu \frac{1}{2} G_A^3 \tag{77}$$

$$\langle p, s | A_\mu^8 | p, s \rangle = s_\mu \frac{1}{2\sqrt{3}} G_A^8 \tag{78}$$

$$\langle p, s | A_\mu^0 | p, s \rangle = s_\mu G_A^1, \tag{79}$$

with

$$\begin{aligned}
A_\mu^3 &= \mathcal{Z}_A^{NS} \frac{1}{2} (\bar{u} \gamma_\mu \gamma_5 u - \bar{d} \gamma_\mu \gamma_5 d) \\
A_\mu^8 &= \mathcal{Z}_A^{NS} \frac{1}{2\sqrt{3}} (\bar{u} \gamma_\mu \gamma_5 u + \bar{d} \gamma_\mu \gamma_5 d - 2\bar{s} \gamma_\mu \gamma_5 s) \\
A_\mu^0 &= \mathcal{Z}_A^S \sum_{q=u,d,s} \bar{q} \gamma_\mu \gamma_5 q .
\end{aligned} \tag{80}$$

Note that we have introduced different renormalization factors for the non-singlet (\mathcal{Z}_A^{NS}) and the singlet (\mathcal{Z}_A^S) axial currents. This is necessary, since the conservation of $A_\mu^{3,8}$ is only violated by the quark mass, whereas the singlet current is not conserved in the limit of vanishing quark mass, due to the presence of the axial anomaly.

The non-singlet couplings can be extracted from neutron and hyperon β decays. One finds²¹ [84, 85]

$$G_A^3 = 1.2670 \pm 0.0035, \quad G_A^8 = 0.579 \pm 0.025. \tag{81}$$

Thus, the flavor singlet coupling G_A^1 is determined by the measurement of Γ_1^p .

In the OZI limit of QCD, where (strange) quark loops do not contribute, eq's. (78) and (79) imply $G_A^1 = G_A^8$, in sharp contrast to the experimental result and to the fact that the Q^2 dependence of G_A^1 is different from that of G_A^8 . The QCD parton model can qualitatively repair this failure by the assumption of a large gluonic contribution to g_1^p . It turns out that singlet quark and gluon distributions mix under renormalization [86]. In a particular renormalization scheme, the Adler-Bardeen scheme, it is possible to shift the anomalous Q^2 dependence completely to the gluonic part, leaving intact the naive interpretation of the singlet quark distributions as the fraction of the proton spin carried by the quarks. However, the QCD parton model is unable to make any quantitative prediction for G_A^1 .

In this situation, a non-perturbative method, which has direct access to the singlet proton amplitude, c.f. eq. (79), is badly needed. A lattice computation of this amplitude can reveal whether, and to what extent, QZI violating contributions determine the value of G_A^1 . In the language of fig.1, the latter correspond to the disconnected parts of the singlet proton amplitude, whereas the connected contributions should still obey the Ellis-Jaffe sum rule.

Before we explain how such a *direct* calculation can be performed on the lattice we will discuss shortly the second approach to G_A^1 which exploits the close connection between flavor singlet axial current, axial anomaly and topological charge.

The axial vector Ward identity

$$\partial_\mu A_\mu^0 = 2i \sum_{i=1, n_f} m_{q_i} \bar{q}_i \gamma_5 q_i + 2n_f \frac{\alpha_s}{4\pi} \text{tr} G_{\mu\nu} \tilde{G}^{\mu\nu}, \tag{82}$$

²¹ G_A^8 has been determined from hyperon decays under the assumption of $SU(3)$ flavor symmetry. Thus, the uncertainty on this quantity might be underestimated.

with n_f being the number of quark flavors and $G(\tilde{G})$ the (dual) tensor of gluon field strength, states that the axial vector flavor singlet current is not conserved in the chiral limit due to existence of an anomalous pure vacuum contribution $tr G_{\mu\nu} \tilde{G}^{\mu\nu}$, called the axial anomaly.

The anomaly is deeply connected to the topological structure of the vacuum [87]. In particular, the topological charge Q (topological index, Pontryagin index), which labels the different topological sectors of the vacuum, can be expressed by

$$Q = -\frac{1}{16\pi^2} \int d^4x \, tr G_{\mu\nu} \tilde{G}^{\mu\nu} . \quad (83)$$

Thus, the axial anomaly is just the topological (charge) density $\mathcal{Q}(x) \equiv tr G_{\mu\nu} \tilde{G}^{\mu\nu}$ of the vacuum.

We can now reformulate eq. (79) in terms of \mathcal{Q} . In the chiral limit ($m_q = 0$), a Fourier transformation of eq. (82) yields

$$iq_\mu \langle p', s | A_\mu^0(q) | p, s \rangle = 2n_f \frac{\alpha_s}{4\pi} \langle p', s | \mathcal{Q}(q) | p, s \rangle , \quad (84)$$

where p, p' are the 4-momenta of the incoming and outgoing proton, and $\vec{q} = \vec{p} - \vec{p}'$. If we choose the proton polarization s to be (anti)parallel to the direction of the momentum transfer q ,

$$\frac{\vec{s}}{|\vec{s}|} = \pm \frac{\vec{q}}{|\vec{q}|} , \quad (85)$$

we obtain in the rest frame of the proton at zero momentum transfer

$$G_A^1 = s_\mu \langle p, s | A_\mu^0 | p, s \rangle = \lim_{\vec{q} \rightarrow \vec{0}} 2n_f \frac{\alpha_s}{4\pi} \frac{-i|\vec{s}|^2}{\vec{q} \cdot \vec{s}} \langle p', s | \mathcal{Q} | p, s \rangle . \quad (86)$$

Thus, one arrives at a topological expression for the singlet axial coupling. We call the lattice procedure to determine the disconnected matrix element on the r.h.s. the *topological method*. Details will be given below. Let us mention however, that this method has a serious shortcoming in the quenched approximation [88]. Because of the fact that the η' meson becomes massless in the chiral limit of quenched QCD, the desired matrix element $\langle p', s | \mathcal{Q} | p, s \rangle$ diverges in this limit. Therefore, such calculations can be done only in full QCD.

An alternative, less fundamental, expression for G_A^1 in terms of topological quantities can be found using the composite operator propagator-vertex (CVP) method [15, 16, 89]. Here one uses the OPE to decompose the singlet part of Γ_1^p , eq. (74), into composite operator propagators $\langle 0 | T \mathcal{O}_i \mathcal{O}_j | 0 \rangle$ at zero momentum and vertex functions Γ

$$(\Gamma_1^p)_{sing} = \frac{1}{9} \frac{2}{2M} 2n_f C_1^s(\alpha_s) [\langle 0 | T \mathcal{Q} \mathcal{Q} | 0 \rangle \Gamma_{\mathcal{Q}pp} + \langle 0 | T \mathcal{Q} \Phi_5 | 0 \rangle \Gamma_{\Phi_5 pp}] , \quad (87)$$

with $\Phi_5 = \sum_{i=1, n_f} \bar{q}_i \gamma_5 q_i$. The topological susceptibility

$$\chi(k^2) = \int dx e^{ikx} i \langle 0 | T \mathcal{Q}(x) \mathcal{Q}(0) | 0 \rangle \quad (88)$$

vanishes in the chiral limit of full QCD at zero momentum transfer. The remaining propagator on the r.h.s. of eq. (87) is given by the square root of the first moment χ' of the topological susceptibility [15]. Thus, if the vertex function $\Gamma_{\Phi_5 pp}$ and the first moment of χ would be known, one could calculate the singlet axial vector coupling. Unfortunately, the vertex function cannot be calculated directly from first principles, making the CPV approach somewhat less rigorous than the *topological method*. However, it can be estimated e.g. in the QZI limit of QCD. The determination of χ' is a typical task for non-perturbative methods like lattice QCD or QCD spectral sum rules (QSSOR). The authors of ref. [16] have used the latter. They found²² $\sqrt{\chi'(0)}/Q_0^2=10\text{GeV}^2 = 23.2 \pm 2.4 \text{ MeV}$ and, correspondingly $G_A^1 = 0.35 \pm 0.05$, consistent with the result of the latest experimental determination, quoted in eq. (70). It will be interesting to see, whether this result can be consolidated by a full QCD lattice computation.

Finally, let us comment on the apparent incompatibility in the physical interpretation of the two approaches. From a success of the *direct method* one would conclude that the correlation of vacuum quark loops with the proton is responsible for the small value of G_A^1 , whereas one expects in the *topological method* that topological excitations of the vacuum decrease the flavor singlet axial coupling. We want to emphasize that these are not different mechanisms: Topologically non trivial vacuum configurations influence of course the correlation of quark loops with the proton, since it is exclusively mediated by the vacuum. From that point of view, one would consider the (disconnected) quark loop contributions to G_A^1 as being induced by the topological properties of the vacuum.

3.2 Direct Method

According to eq. (79) we need to compute the matrix element $\langle p, s | \bar{q} \gamma_\mu \gamma_5 q | p, s \rangle$. The techniques which are employed for this task are quite similar to those introduced in section 2.1. Again, one exploits ratios of 3- and 2-point correlation functions at large time distances, namely

$$R_A^{SUM}(x_0, \mu) = \frac{G_{NqN}^A(x_0, \mu)}{G_{NN}(x_0)} - \langle \sum_{\vec{y}, y_0} (\bar{q} \gamma_\mu \gamma_5 q)(\vec{y}, y_0) \rangle \xrightarrow{x_0 \rightarrow \infty} A + \langle N | \bar{q} \gamma_\mu \gamma_5 q | N \rangle x_0, \quad (89)$$

$$R_A^{PLA}(x_0, y_0, \mu) = \frac{C_{NqN}^A(x_0, y_0, \mu)}{G_{NN}(x_0)} - \langle \sum_{\vec{y}} (\bar{q} \gamma_\mu \gamma_5 q)(\vec{y}, y_0) \rangle \xrightarrow{x_0 \rightarrow \infty} \langle N | \bar{q} \gamma_\mu \gamma_5 q | N \rangle, \quad 0 \ll y_0 \ll x_0, \quad (90)$$

²²A very preliminary result of an exploratory full QCD lattice simulation with Kogut-Susskind fermions has been reported by the authors of ref. [90]: $\sqrt{\chi'(0)} = 16(3)\text{MeV}$.

and

$$R_A^{PAM}(x_0, \Delta x_0, \Delta x'_0, \mu) = \sum_{y_0=\Delta x_0}^{x_0-\Delta x'_0} R_A^{PLA}(x_0, y_0, \mu) . \quad (91)$$

The axial 3-point functions G_{NqN}^A and C_{NqN}^A are defined as

$$C_{NqN}^A(x_0, y_0, \mu) = \sum_{\vec{x}} \sum_{\vec{y}} \langle N^\dagger(\vec{0}, 0) (\bar{q}\gamma_\mu\gamma_5 q)(\vec{y}, y_0) N(\vec{x}, x_0) \rangle , \quad (92)$$

$$G_{NqN}^A(x_0, \mu) = \sum_{y_0} C_{NqN}^A(x_0, y_0, \mu) . \quad (93)$$

One might suspect that the application of the *summation method* is not justified, since a term $\sim \bar{q}\gamma_\mu\gamma_5 q$ is not present in the QCD action S_{QCD} , and thus the Feynman-Hellmann theorem cannot be used directly to derive eq. (89). However, if one starts from a slightly modified action

$$S_{QCD}(\lambda) = S_{QCD} + \lambda \sum_y (\bar{q}\Gamma q)(y) \quad , \quad \Gamma = \gamma_\mu, \gamma_5, \gamma_\mu\gamma_5, \dots \quad (94)$$

and repeats the steps which lead to eq. (31) one arrives at

$$R_A^{SUM}(x_0, \lambda) = \frac{G_{NqN}^A(x_0, \lambda)}{G_{NN}(x_0, \lambda)} - \langle \sum_y (\bar{q}\Gamma q)(y) \rangle = A(\lambda) + \frac{\partial M_N(\lambda)}{\partial \lambda} x_0 . \quad (95)$$

The Feynman-Hellmann theorem, see eq. (33), yields

$$\frac{\partial M_N(\lambda)}{\partial \lambda} = \langle N(\lambda) | \bar{q}\Gamma q | N(\lambda) \rangle . \quad (96)$$

Finally, in the limit $\lambda \rightarrow 0$, one obtains eq. (89).

The numerical methods used to calculate the connected contributions to R_A^{SUM} and R_A^{PLA} are identical with those described in section 2.2.

To determine the disconnected contributions, one has to evaluate

$$(C_{NqN}^A)^{disc} = \langle F_{G_{NN}}(0, x) \sum_{\vec{y}} Tr(\gamma_\mu\gamma_5 M^{-1}(\vec{y}, y_0; \vec{y}, y_0)) \rangle \quad (97)$$

and

$$(G_{NqN}^A)^{disc} = \sum_{y_0} (C_{NqN}^A)^{disc} . \quad (98)$$

In principle, the standard estimator techniques, described in section 2.2, can be applied. However, these methods become inefficient if one computes off-diagonal elements of M^{-1} in spin space, which occur for example in the combinations $Tr(\gamma_{1,2}\gamma_5 M^{-1})$. In these cases, large diagonal contributions add to the 'noise term' on the r.h.s. of eq. (58), and one would

have to enhance the number of estimates or gauge configurations drastically to suppress these terms.

Two alternative ways to cope with this problem have been proposed in ref's. [73, 91] and ref. [92]. The first method simply circumvents the problem by splitting the stochastic inversion, eq. (56), into four pieces, each of them corresponding to one spin component. It turns out that, with an equal computational effort, this *spin explicit method* reduces the statistical error on the estimate of $Tr(\gamma_{1,2}\gamma_5 M^{-1})$ by about 40 - 50%.

The second technique reduces the fluctuations from large diagonal contributions by subtracting the estimate for the on-diagonals

$$E[M^{-1}(x_0, x_0)] = \frac{1}{N_E} \sum_{s=1}^{N_E} \sum_y \eta_{x_0}^s M^{-1}(x_0, y) \eta_y^s \quad (99)$$

from the estimate $E[M^{-1}(x_0, z_0)]$ for the off-diagonals, given by eq. (58). This yields an improved estimate

$$E[M^{-1}(x_0, z_0)]^{impr} = E[M^{-1}(x_0, z_0)] - E[M^{-1}(x_0, x_0)] \frac{1}{N_E} \sum_{s=1}^{N_E} \eta_{z_0}^s \eta_{x_0}^s . \quad (100)$$

We emphasize that this *diagonal improved method* works equally well as the *spin explicit method*.

3.2.1 Renormalization

The axial current A_μ is not conserved in the continuum due to the presence of finite quark masses and to the axial anomaly. Thus it gets renormalized by quantum fluctuations. The effects of the two chiral symmetry breaking mechanisms on the renormalization of A_μ are however quite different.

The quark masses induce only a soft symmetry breaking, i.e. the dimension of the relevant operator is less than 4, and the renormalization factor \mathcal{Z}_A^{NS} is cutoff independent and finite. In particular, one obtains $\mathcal{Z}_A^{NS} = 1$ in the limit of vanishing quark mass. Non-singlet axial currents are renormalized by \mathcal{Z}_A^{NS} alone, as the axial anomaly is absent in this case.

The symmetry breaking caused by the axial anomaly is not soft (dimension=4), and A_μ picks up an additional renormalization which diverges logarithmically if the cutoff is removed [93]. This leads to a non-zero anomalous dimension which induces a renormalization point dependence on \mathcal{Z}_A^S [94]. Fortunately, the renormalization point dependence of G_A^1 is weak. Increasing the renormalization scale μ^2 from 10GeV^2 to infinity decreases the value of G_A^1 by about 10% [23].

The situation is more complicated in lattice QCD. Lattice discretizations of the fermion action, which avoid the fermion doubling problem, introduce additional chiral symmetry breaking terms. It has been shown by Karsten and Smit [31] for the Wilson type of discretization that these terms are essential in reproducing the correct form of the axial anomaly in the continuum limit. However, the renormalization of the (axial) currents

becomes non-trivial. Although the lattice value, Z_A^{NS} , is still finite, the condition $Z_A^{NS} = 1$ at $m_q = 0$ is no longer valid.

Much progress has been achieved in the determination of the lattice values of Z_A^{NS} , which depend on the lattice coupling and quark mass. We will comment on the different methods below.

Not much is known about the lattice renormalization factor Z_A^S of the singlet axial current. In first order lattice perturbation theory, the logarithmically divergent contribution from axial anomaly is absent, and $Z_A^S = Z_A^{NS}$ [31]. Unfortunately, a two loop or even a non-perturbative determination of Z_A^{NS} has not been performed yet. In view of the large statistical uncertainties in the disconnected parts of flavor singlet axial current matrix elements (see below) it appears to be justified to work with the assumption $Z_A^S = Z_A^{NS}$. However, one should keep in mind that a possible improvement of the statistical quality would have to go hand in hand with a more precise determination of Z_A^S .

The early estimates of Z_A^{NS} were based on first order lattice perturbation theory calculations, where the bare lattice coupling was taken as the expansion parameter [31, 95]. It was demonstrated however through several examples [39] that lattice perturbation theory in the bare coupling g_0 is ill behaved, and that large higher order corrections can introduce considerable uncertainties on the renormalized matrix elements.

The convergence of the perturbative expansion can be improved, if one uses a renormalized coupling rather than g_0 , defined by a proper renormalization condition [39, 96]. Defining an improved coupling α_V by the static potential V

$$V(q) = -\frac{C_f 4\pi\alpha_V(q)}{q^2} \quad , \quad C_f = \frac{4}{3} \quad (101)$$

Lepage and Mackenzie [39] have worked out an improved perturbative expansion on the lattice, which in many cases exhibits a faster convergence than the expansion in g_0 . Moreover they demonstrated that the improvement is mainly due to the inclusion of tadpole-like diagrams, which, if ignored, induce a slow convergence of the expansion. Most of the recent lattice simulations have used this 'tadpole improved' perturbation theory in first order to renormalize their results. We emphasize however that even with this method higher order contributions can be sizable. Thus, a scaling analysis of the renormalized results is still mandatory.

To overcome this problem, non-perturbative renormalization techniques have been developed, which avoid the use of lattice perturbation theory [97–100]. For the determination of Z_A^{NS} two different procedures, the Ward identity method (WI) [97] and the regularization scheme independent method (RI) [99] are equally appropriate. The WI method exploits the fact that the Ward identities on the lattice have the same structure as in the continuum. This defines a set of non-linear equations for the renormalization factors, which can be solved numerically on a given lattice.

Clearly, the WI method is restricted to those operators where Ward identities do exist for. The RI method is more general in that respect and can be applied in principle to arbitrary composite operators. In this scheme the renormalization condition for an operator \mathcal{O} is imposed on the corresponding amputated Green function, computed between off shell

quark states of large virtuality. This defines a renormalized operator $\mathcal{O}^{\mathcal{R}}$, and thus a renormalization constant $Z_{\mathcal{O}}$, which is independent of the regularization scheme [101]. A disadvantage of the RI method is that one has to work in a fixed gauge. This makes it necessary to study the influence of lattice Gribov copies on the results [102].

Both non-perturbative methods imply a numerical lattice determination of several correlation functions. Thus, uncertainties due to finite size effects, statistical accuracy and, in the case of the WI method, ground state identification may still be present.

One may ask of course to what extent the value of Z_A^{NS} depends on the method used for its determination. To illustrate this point we show²³ in tab.2 the results for Z_A^{NS} from the different methods, calculated with the Wilson action in the quenched approximation and at several lattice couplings $\beta = 6/g_0^2$.

β	$a^{-1}[\text{GeV}]$ [103]	SPT	TIPT	WI [98]	RI [103]
6.0	2.258(50)	0.87	0.78	0.85(7)	0.81(1)
6.2	2.993(94)	0.87	0.79		0.81(1)
6.4	4.149(161)	0.87	0.80		0.82(2)

Table 2: Results for Z_A^{NS} in the chiral limit at a renormalization scale $\mu = a^{-1}$ in the standard Wilson discretization. Denotation: SPT: first order standard (bare) perturbation theory; TIPT: first order tadpole improved perturbation theory; WI: non-perturbative Ward identity method; RI: non-perturbative regularization scheme independent method.

Obviously, the effect of variation of methods is not dramatic (5 – 10%), compared to the large statistical uncertainties on the disconnected part of the axial flavor singlet current. Given that, together with the fact that renormalization effects on G_A^1 are small in the continuum, one can hope, for lack of better wisdom, that the one loop result for the renormalization of this current, $Z_A^S = Z_A^{NS}$, is a currently tolerable approximation.

3.3 Topological Method

To determine G_A^1 from eq. (86) by a lattice calculation one needs to define a discretized lattice operator for the topological charge density \mathcal{Q}^L which agrees with the continuum definition of \mathcal{Q} in the limit $a \rightarrow 0$, e.g.

$$\mathcal{Q}^L(x) \xrightarrow{a \rightarrow 0} a^4 \mathcal{Q}(x) + O(a^6) . \quad (102)$$

²³This table has been originally compiled by the authors of ref. [103].

A straightforward way to define \mathcal{Q}^L starts from the discretized version of the field strength tensor $G_{\mu\nu}^L$,

$$G_{\mu\nu}^L(x) = \frac{1}{8} [P_{\mu,\nu}(x) + P_{-\mu,-\nu}(x) + P_{\nu,-\mu}(x) + P_{-\nu,\mu}(x) - P_{\nu,\mu}(x) - P_{-\nu,-\mu}(x) - P_{-\mu,\nu}(x) - P_{\mu,-\nu}(x)] , \quad (103)$$

where $P_{\mu,\nu}(x)$ is the product of gauge parallel transporters $U(x)$ around an elementary plaquette

$$P_{\mu,\nu}(x) = U_\mu(x)U_\nu(x + a\hat{\mu})U_{-\mu}(x + a\hat{\mu} + a\hat{\nu})U_{-\nu}(x + a\hat{\nu}) . \quad (104)$$

From that it follows for the topological charge density [104]

$$\mathcal{Q}^L(x) = \frac{1}{64} \sum_{\mu\nu\rho\sigma}^{\pm 4} \tilde{\epsilon}_{\mu\nu\rho\sigma} Tr (P_{\mu,\nu}(x)P_{\rho\sigma}(x)) , \quad (105)$$

where $\tilde{\epsilon}_{\mu\nu\rho\sigma}$ is the Levi-Civita tensor for $\mu, \nu, \rho, \sigma > 0$, and $\tilde{\epsilon}_{\mu\nu\rho\sigma} = -\tilde{\epsilon}_{-\mu\nu\rho\sigma}$, etc. .

To relate the lattice definition of the topological charge density to the respective continuum quantity one needs to renormalize \mathcal{Q}^L . In principle, this is a highly non-trivial task, since \mathcal{Q} mixes with $\partial_\mu A_\mu$ and with the pseudo scalar current $\sum_{i=1}^{n_f} m_i \bar{q}_i \gamma_5 q_i$ under renormalization [15]. It has been shown however in first order lattice perturbation theory [105] that the mixing is quite small ($\leq 5\%$) for bare lattice couplings $g_0 \leq 1$. Thus one can concentrate on the determination of one multiplicative renormalization constant Z_Q ,

$$\mathcal{Q} \simeq Z_Q \mathcal{Q}^L . \quad (106)$$

Unfortunately, it turns out that the one loop correction to Z_Q is large [105,106], making a non-perturbative determination highly desirable. Such a non-perturbative renormalization method has been developed by the authors of ref's. [107,108]. Roughly speaking it consists of preparing a classical gauge configuration of given topological charge and then to add gauge fluctuations by a Monte Carlo process. A comparison of the integer valued 'classical' topological charge with the one extracted from the 'fluctuating' gauge configurations allows for the determination of Z_Q .

On the other hand one can try to improve the lattice operator \mathcal{Q}^L , eq. (105), such that the higher order corrections to Z_Q are made small or might even vanish. The link smearing technique [109], which supplies a non-local version of eq. (105), reduces the higher order corrections substantially. However, the 'ultima ratio' with respect to renormalization properties is the so called geometric definition of \mathcal{Q}^L , given by M. Lüscher [110]. Here, \mathcal{Q}^L is constructed such that the corresponding topological charge takes only integer values even in the case of 'fluctuating' gauge configurations. It follows that $Z_Q = 1$, i.e. higher order corrections are absent.

A comparison of the different definitions of topological charge on the lattice has been given by the authors of ref. [111] in the quenched approximation. It turns out that, using the non-perturbative renormalization procedure described above, all definitions lead

to consistent results. However, the geometrical definition and the definition of eq. (105) suffer from large statistical noise. Thus, for practical simulations, one should use²⁴ the link smearing technique [109] to calculate $\mathcal{Q}^{\mathcal{L}}$.

Having succeeded in defining suitable lattice operators $\mathcal{Q}^{\mathcal{L}}$ there remains still a potentially severe problem for full QCD lattice applications²⁵ to extract reliable results from numerical simulations. It has been obtained in ref. [114] for the staggered formulation of lattice fermions that the standard updating algorithm, the Hybrid Monte Carlo, tends to lose its ability to move between different sectors of topological charge if the lattice quark mass is chosen at or below $ma \simeq 0.01$, which corresponds to $m_{\pi}/m_{\rho} \simeq 0.57$. Thus, in this region of quark mass, the results might be biased by a non-Gaussian distribution of gauge configurations with respect to topology. The authors of ref. [115] have performed a similar investigation using dynamical Wilson fermions with quark masses down to a value corresponding to $m_{\pi}/m_{\rho} \simeq 0.69$, finding no significant decrease of the Hybrid Monte Carlo's mobility. At $m_{\pi}/m_{\rho} \simeq 0.56$ ref. [115] obtains still transitions between different topological sectors, but with a reduced frequency. This indicates that either the number of Hybrid Monte Carlo updates has to be increased at small quark mass²⁶ or one has to find an alternative updating algorithm which does not suffer from this kind of immobility.

Assuming that we have successfully created a statistically representative sample of vacuum configurations we are now prepared to evaluate the r.h.s. of eq. (86) on the lattice. Obviously, two steps are necessary for this task: First one has to determine the matrix element $\langle p', s | \mathcal{Q}^{\mathcal{L}}(q) | p, s \rangle$ for several momenta p, p' and secondly one has to extrapolate the results to the point $q = p - p' = 0$. Concerning the second step we emphasize that it is advantageous to work in the brick-wall system

$$|\vec{p}\uparrow\rangle = |\vec{p}'\uparrow\rangle \quad , \quad q_0 = 0 . \quad (108)$$

Within this setting, the (unwanted) matrix element $q_0 \langle p', s | A_0^0 | p, s \rangle$ is absent in eq. (84) even for $\vec{q} \neq 0$. Thus, there is no need to remove it by the extrapolation $\vec{q} \rightarrow 0$ in eq. (86).

To extract the matrix element $\langle p', s | \mathcal{Q}^{\mathcal{L}}(q) | p, s \rangle$ one starts from the 3-point correlation function

$$A(\vec{y}, \tau, \vec{x}, t) = \langle P^\dagger(\vec{0}, 0) T_s \mathcal{Q}(\vec{y}, \tau) P(\vec{x}, t) \rangle , \quad (109)$$

²⁴We did not discuss the ‘fermionic’ definition of the topological charge density

$$\mathcal{Q}^{\mathcal{L}} = m_q \langle Tr(\gamma_5 M^{-1}) \rangle , \quad (107)$$

where m_q is the quark mass and M^{-1} the quark propagator, which has been proposed by Smit and Vink [112], inspired by the Atiyah-Singer index theorem. Although stochastic estimator techniques enable for an accurate calculation [113] of the r.h.s. of eq.(107), the renormalization properties of have not been studied yet in detail.

²⁵Quenched QCD does not suffer from this problem.

²⁶Ref. [115] estimates an increase by a factor of four when decreasing the quark mass from $m_{\pi}/m_{\rho} \simeq 0.69$ to $m_{\pi}/m_{\rho} \simeq 0.56$.

where P, P^\dagger are interpolating proton operators and T_s is the spin projection operator. The expectation value A can be determined on the lattice by calculating the correlation of the (spin projected) proton propagator with the topological charge density.

In Fourier space one obtains for given final momentum of the proton \vec{p} and momentum transfer²⁷ q

$$\tilde{A}(\vec{q}, \tau, \vec{p}, t) = \sum_{\vec{x}, \vec{y}} A(\vec{y}, \tau, \vec{x}, t) e^{i\vec{y}\vec{q}} e^{i\vec{x}\vec{p}}. \quad (110)$$

At large time distances $t - \tau$ and τ the interpolating proton operator projects only on the proton ground state. This yields

$$\tilde{A}(\vec{q}, \tau, \vec{p}, t) \xrightarrow{t-\tau, \tau \rightarrow \infty} \langle 0 | P^\dagger | P(p', s) \rangle \langle P(p, s) | P | 0 \rangle \langle P(p', s) | \mathcal{Q} | P(p, s) \rangle \times e^{-E(p)(t-\tau)} e^{-E(p')\tau}. \quad (111)$$

The proton amplitudes $\langle 0 | P^\dagger | P(p', s) \rangle$ and $\langle P(p, s) | P | 0 \rangle$ are determined from the asymptotic time dependence of the proton propagator $\Delta_P(p, t)$, see eq. (28). Using the condition $|\vec{p}| = |\vec{p}'|$ (see above) one finally gets

$$\langle P(p', s) | \mathcal{Q} | P(p, s) \rangle = \lim_{t-\tau, \tau \rightarrow \infty} \frac{\tilde{A}(\vec{q}, \tau, \vec{p}, t)}{\Delta_P(p, t)}. \quad (112)$$

From a computational point of view one might think that the topological method is superior to the direct method since it circumvents the very costly and statistically noisy calculation of disconnected (fermionic) contributions with stochastic estimator methods. However it has some serious disadvantages which might be quite difficult to overcome. First of all, eq. (84), which connects the axial current matrix element with the topological charge density, is valid only in the chiral limit. Apart from the fact that this makes an extrapolation in m_q necessary²⁸ one has to neglect symmetry breaking effects according to $m_{u,d} \neq 0$. Secondly one has to calculate \tilde{A} and Δ_P at several momenta \vec{p}, \vec{q} . The signals from momentum nonzero correlation functions are however very noisy on the lattice and one needs high statistics and well suited guesses for the wavefunctions to extract the required ground state information. On top of this the extrapolation in q might have to span a quite long range. The smallest nonzero momentum on a lattice with periodic boundary conditions is given by

$$p_{min} = \frac{2\pi}{N_s} \times a^{-1}. \quad (113)$$

With typical lattice parameters $N_s \simeq 20$ and $a^{-1} \simeq 2\text{GeV}$ one gets the rather large value $p_{min} \simeq 600\text{MeV}$.

Last not least, as we mentioned above, the application of the topological method is not justified in the quenched approximation [88]. In full QCD one has to fight with a possible

²⁷Note that the initial proton momentum \vec{p}' is implicitly fixed by $\vec{p}' = \vec{p} - \vec{q}$.

²⁸The fermion matrix approaches a zero mode at $m_q = 0$. Thus, the quark propagator diverges at this point. A direct lattice simulation at $m_q = 0$ is therefore excluded.

stiffness of the updating algorithm at small sea quark masses with respect to tunneling between different topological sectors²⁹.

Exploratory lattice studies have been performed in quenched [88, 116] and in full [117, 118] QCD to check on the feasibility of this method. It turned out that the statistical quality of the momentum nonzero correlation functions and, in full QCD, the stiffness of the updating algorithm with staggered fermions are the major hindrances in extracting reliable results. Thus, being optimistic, one can hope that the topological method might become useful with high statistics full QCD simulations using Wilson-like fermions. Such simulations are being performed currently by the CP-PACS [77] and T χ L [119] collaborations.

3.4 Lattice Results

3.4.1 Quenched QCD

The first steps towards a lattice determination of G_A^1 have been done several years ago by calculating the connected contributions to the matrix elements $\langle P|\bar{u}u|P\rangle$ and $\langle P|\bar{d}d|P\rangle$ [72, 120, 121]. Although the statistical accuracy of these simulations has been rather low (less than 40 gauge configurations have been used), the results have been quite encouraging as they yielded estimates for the non-singlet axial couplings G_A^3 and G_A^8 in the ball-park of the experimental findings, eq. (81).

Recently, a more precise estimate of G_A^3 in the quenched approximation has been calculated by the QCDSF collaboration [122]. They used the $O(a)$ improved Sheikoleslami-Wohlert action with a non-perturbatively determined [38] ‘clover’ coefficient c_{sw} , and non-perturbative estimates for the axial vector renormalization constant Z_A^{NS} . The simulation has been performed at 3 different values of the bare coupling, $\beta = 6.0, 6.2, 6.4$, which correspond to lattice cutoffs in the range $a^{-1} \simeq 2 - 3.5\text{Gev}$. The size of their statistical samples varies from $O(500)$ gauge configurations at $\beta = 6.0$ to $O(100)$ at $\beta = 6.4$. Fig. 9 displays the results for G_A^3 as a function of the (square of) the lattice spacing a in units of the string tension \sqrt{K} . It turns out that the cutoff effects in this range of the bare coupling are small ($O(10\%)$). A linear extrapolation³⁰ to the continuum limit, $a = 0$, yields a value for G_A^3 which is slightly lower, but, within errors, still consistent with the experimental result. Thus, one can expect from quenched lattice simulations to find a value of G_A^3 , which is close to experiment. Turning this conclusion around, the deviation of a lattice estimate of G_A^3 at a finite cutoff a^{-1} from the experimental result can serve as an indicator for systematic effects in the lattice calculations of the flavor non-singlet couplings. For want of something more precise, this deviation may be used also as an (lower limit) estimate for cutoff effects present in lattice determinations of G_A^1 .

²⁹Of course this problem affects also the direct method.

³⁰Using an $O(a)$ improved action one expects the cutoff effects to appear at $O(a^2)$. Thus, a linear extrapolation of $G_A^3(a^2)$ is justified.

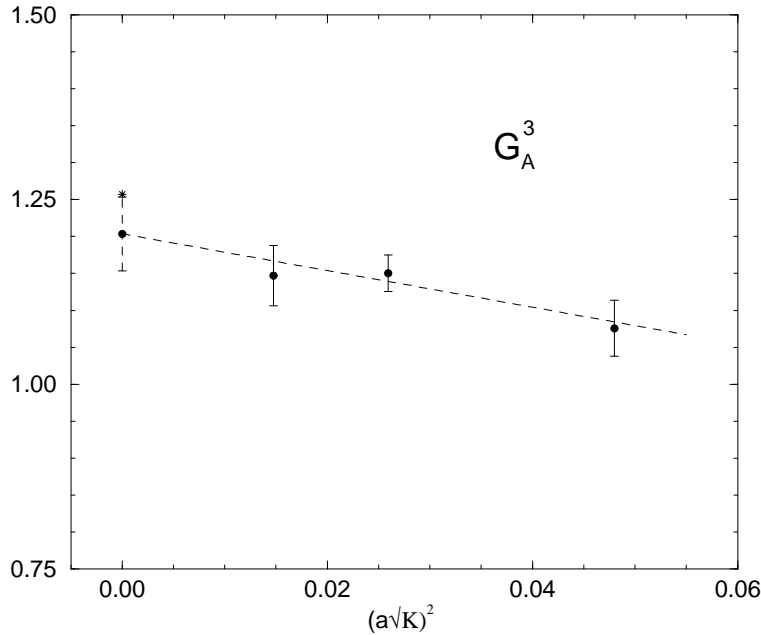


Figure 9: *QCDSF collaboration [122]: Continuum extrapolation of $G_A^3(a^2)$. The star indicates the position of the experimental result.*

In quenched QCD, two such simulations have been performed up to now with the standard Wilson action, one by Fukugita et al. [123] and one by Dong et al. [124]. The former has been done with accurate statistics ($O(300)$ gauge configurations), but at a somewhat large coupling, $\beta = 5.7$, which corresponds to $a^{-1} \simeq 1.5\text{GeV}$. The latter has operated closer to the continuum, at $\beta = 6.0$, but with a very low statistics (24 configurations), which might lead to a substantial under-estimation of the errors.

Using G_A^3 as an indicator for the size of cutoff effects, one finds in both cases that the uncertainty of their lattice estimates for G_A^1 is dominated by the large statistical noise found in the disconnected contributions. Before we discuss the results of ref's. [123,124] in somewhat more detail we will illustrate briefly why one indeed expects considerable statistical fluctuations in those parts.

We have seen in chapter 2.3 that the disconnected contribution to $\sigma_{\pi N}$ is much more noisy than the connected one. This is because both, the noise from the estimator method and from the inherent quantum fluctuations add up on top of the disconnected signal. From a numerical point of view the situation is even more disadvantageous for the disconnected contributions to G_A^1 . This is illustrated in fig. 10. According to eq. (47) the disconnected part of $\sigma_{\pi N}$ is given by the correlator of the nucleon propagator and the sum over quark loops with Dirac components (μ, μ) , $\mu = 1, 2, 3, 4$. Since the contributions are of similar size for each of the Dirac components, the summation helps to stabilize the signal. The disconnected part of G_A^1 , see eq. (98), however is determined by the difference of two such

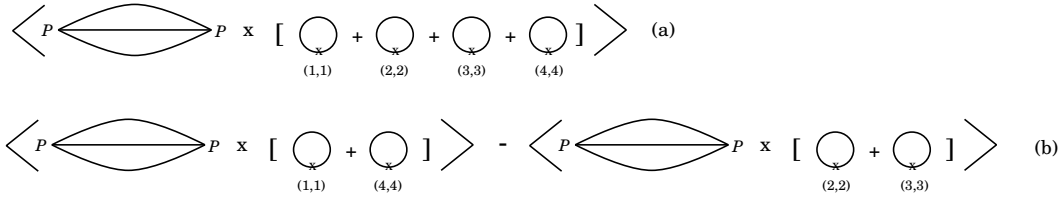


Figure 10: (a) Disconnected contribution to $\sigma_{\pi N}$; (b) Disconnected contribution to $\langle P | \bar{q} \gamma_3 \gamma_5 q | P \rangle$.

noisy correlators.

In fig. 11 we display the signals for connected and disconnected contributions to G_A^1 as found by the authors of ref. [123], at a quark mass corresponding to $m_\pi/m_\rho \simeq 0.745$. The connected parts exhibit a clear linear slope, see eq. (89), whereas the disconnected contribution is very noisy and disappears at $t = 12$.

Using the results of linear fits to the signals at several quark masses one can perform an extrapolation to the chiral limit. The quark mass dependence of connected and disconnected contributions is shown in fig. 12. Note that the amplitudes have been multiplied by the 1st order tadpole improved renormalization constant $Z_A^S = Z_A^{NS}$. To obtain the strange quark contribution to the singlet coupling, the ‘loop’ quark mass has been fixed to the strange quark mass³¹, while extrapolating in the light (valence) quark mass of the proton.

We emphasize that the disconnected parts are of opposite sign to the connected ones, thus lowering the value of G_A^1 . Obviously, they agree within errors over the entire mass range. This indicates flavor symmetry of the disconnected amplitudes. The mass dependence of all the amplitudes is weak, and a linear extrapolation seems well justified.

At the chiral limit, the authors of ref. [123] obtain

$$G_A^3 = \Delta u - \Delta d = 0.638(54) + 0.347(46) = 0.985(25) \quad (114)$$

and

$$G_A^1 = \Delta u + \Delta d + \Delta s = 0.638(54) - 0.347(46) - 0.109(30) = 0.18(10), \quad (115)$$

where $\Delta q = \langle P | \bar{q} \gamma_3 \gamma_5 q | P \rangle$. Note that G_A^1 is significantly lower than the OZI estimate $G_A^1 \simeq G_A^8 = 0.579(25)$, even within a statistical uncertainty of about 50%.

Unfortunately, the systematical errors are not well under control. As mentioned above, the comparison of the lattice estimate of G_A^3 with the experimental result can be taken to give at least a rough impression on the size of systematical effects. From the inspection of eq. (114) and eq. (81) one estimates that those are of the order of 30%.

³¹The lattice value of the strange quark mass m_s is determined by the condition $m_K(m_s, m_l)/m_\rho(m_l) = 0.64$, where m_l is the light quark mass.

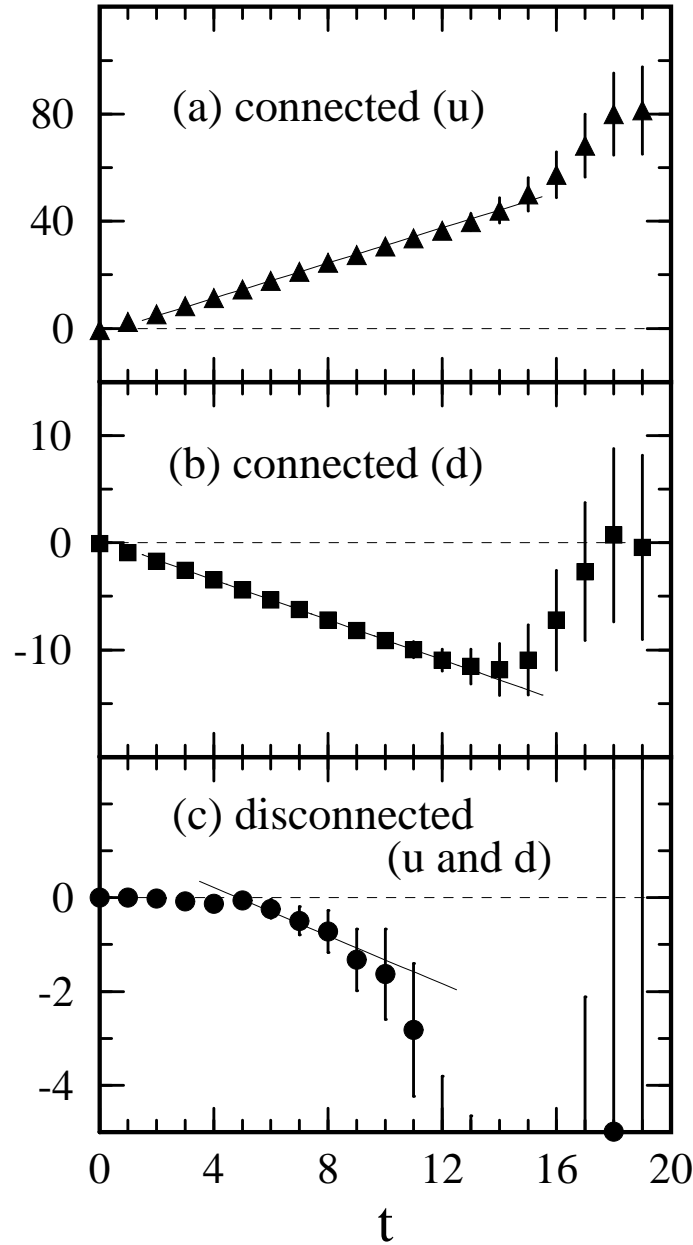


Figure 11: *Connected u-quark (a), connected d-quark (b) and disconnected contributions G_A^1 as found by ref. [123] at a quark mass corresponding to $m_\pi/m_\rho \simeq 0.745$. The disconnected part has been estimated with the (modified) volume source technique. The solid lines indicate the results of the fits according to eq. (89).*

A similar behavior of connected and disconnected amplitudes has been obtained by the authors of ref. [124]. They find estimates $G_A^1 = 0.25(12)$, $G_A^3 = 1.20(10)$, and

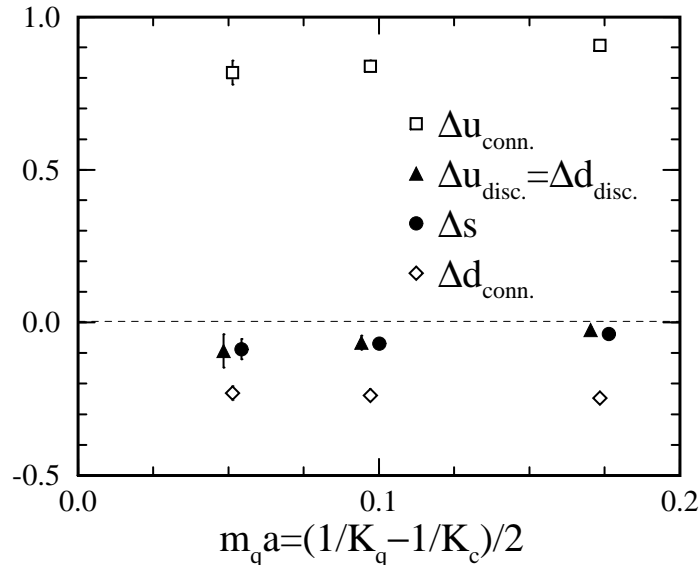


Figure 12: Ref. [123]: Connected and disconnected amplitudes $\Delta q = \langle P | \bar{q} \gamma_3 \gamma_5 q | P \rangle$ as a function of the bare quark mass in lattice units. The data has been multiplied by the 1st order tadpole improved renormalization constant $Z_A^S = Z_A^{NS}$.

$G_A^8 = 0.61(13)$, which are much closer to the experimental results. Since they have worked at a larger cutoff, $a^{-1} \simeq 2\text{GeV}$ compared to $a^{-1} \simeq 1.5\text{GeV}$ in ref. [123], the systematical errors might be indeed reduced. However, as mentioned above, the statistical sample which underlies this calculation is rather small, i.e. 1/10 of the sample used in ref. [123]. Thus, some caution in interpreting these findings is in order.

Nevertheless, the results found in quenched lattice calculations of G_A^1 are encouraging, as they yield quantitative support for the assumption that the small value of G_A^1 can be explained by negative contributions from quantum fluctuations.

It will be interesting to see whether this remains valid in full QCD.

3.4.2 Full QCD

Recently, the SESAM collaboration has performed a full QCD lattice calculation of G_A^1 [125]. The analysis is based on 4 sets of 200 statistically independent gauge configurations, which have been generated in the Wilson discretization scheme with $n_f = 2$ dynamical fermions at $\beta = 5.6$. The cutoff $a_\rho^{-1} = 2.3\text{GeV}$ corresponds approximately to that of a quenched calculation at $\beta = 6.0$ [70].

SESAM has applied the summation method, see eq. (89), and the standard insertion technique, c.f. section 2.2, to calculate the connected contributions. We illustrate the quality of the corresponding signals in fig. 13. Obviously the expected linear rise of

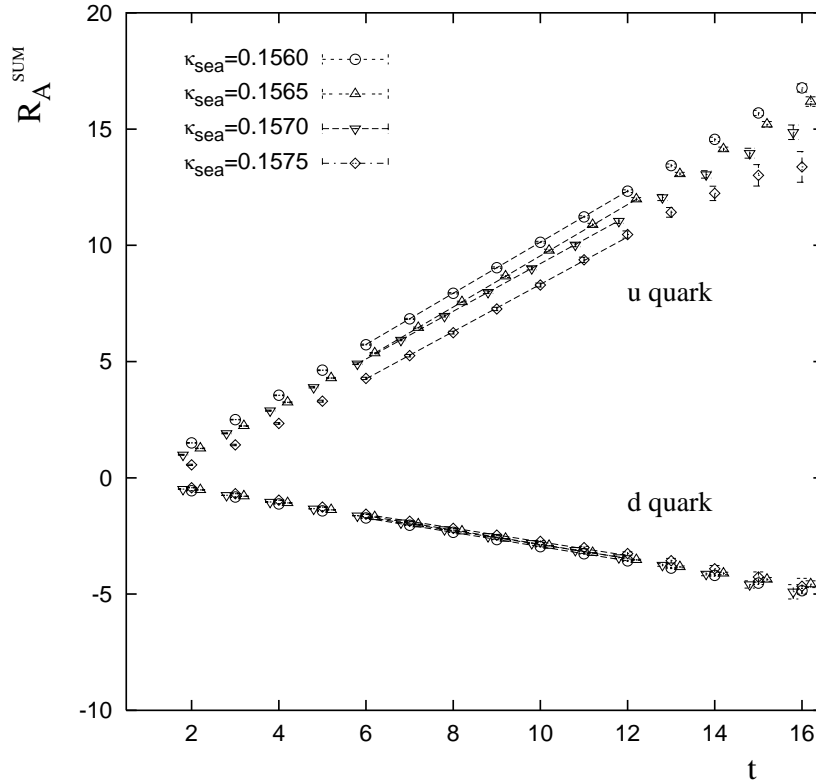


Figure 13: *Full QCD, SESAM collaboration [125]: Connected contributions to G_A^1 at different quark masses. The slope of the ‘u quark’ signals corresponds to the (spin averaged) amplitude $s_\mu \langle P | \bar{u} \gamma_m u \gamma_5 u | P \rangle$, that of the ‘d quark’ signals to $s_\mu \langle P | \bar{d} \gamma_m u \gamma_5 d | P \rangle$. The fits (range and value) are indicated by dashed lines.*

$R_A^{SUM}(t)$ is manifest for all four quark masses.

The disconnected amplitudes have been determined with the PAM method, eq. (91). To calculate the numerator of R_A^{PAM} SESAM has used the spin explicit stochastic estimator method, see section 3.2, with complex Z_2 noise and 100 estimates per spin component. This procedure has been proven to be much more advantageous than the standard summation method in calculations of the disconnected contributions to $\sigma_{\pi N}$ [73]. The signals for the axial vector insertions are shown in fig. 14. Although a linear behavior can be identified, the statistical quality of the data is low. This is similar to the situation found in the quenched calculations with (un-improved) volume source and summation methods, see fig. 11. The apparent non-improvement of PAM and spin explicit stochastic estimator technique might be due to larger statistical fluctuations in full QCD compared to quenched QCD. As mentioned above, such a behavior has been recognized in the analysis of the light spectrum, where, at equal sample size and lattice setup, the statistical errors in full QCD

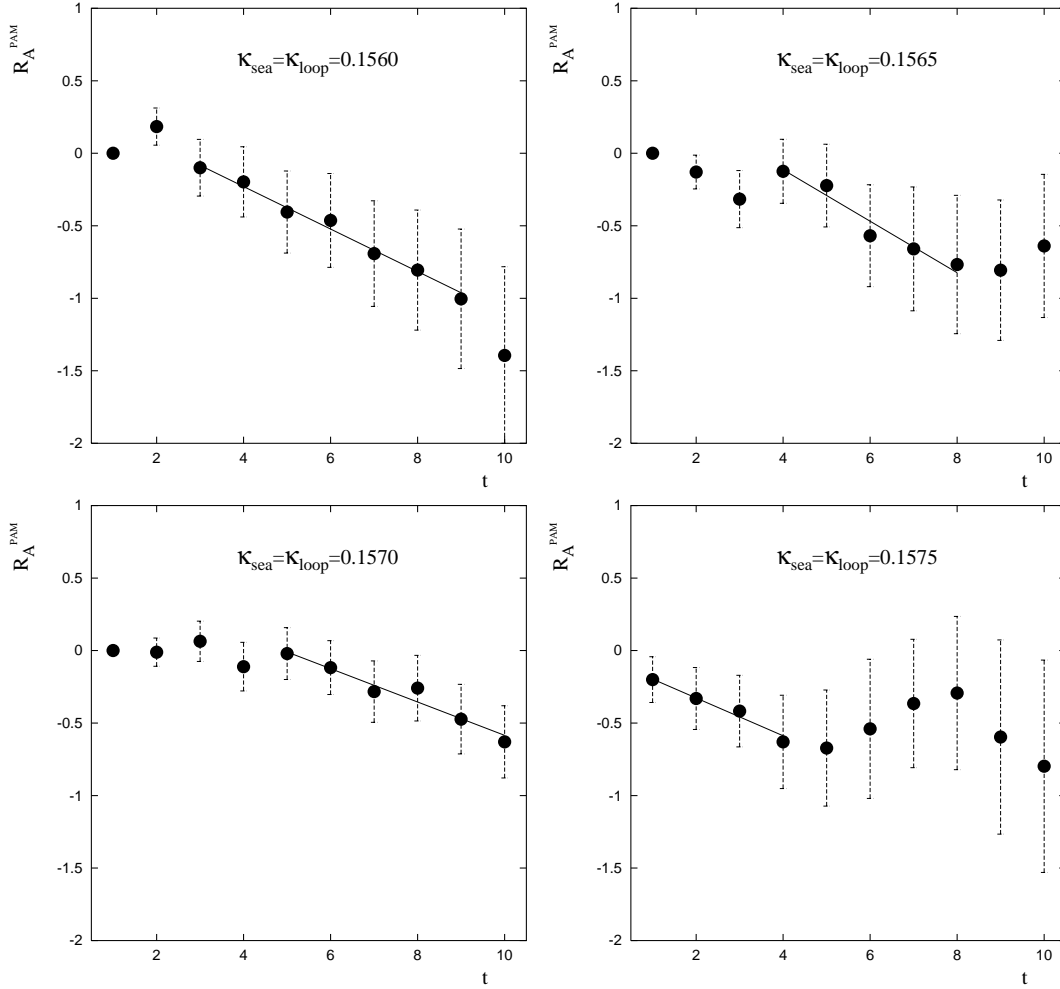


Figure 14: Full QCD, SESAM collaboration [125]: The ratio $R_A^{PAM}(t)$ with $\Delta t_0 = \Delta t = 1$ for the disconnected amplitudes $D_q = \langle P(\kappa_{sea}) | (\bar{q}\gamma_3\gamma_5q)(\kappa_{sea}) | P(\kappa_{sea}) \rangle$ at four sea quark masses. The fits (range and value) are indicated by solid lines.

exceed those of quenched QCD by more than a factor of 2 [70].

From the analysis of R_A^{SUM} and R_A^{PAM} at several quark masses one extracts the mass dependence of connected and disconnected contributions and extrapolates to the light quark mass. The data and the extrapolations are compiled in fig. 15. Obviously, the full QCD results are not very different from the quenched estimates of ref. [123], which are shown in fig. 12. In both cases one finds a weak mass dependence of the amplitudes. The disconnected insertions are less than zero, and their flavor symmetry appears to be maintained.

At the light quark mass, the full QCD estimates for the axial vector coupling constants

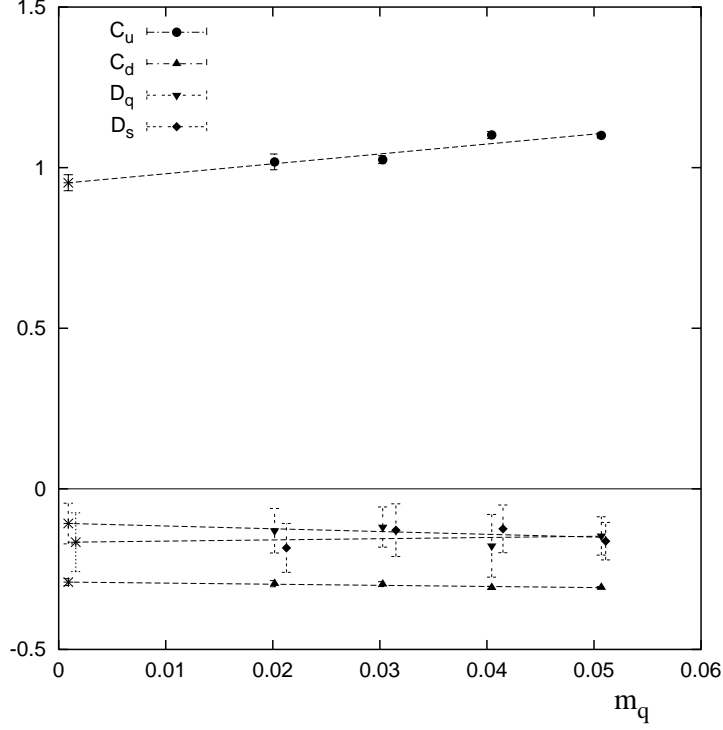


Figure 15: *Full QCD, ref. [125]: Extrapolation of the unrenormalized lattice amplitudes to the light quark mass. The fits are indicated by dashed lines, the results of the fits by bursts. The amplitudes are defined as follows: $C_u = s_\mu \langle P(m_q) | (\bar{u} \gamma_\mu \gamma_5 u)(m_q) | P(m_q) \rangle_{con}$ (spin averaged); $C_d = s_\mu \langle P(m_q) | (\bar{d} \gamma_\mu \gamma_5 d)(m_q) | P(m_q) \rangle_{con}$ (spin averaged); $D_q = \langle P(m_q) | (\bar{q} \gamma_3 \gamma_5 q)(m_q) | P(m_q) \rangle_{disc}$; $D_s = \langle P(m_q) | (\bar{s} \gamma_3 \gamma_5 s)(m_s) | P(m_q) \rangle_{disc}$.*

read

$$G_A^1 = Z_A^S [C_u + C_d + 2D_q + D_s] = 0.20(12) \quad (116)$$

and

$$G_A^3 = Z_A^{NS} [C_u - C_d] = 0.907(20), \quad G_A^8 = Z_A^{NS} [C_u + C_d] = 0.484(18), \quad (117)$$

where the 1st order tadpole improved renormalization

$$Z_A^S = Z_A^{NS} = \frac{1}{2\kappa} \left(1 - \frac{3\kappa}{4\kappa_c}\right) \left(1 - 0.31 \alpha_{\overline{MS}} \left(\frac{1}{a}\right)\right) \quad (118)$$

has been applied³². As in the quenched case at $\beta = 5.7$, the estimate of the triplet coupling differs from the experimental result by about 30%. This points to the presence

³²SESAM has used $\alpha_{\overline{MS}}(\frac{1}{a}) = 0.215$, $\kappa = \kappa_l = 0.15846$ for the light quark insertions (C_u, C_d, D_q), and $\kappa = \kappa_s = 0.15608$ for D_s .

of sizeable systematic uncertainties due to insufficient renormalization and finite cutoff effects. However, the major source of uncertainty in G_A^1 is given by the substantial amount of statistical fluctuations.

Within these uncertainties one finds no significant difference between quenched and full QCD results. This might indicate that the disconnected contributions to the flavor singlet axial coupling of the proton are dominated by the gluonic properties of the vacuum.

3.5 Summary

Within statistical and systematic uncertainties of about 50%, lattice simulations consolidate the assumption that the influence of QCD vacuum properties leads to a small value of G_A^1 . With the direct method, the latter are reflected in the disconnected contributions to the flavor singlet axial vector amplitude of the proton. Since quenched and full QCD calculations yield similar results, one might suspect that this phenomenon is dominated by gluons.

Use of the topological method would allow to investigate the influence of the axial anomaly on the value of G_A^1 in more detail. In particular one could study explicitly its dependence on the topological sectors of the QCD vacuum. However, as we have pointed out above, this approach suffers from serious numerical problems, and one has not succeeded yet to extract reliable estimates for G_A^1 by application of this technique.

Several strategies to improve this situation come in mind. With the direct method, the accuracy limiting factors are the statistical noise of the disconnected amplitudes and the neglect of higher order or non-perturbative contributions to Z_A^S . The former can be reduced by use of larger lattices, where self averaging effects will help, higher statistics and adapted estimator techniques. To improve on the latter one needs, at least, a 2nd order calculation of Z_A^S in the framework of lattice perturbation theory. Even then, as can be seen from the findings of the QCDSF collaboration, one might have to fight against cutoff effects. Thus, a scaling analysis of G_A^1 appears to be unavoidable.

To apply the topological method successfully, one needs to generate (physically) large vacuum configurations at small cutoff. This would enable for a calculation of the correlation of the proton with the topological charge density at small quark masses and momentum transfer. Fortunately, a non-perturbative renormalization procedure for the topological charge is available.

With current quenched or ($n_f = 2$) full QCD simulations, the strange quark contribution to G_A^1 might not be estimated correctly. In a realistic setup one would have to include a strange sea quark. From the numerical point of view a lattice simulation with 2 (degenerate) light quarks and 2 (degenerate) strange quarks appears feasible.

4 The Mass of the η' Meson and the $U(1)$ Problem

4.1 The Problem

In a classical field theory, symmetries of the Lagrangian must be reflected by symmetries of the physical phenomena which such a theory is supposed to describe. In a quantum field theory, this is not necessarily true, since quantum fluctuations of the vacuum can spoil the classical symmetries. However, one then expects to obtain remnants of this symmetry breaking in the physical observables, e.g. the occurrence of (massless) Goldstone bosons in case of a spontaneously broken global symmetry and of massive gauge bosons and Higgs particles if a (local) gauge symmetry is violated.

The QCD Lagrangian exhibits a $U(3) \times U(3) = SU(3) \times SU_A(3) \times U(1) \times U_A(1)$ global flavor symmetry [126] in the chiral limit, $m_u = m_d = m_s = 0$. Most of the implications of this large symmetry on the physics of strong interaction has been understood already in the early days of current algebra and the quark model.

The $SU(3)$ flavor symmetry is reflected in the multiplet structure of the particle spectrum [127], whereas the $SU_A(3)$ axial flavor symmetry is supposed to be broken spontaneously. The corresponding Goldstone bosons can be identified with the 8 light pseudo scalar mesons ($\pi^{0,\pm}, K^0, \bar{K}^0, K^\pm, \eta$), and the fact that those have non vanishing and non degenerate masses can be explained by an additional explicit breaking of the $SU(3)$ and $SU_A(3)$ symmetries due to $m_s \neq m_d \neq m_u \neq 0$.

The $U(1)$ flavor symmetry predicts baryon number conservation, which is well realized in nature. Likewise, one would expect an ‘axial baryon number conservation’, i.e. a parity doubling of baryon states, from the $U_A(1)$ symmetry. Since the particle spectrum does not exhibit such a parity doubling, one would suppose that this symmetry is broken spontaneously. However, there is no light pseudo scalar meson which could be identified with the corresponding Goldstone boson. The η' meson has the correct quantum numbers, but it is simply too heavy. This is the so called $U(1)$ problem of QCD: The $U_A(1)$ symmetry of the QCD Lagrangian seems to be broken by quantum fluctuations, but apparently there is no remnant of this symmetry breaking visible in the particle spectrum.

This problem is nearly as old as QCD itself. After Glashow [126] had noted in 1968 the cogency of a pseudo scalar meson with a mass of the order of the pion mass, it was shown by Weinberg [128], using conventional soft pion methods, that this mass should indeed be smaller than $\sqrt{3} \times m_\pi$.

Since then a natural solution to the $U(1)$ problem has been achieved³³ by the study of the connection between the axial anomaly, topological excitations of the vacuum and instantons [11, 129].

The physical picture which emerges from this work is (roughly) as follows. The conservation of the $U_A(1)$ symmetry current A_μ^0 , eq. (69), is formally violated by the presence of the axial anomaly $2n_f \frac{\alpha_s}{4\pi} \text{tr} G_{\mu\nu} \tilde{G}^{\mu\nu}$, c.f. eq. (82). One might wonder however, how such a

³³For reviews on the $U(1)$ problem see [130–132].

contribution can make a physical effect at all, if one assumes *random* quantum fluctuations of the gauge fields. In this case, a possible contribution from the axial anomaly should just average away.

A possible solution to this problem came from G.'t Hooft [11], who showed that non-trivial topological excitations of the vacuum, instantons, can produce a non vanishing contribution to physical observables.

In this scenario, the $U_A(1)$ symmetry breaking would not be spontaneous and thus one would not expect to find a corresponding pseudo scalar Goldstone boson³⁴. Remnants of this new kind of symmetry breaking would however still be observable in nature. For example the η' meson would acquire it's large mass from instanton contributions. If it were possible to switch off the topological vacuum excitations, the η' meson should become light and would behave like an 'ordinary' Goldstone particle.

Indeed, such a behavior has been obtained in the framework of a $1/N_c$ expansion, N_c being the number of colors, by Witten [12] and Veneziano [13]. They showed that in the limit $N_c \rightarrow \infty$, where the axial anomaly is absent, the masses of η' and π become degenerate. In first order $1/N_c$ this degeneracy is lifted and, in an $SU(3)$ flavor symmetric world, one obtains

$$m_{\eta'}^2 - m_{\pi}^2 = m_0^2 = \frac{2n_f\chi}{f_{\pi}^2}. \quad (119)$$

Here n_f denotes the number of flavors and χ is the topological susceptibility defined in eq. (88), at $k^2 = 0$. Taking into account an explicit $SU(3)$ flavor symmetry breaking and neglecting the effects of a (small) $\eta - \eta'$ mixing, one would expect

$$m_0^2 \simeq m_{\eta'}^2 - (4m_K^2 + 3m_{\pi}^2 + m_{\eta'}^2)/8 \simeq (867\text{MeV})^2, \quad \chi \simeq (182\text{MeV})^4. \quad (120)$$

In summary, there is a lot of (theoretical) evidence, that the topological properties of the QCD vacuum are indeed likely to solve the $U(1)$ problem. The question remains however, whether this qualitative evidence holds also quantitatively. To answer this question one would first have to show that the large η' mass, $m_{\eta'} = 958\text{MeV}$, is really a property of QCD. Secondly, one would like to see that the topological excitations in full QCD are such that they yield an additional contribution to $m_{\eta'}$ of size $m_0 \simeq 867\text{MeV}$. Last not least one would have to study the instanton content of QCD in detail to learn about the mechanism of how the η' acquires it's mass.

Being a non-perturbative method, lattice gauge theory is perfectly suited to study quark-antiquark bound states like octet and singlet mesons. It has been argued in ref's.

³⁴It has been argued frequently, see e.g. ref. [133], that, even in the presence of the axial anomaly, it is still possible to define a conserved flavor singlet axial vector current. Thus, the $U(1)$ symmetry would be broken spontaneously and there should still exist a corresponding Goldstone boson. Since this conserved current is not gauge invariant, the Goldstone boson could be realized as a Kogut-Susskind ghost [134] in the unphysical, gauge variant sector of QCD. The physical interpretation of such an unphysical construction however is by far not clear and requires at least additional assumptions about the nature of the vacuum [132].

[131, 132] that the contributions of topological vacuum excitations could be overlooked by standard perturbative expansions. Clearly, with lattice QCD this flaw is absent. Within the course of a Monte Carlo process, QCD vacuum configurations are explicitly generated³⁵. Thus, one has direct access to topological properties of each single configuration. This enables, in principle, for a detailed study of the connection between instantons, topological excitations and the η' mass.

4.2 Lattice Technique

The mass of a (full) QCD bound state can be extracted from the asymptotic behavior of the momentum zero projection of it's propagator.

Let us consider, for example, a one flavor pseudo scalar meson with an interpolating operator $P = \bar{q}\gamma_5 q$. The time dependence of it's (momentum zero) propagator is given by³⁶

$$G_P(0, t) = \sum_{\vec{x}} \langle P^\dagger(\vec{0}, 0) P(t, \vec{x}) \rangle = \sum_n |\langle 0 | P^\dagger | n \rangle|^2 e^{-m_n t} \xrightarrow{t \rightarrow \infty} |\langle 0 | P^\dagger | n_0 \rangle|^2 e^{-m_{n_0} t}, \quad (121)$$

where n_0 is the lowest eigenstate of the QCD Hamiltonian with quantum numbers $J^{PC} = 0^{-+}$.

Alternatively one can express $G_P(0, t)$ in terms of quark operators

$$G_P(0, t) = \sum_{\vec{x}} \langle (q\gamma_5\bar{q})(\vec{0}, 0) (\bar{q}\gamma_5 q)(\vec{x}, t) \rangle, \quad (122)$$

or, performing all possible contractions of quark operators, in terms of quark propagators Δ_q , defined in eq.(42)

$$G_P(0, t) = \sum_{\vec{x}} \left\{ \langle Tr(\Delta_q \Delta_q^\dagger)(0, t) \rangle - \langle Tr(\Delta_q \gamma_5)(0, 0) Tr(\Delta_q \gamma_5)(t, t) \rangle \right\} \equiv C_P(0, t) - D_P(0, t). \quad (123)$$

Thus, a one flavor meson propagator has always two contributions: The first term on the r.h.s. of eq.(123), C_P , is called 'connected', since the meson states at time 0 and time t are explicitly connected by quark lines. Correspondingly, the second term, D_P , is called 'disconnected'. Note that this term violates the OZI rule. It is highly sensitive to the details of the vacuum structure since the correlation between the quark loops $Tr(\Delta_q \gamma_5)$ at time 0 and t is mediated by quantum effects (multiple gluons and internal quark loops). Both contributions are schematically depicted in fig.2.

³⁵One has to ensure of course that the Monte Carlo algorithm tunnels sufficiently often between different topological sectors [115]

³⁶This is true for an infinitely extended lattice in time. For a finite lattice with time extend T and (anti)periodic boundary conditions the asymptotic form is given by $\lim_{t \rightarrow \infty} G(0, t) = |\langle 0 | P^\dagger | n_0 \rangle|^2 [e^{-m_{n_0} t} + e^{-m_{n_0}(T-t)}]$. For the sake of clarity we will however restrict the discussion to infinitely extended lattices.

The physical light mesons are not made of one quark flavor. They are rather 2-flavor triplet (pions), 3-flavor octet (Kaons, η) or 3-flavor singlet (η') combinations of quarks. Just from combinatorics one expects the disconnected contributions to cancel each other largely for the non singlet combinations³⁷, and to contribute additively to the singlet state.

From this point of view, one can identify the connected contribution with the normal ‘Goldstone part’ of the pseudo scalar mesons and the disconnected contribution with the anomalous ‘topological part’.

We could now proceed and calculate G_P according to eq.(123) on a representative sample of gauge configurations. Then one would extract $m_{\eta'}$ from a fit to its asymptotic form, eq.(121). However this might not be advantageous for several reasons. First, one would like to concentrate on the (anomalous) mass contribution from the disconnected part. Secondly, one should try to keep statistical errors, which arise mostly from the large fluctuations of the disconnected part, as small as possible. For both these reasons one favors to consider the ratio

$$R_{DC}(t) = \frac{n_f D_P(0, t)}{C_P(0, t)}, \quad (124)$$

rather than to G_P itself. The factor n_f (number of flavors) has been inserted in the numerator because a n_f -flavor singlet meson has n_f contributions C_P , but n_f^2 contributions D_P .

In full QCD, the asymptotic time dependence of G_P and C_P is given by eq.(121). Thus, it follows

$$R_{DC}(t) = 1 - C e^{(m_{\eta'} - m_8)t} \quad (125)$$

at large t . Here we have identified mass of the full singlet propagator (G_P) with $m_{\eta'}$ and the mass of the ‘Goldstone part’ (C_P) with m_8 . Note that R_{DC} is sensitive to the difference of these masses. The ‘Goldstone mass’ m_8 vanishes in the chiral limit. Therefore, one can extract m_0 , see eq. (119), from an extrapolation to this point.

The situation is slightly more complicated in quenched QCD. In this case eq.(121) does not describe the asymptotic time dependence of G_P correctly since higher quark loop contributions to the singlet propagator are not taken into account. In the $1/N_c$ expansion of Witten and Veneziano [12,13], which in first order leads to eq.(119), the η' propagator in momentum space, \tilde{G}_P , is described by an infinite sum over virtual quark loops, connected by an effective gluonic coupling m_0^2

$$\tilde{G}_P(p^2) \sim \frac{1}{p^2 + m_8^2} - \frac{m_0^2}{(p^2 + m_8^2)^2} + \frac{m_0^4}{(p^2 + m_8^2)^3} - \dots = \frac{1}{p^2 + m_8^2 + m_0^2}. \quad (126)$$

This is shown in fig.16. The quenched approximation neglects virtual quark loops, which corresponds to a truncation of the geometric series in eq.(126) after the second term. Obviously, the first term can be identified with the connected contribution to the truncated

³⁷Up to a presumably negligible flavor symmetry breaking, they cancel exactly.

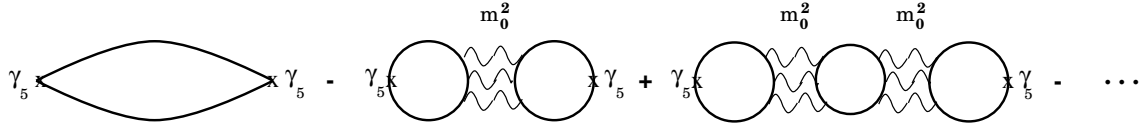


Figure 16: Contributions to the flavor singlet propagator in the scheme of Witten and Veneziano.

propagator, whereas the second term belongs to its disconnected part. A Fourier transform of both terms yields³⁸

$$(R_{DC}(t))^{quen} = A + \frac{m_0^2}{2m_8} t, \quad A = \frac{m_0^2}{2m_8^2}. \quad (127)$$

Thus, under the assumption that the Witten-Veneziano expansion is valid, one can determine $m_{\eta'}$ even in the quenched approximation from a linear fit to $(R_{DC}(t))^{quen}$. It is however by no means obvious, that quenched and full QCD calculations should yield the same value for $m_{\eta'}$. Full QCD simulations with reliable statistics are therefore urgently needed.

A peculiar situation arises in the partially quenched approximation, i.e. in the case where not all valence quarks have their counterparts in the quark sea. Such a setting can be useful if one wants to exploit gauge configurations with light sea quarks with respect to the strange quark sector of QCD or if one works with $n_f = 2$ dynamical fermions in the Kogut-Susskind discretization. The form of the corresponding η' propagator, i.e. the analogon to eq.(126), has been worked out by Bernard and Golterman in the framework of the partially quenched chiral perturbation theory [135].

The numerical techniques which are used to calculate the connected and disconnected contributions to the η' propagator, eq. (123), are quite similar to those already explained in the previous sections. The connected part can be composed from solutions to eq.(46), and for the disconnected contribution one can use the estimator techniques discussed in sections 2.2 and 3.2. We emphasize again that the computationally expensive and statistically noisy part of this calculation is the disconnected one. In order to gain statistics one exploits the translational invariance of the propagator, $G(0, t) = G(t_0, t_0 + t)$, and performs the average over all timeslices N_t , $D_P(0, t) = 1/N_t \sum_{t_0} D_P(t_0, t_0 + t)$.

We mentioned at the beginning of this section that the calculation of $m_{\eta'}$ and the proof that it does not vanish in the chiral limit are not sufficient to prove that the 't Hooft scenario of the $U(1)$ problem is realized in QCD. One rather has to demonstrate that non-trivial topological excitations of the vacuum really exist in QCD, and that those excitations are responsible for the large mass of the η' meson.

³⁸Using the Witten-Veneziano expansion one can also estimate the amplitude C in eq.(125). One finds $C = m_8/m_{\eta'}$.

One method to study the connection between topology and $m_{\eta'}$ is to determine the topological charge Q , see eq.(83), in addition to $m_{\eta'}$ and m_0 , on a given set of gauge configurations³⁹. With this information in hands one can analyze the dependence of $m_{\eta'}$ (or equivalently of m_0) on Q . A finding $m_{\eta'} = m_8$, ($m_0 = 0$), at $Q = 0$ and $m_{\eta'} \neq m_8$, ($m_0 \neq 0$), at $Q \neq 0$ would favor strongly the ‘topological solution’ of the $U(1)$ problem.

Additional information on this connection can be extracted from the lowest eigenmodes of the Dirac operator. The Atiyah-Singer index theorem [136]

$$Q = n^+ - n^- \quad (128)$$

states that the topological charge Q in the continuum is given by the difference between the number of positive (n^+) and negative (n^-) chirality eigenmodes Ψ^\pm of the Dirac operator with zero eigenvalue

$$\not{D}\Psi^\pm = \gamma^\mu(\partial_\mu - ig\frac{\lambda_a}{2}A_\mu^a)\Psi^\pm = i\lambda\Psi^\pm \quad , \quad \lambda = 0 \quad (129)$$

$$\gamma_5\Psi^+ = +\Psi^+ \quad , \quad \gamma_5\Psi^- = -\Psi^- \quad . \quad (130)$$

Thus , if m_0 is determined by topology, one would expect that the related correlator, i.e. the disconnected part of eq.(123), could be calculated using only the zero modes of the Dirac operator, whereas the latter should be insufficient for a complete determination of the connected part.

Unfortunately, the Atiyah-Singer theorem does not hold (exactly) in a discrete formulation (Wilson or Kogut-Susskind) of QCD on a finite lattice. This is due to the fact that the fundamental property $\gamma_5\not{D} = -\not{D}\gamma_5$ of the (anti hermitian) Dirac operator, is not fulfilled in the discretized case. It follows that, in principle, all eigenmodes of the lattice Dirac operator can contribute to the topological charge.

It has been shown however, by Smit and Vink [112] and Itoh, Iwasaki and Yoshié [137], that the Atiyah-Singer theorem holds still approximately on the lattice. Instead of taking into account only the zero eigenmodes one now needs the ‘lowest’ eigenmodes to make up for the topological charge. Since it is not a priori known how many of these ‘lowest’ eigenmodes are really needed, one has to study the influence of the number of lowest eigenmodes on the connected and disconnected contributions to the η' propagator numerically.

We mention that the determination of the spectrum of the Dirac operator on a (large) lattice represents a non-trivial numerical problem. Algorithms suited for this task are explained in ref’s. [138–141].

4.3 Lattice Results

The ‘topological’ scenario to explain the $U(1)$ puzzle has been proposed more than 20 years ago, but it is only in these days that the lattice method may become powerful

³⁹Lattice definitions and numerical methods to determine Q have been discussed in section 3.3

enough to prove that the proposed solution is actually realized in QCD. This is mostly due to the substantial computational effort which is necessary to calculate the disconnected contributions to the η' propagator with reliable statistics.

Nevertheless there is already a handful of pioneering simulations in quenched QCD and, to an even lesser extend, in full QCD, which find promising evidence that the 't Hooft mechanism explains the large mass of the η' meson.

After early exploratory studies [137, 142] from the time where estimator techniques for the disconnected part of the η' propagator were not yet available, the first quenched simulation with reliable statistics (200-300 gauge configurations) was performed by the authors of ref. [143], using Wilson fermions⁴⁰ on a $12^3 \times 20$ lattice and a somewhat large lattice spacing, $a \simeq 0.14\text{fm}$ ($a^{-1} = 1.45(3)\text{GeV}$, $\beta = 5.7$). They employed the volume source technique, see eq's. (53),(54), to calculate the disconnected contribution.

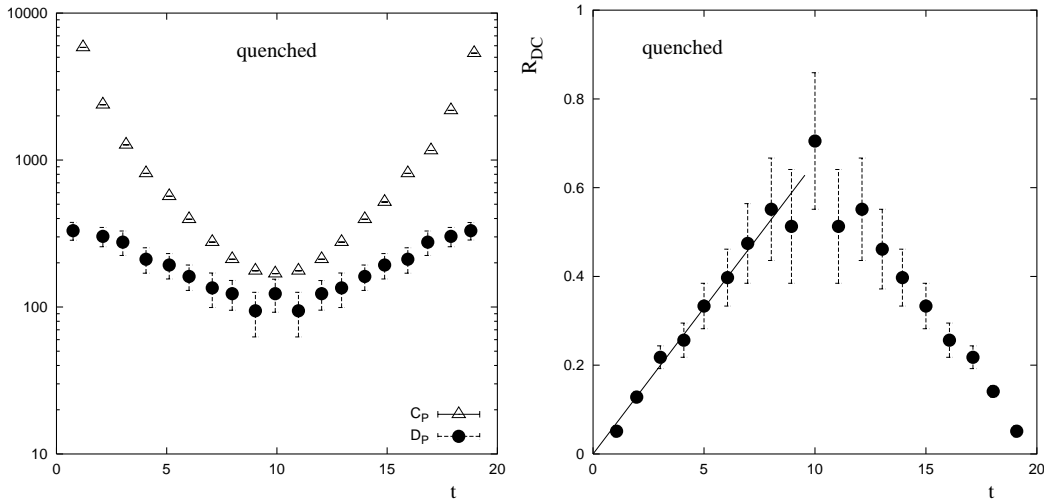


Figure 17: *Left: Connected (C_P) and disconnected (D_P) contributions to the η' propagator at a quark mass corresponding to $m_\pi/m_\rho = 0.59$. Right: The ratio R_{DC} at the same quark mass. The solid line indicates the result of a linear fit to R_{DC} in the range $4 \leq t \leq 8$. The data has been extracted from ref. [143].*

We illustrate the statistical quality of the corresponding signals in fig.17, where we display connected and disconnected contributions to the η' propagator as well as the ratio R_{DC} . The disconnected part is much more noisy than the connected one, as expected. The ratio R_{DC} is reasonably consistent with the predicted linear behavior in the quenched approximation, see eq. (127). From this data, one can extract m_0 at a given quark mass.

⁴⁰They chose quark masses corresponding to $m_\pi/m_\rho = 0.74, 0.70, 0.59, 0.42$. Unfortunately, the results for the lightest quark mass were achieved with only 40 gauge configurations.

To mimic the physical situation of $n_f = 3$ quarks, one multiplies m_0 by $\sqrt{3}$. Clearly, such a procedure is justified only in a flavor symmetric situation.

The physical value for m_0 in this flavor symmetric world, i.e. its value at the light quark mass⁴¹ can be read off from the result of a fit to $m_0(m_q)$.

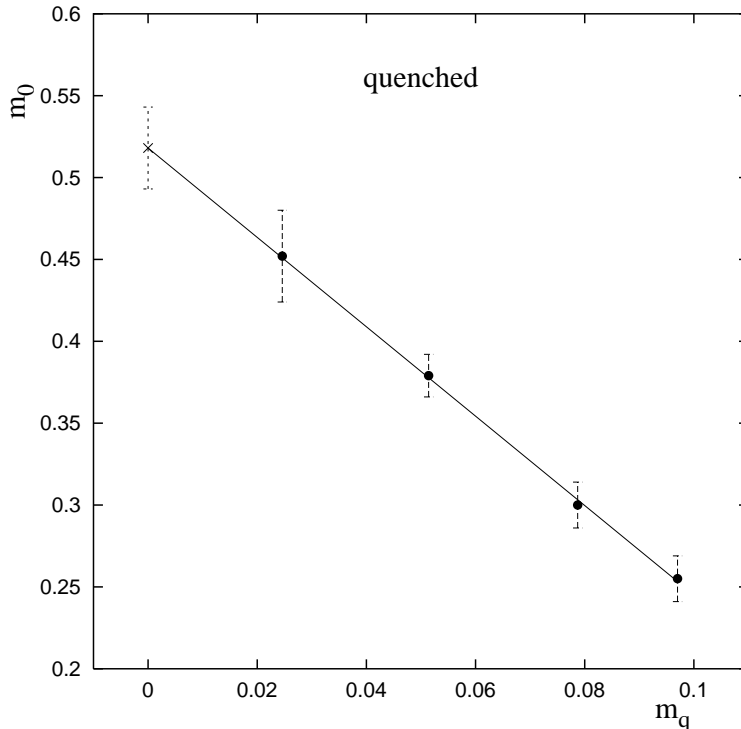


Figure 18: Ref. [143]: Dependence of m_0 on the bare quark mass m_q . The solid line shows a linear fit to $m_0(m_q)$. The cross indicates the result of the fit at the chiral point. Its value in lattice units is $m_0 = 0.518(25)$, which corresponds to $m_0 = 751(39)\text{MeV}$. Note that all m_0 data have been multiplied by $\sqrt{n_f} = \sqrt{3}$.

As shown in fig. 18, the authors of ref. [143] find a linear increase of $m_0(m_q)$ with decreasing m_q . Note that this is in contrast to the behavior of non-singlet pseudo scalar masses, where one obtains a linear decrease of $m_P^2(m_q)$. At the chiral point, ($m_q = 0$), they get $m_0 = 751(39)\text{MeV}$, where the number in brackets denotes the statistical error.

One should, for various reasons, not be worried too much about the mismatch ($2 - 3\sigma$) of this result with the physical estimate, see eq.(120). As we mentioned above, the

⁴¹The light quark mass m_l (in lattice units) can be determined by the condition $m_\pi/m_\rho = 0.1766$. Alternatively one can extrapolate to the chiral point $m_l = 0$. The difference between these methods with respect to m_0 is negligible.

disconnected part has been obtained with the volume source technique, which does not allow to monitor the cancellation of the unwanted gauge variant parts. Furthermore, the simulation has been performed at a coarse lattice spacing, but the influence of finite cutoff effects has not been taken into account. Moreover, one has assumed flavor symmetry with respect to m_0 , which might not be realized in nature. Last not least, the result has been achieved in the quenched approximation. Since vacuum contributions are essential in the determination of m_0 , this could introduce a systematic bias. For all these reasons one should expect that the true error on m_0 is actually much larger.

The good news from the findings of ref. [143] is of course that m_0 is in the right range. Thus, there is a good chance that, once all the uncertainties listed above have been removed, one will indeed obtain the experimental η' mass in full QCD lattice calculations.

Given that, one can proceed to study the connection between vacuum topology and m_0 . The authors of ref. [144] have calculated the topological charge Q according to the standard definition⁴², see eq.(105), on the same set of gauge configurations as used in ref. [143], at a quark mass corresponding to $m_\pi/m_\rho = 0.59$. Thus one can analyze the dependence of m_0 on Q for this setup. We display the result of ref. [144] in fig.19. It appears that m_0 correlates to the value of Q : m_0 increases as Q increases. This indicates that the proposed solution of the $U(1)$ problem is realized in QCD. Unfortunately, the authors of ref. [144] have used an ‘integerized’ value of Q instead of a renormalized one, i.e. they set the lattice value of Q to the nearest integer instead of applying the renormalization procedure described in section 3.3. However, it is unlikely that this inaccuracy alters the conclusions of their work.

In order to consolidate this result one needs to perform lattice simulations which avoid the insufficiencies discussed above. As this is, after all, a question of compute power and of the capacity of stochastic algorithms, this goal can be achieved only in small steps.

Recently, Venkataraman and Kilcup [146] analyzed full QCD gauge configurations with 2 flavors of Kogut-Susskind fermions with respect to the η' mass. The configurations have been generated by the QCDSF collaboration [147, 148] on $16^3 \times 32$ lattices, at 3 different values of the sea quark mass, corresponding to $m_\pi/m_\rho = 0.704, 0.644$, and 0.572 , and at a lattice cutoff $a^{-1} \simeq 2\text{GeV}$. The disconnected part of the η' propagator has been calculated using a stochastic estimator method, and ‘Wuppertal smearing’ [149] has been employed to improve the ground state projection of the operators. In addition, the authors of ref. [146] have performed a quenched simulation at equal lattice spacing and volume. This allows for a direct comparison of quenched and unquenched results. Thus, this analysis has installed quite a number of improvements to alleviate the deficiencies of ref’s. [143, 144]. Unfortunately, the size of the samples of gauge configurations used here is rather limited (34-79 configurations for full QCD and 83 configurations for quenched QCD).

In fig.20 we display the ratio R_{DC} both for the quenched and full QCD simulations. Obviously the expected t dependence of R_{DC} , c.f. eq’s. (125) and (127), is reasonably well satisfied by the data.

⁴²The definition is applied to ‘cooled’ configurations. The cooling method is explained in ref. [145].

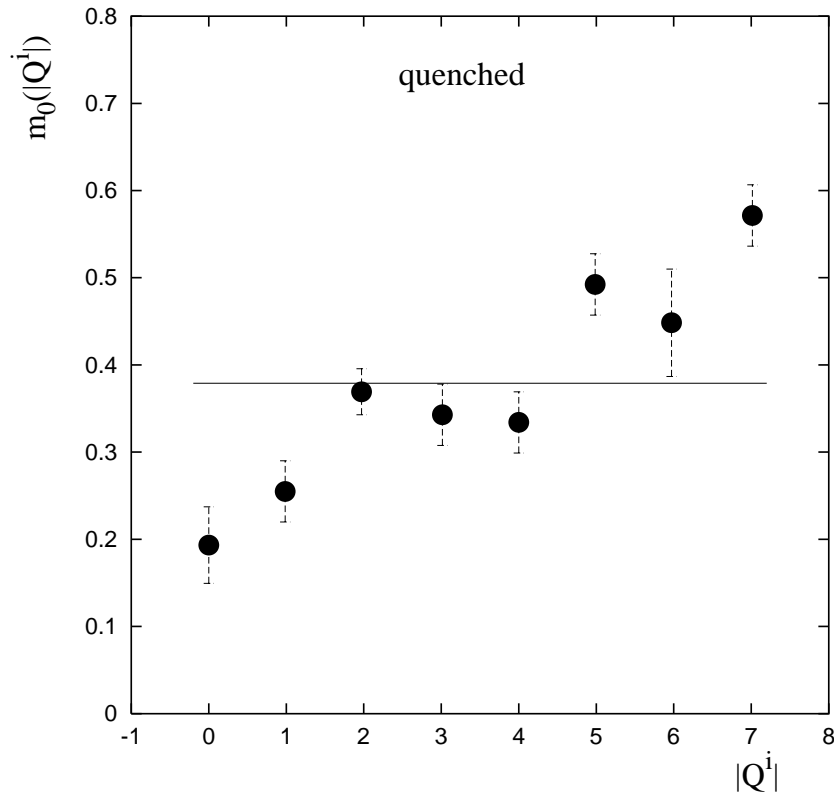


Figure 19: m_0 in lattice units as a function of the ‘integerized’ topological charge Q^i , at a quark mass corresponding to $m_\pi/m_\rho = 0.59$. The solid line indicates the result for the entire ensemble of gauge configurations. The data has been extracted from ref. [144].

An extrapolation⁴³ of the fit results at the various quark mass values to the chiral limit yields $m_{\eta'} = 780(187)\text{MeV}$ for $n_f = 2$ full QCD, and $m_{\eta'} = 891(101)\text{MeV}$ in the quenched approximation. As in ref. [143], these values are obtained by correcting for the case of 3 quark flavors. Within large statistical errors both results, quenched and unquenched, are consistent with experiment. This is similar to the situation found in lattice calculations of the axial flavor singlet coupling G_A^1 . It might indicate, within the given level of accuracy, that the vacuum contribution to $m_{\eta'}$ is determined largely by gluonic properties, rather

⁴³The authors of ref. [146] assume a linear functional behavior of $m_0^2(m_q)$, in contrast to the finding of ref. [143], where m_0 (not m_0^2) increases linearly with with decreasing m_q . Unfortunately, the systematic uncertainty arising from this difference has not been taken into account.

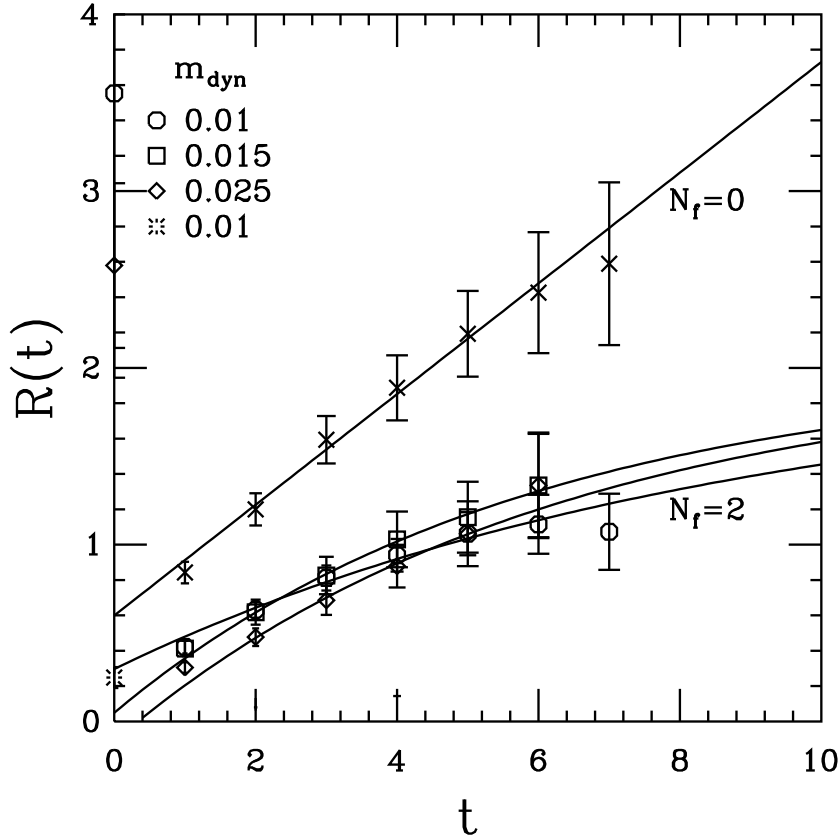


Figure 20: The ratio R_{DC} for quenched ($N_f = 0$) and full ($N_f = 2$) QCD, as found by ref. [146]. The solid lines correspond to fits according to eq. (125) and eq. (127).

than by fermion loops.

We mention that this interpretation is supported by the findings of lattice calculations using the ‘bermion’ approach to QCD [150]. In this method one simulates QCD at negative numbers of flavor, $n_f \leq 0$, where fermions are replaced by ‘bermions’, i.e. bosons with a fermion action, and then extrapolates the results to $n_f > 0$. The authors of ref. [151] have applied this approach to the calculation of m_0 . As a result they find no significant dependence of m_0 on n_f in the range $-8 \leq n_f \leq 0$.

Finally, we comment on the numerical evidence for the connection between topological vacuum excitations and the η' mass from a calculation of the low lying eigenmodes of the Dirac operator. According to the approximate validity of the Atiyah-Singer theorem on the lattice, the lowest eigenmodes reflect the topological properties of the vacuum. Thus, if the disconnected part of the η' propagator is dominated by the latter, it should be possible to compose it exclusively from these contributions. The connected part, which represents the

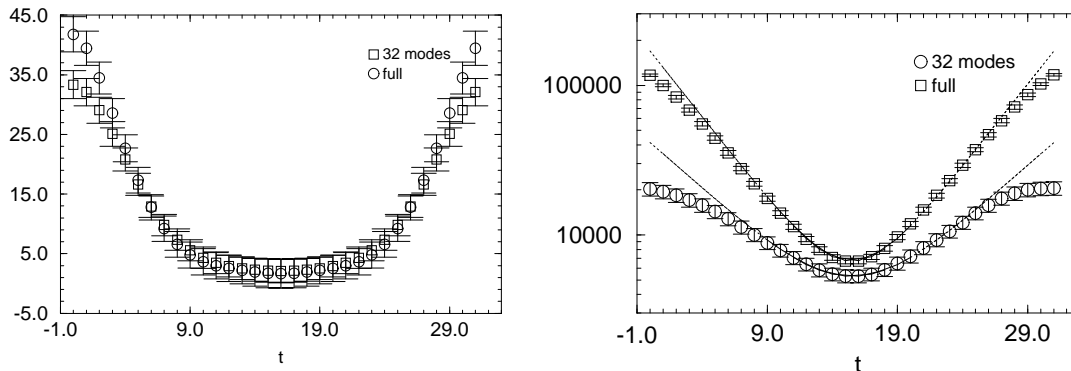


Figure 21: *Disconnected (left) and connected (right) contributions to the η' propagator as found by ref. [146] in a full QCD ($n_f = 2$) simulation with Kogut-Susskind fermions at a (lattice) quark mass $m_q a = 0.01$. The latter corresponds to $m_\pi/m_\rho = 0.572$.*

‘normal’ Goldstone mode, should however not be obtainable from the lowest eigenmodes alone.

The authors of ref. [146] have compared the connected and disconnected parts obtained from a full calculation with those constructed from the lowest 32 eigenmodes. We display their result in fig.21. Obviously the (full) disconnected contribution is well represented by the eigenmodes, in contrast to the connected part.

4.4 Outlook

The final goal to confirm quantitatively that the ‘topological’ solution to the $U(1)$ problem is realized in QCD has not been reached yet. There is however a lot of evidence that this solution is most likely. All results achieved so far with lattice methods point in this direction.

From quenched and unquenched lattice simulations it appears, within the given level of uncertainty, that the mass of the η' meson calculated in QCD is comparable to its experimental value. The fact that both methods yield similar results may indicate that the topological contributions are dominated by the gluonic properties of QCD.

On top of this, the connection to topological vacuum excitations has been established in quenched QCD by studying the dependence of m_0 on the topological charge Q , and in full QCD by a comparison between the η' propagator calculated with all eigenmodes and the one composed from only the low lying states.

To consolidate these findings one has to perform lattice calculations at high statistics and by application of (possibly improved) stochastic estimator techniques. This, as a first step, would enable for a reliable estimate of the statistical error. The next step is then

to vary lattice spacing and volume in order to perform a continuum extrapolation of the lattice results. If this is done within the framework of a ‘conventional’ full QCD simulation with 2 flavors and degenerate quark masses one could extract the QCD result for the η' mass under the assumption of flavor symmetry with respect to m_0 and by neglecting $\eta - \eta'$ mixing effects.

In view of the fact that the results discussed above have been achieved on computers with a speed of less or about 10Gflops this aim is certainly within the range of upcoming TERAflops machines. To include the effects of flavor symmetry breaking and to calculate reliably the influence of $\eta - \eta'$ mixing effects one would have to repeat the whole procedure with $n_f \geq 3$ dynamical quark flavors and non-degenerate masses. Without significantly improved stochastic algorithms, such a program is currently beyond reach. It should however be feasible to perform such a calculation with $n_f = 2$ light and $n_f = 2$ heavy flavors at a fixed lattice spacing. This would help to estimate the size of these effects.

Clearly, high statistics samples of QCD vacuum configurations will allow for a more detailed study of the connection between topology and $m_{\eta'}$. Especially the role of instantons⁴⁴, which we did not discuss here in detail, could be clarified.

⁴⁴For a recent review on instantons on the lattice see [152].

5 Final Remarks

We said in the introduction that a major goal in studying flavor singlet phenomena is to learn about the properties of the QCD vacuum. So, what can we learn from the results of lattice QCD achieved so far in this context? The answer to this question embraces several aspects.

First of all, we have seen that disconnected (vacuum) amplitudes indeed yield substantial contributions to flavor singlet processes. It turns out that they are suited in sign and order of magnitude to explain ‘anomalous’ phenomena like the small value of G_A^1 , the large mass of the η' meson and the high value, compared to the octet estimate σ_0 , of $\sigma_{\pi N}$.

Secondly, the connection between topological excitations of the vacuum and the η' mass could be established. This is evidence, that the $U(1)$ problem can be solved by the ‘t Hooft mechanism. Similarly, one finds that the influence of the axial anomaly, which is (mostly) reflected in the size of the disconnected axial vector insertion of the proton, lowers the value of G_A^1 .

Thirdly, comparing quenched and full QCD lattice results, one can estimate the effect of sea quarks on flavor singlet amplitudes. They seem to have some influence on the scalar insertions, e.g. on $\sigma_{\pi N}$ and y , as they lower the ratio of disconnected to connected amplitudes. Axial vector and pseudo scalar insertions, which are connected to the axial anomaly, do not seem to depend largely on the presence of sea quarks.

Fourthly, flavor symmetry breaking effects in the disconnected (vacuum) contributions appear to be small. This would explain the success of lattice determinations of flavor non-singlet quantities like G_A^3 .

Unfortunately most of the findings mentioned here are still semi-quantitative results. At the current level of statistical and systematical reliability, the estimates of flavor singlet quantities from lattice calculations cannot be used yet for a precise quantitative comparison between experiment and theoretical QCD predictions.

Clearly, one would like to have an idea of what it would take to reduce the uncertainties of the lattice results to the level of about 20%, which corresponds the accuracy currently achieved in experimental measurements of G_A^1 and $\sigma_{\pi N}$.

The various sources of uncertainty have been discussed in some detail in this review. It can be seen from this discussion that the error is dominated by the large statistical fluctuations of the disconnected amplitudes. These amount to 50 to 60%. To reduce the fluctuations to the experimental level of 20% just by ‘brute force’ one would need a factor of 9 in computer speed.

The second largest error is due to cutoff effects and, closely connected to this, uncertainties in the determination of renormalization constants. From the lattice results of G_A^3 one estimates a 20 to 30% contribution to the error. Thus, a rough finite cutoff analysis would be sufficient. Current lattice calculations of flavor singlet quantities have been performed at a cutoff of $a^{-1} \simeq 2\text{GeV}$. An increase of a^{-1} by a factor of 1.5 ($a^{-1} \simeq 2\text{GeV}$) would require an increase of the number of lattice points by a factor of $1.5^4 \simeq 5$. On top of this one has to take into account that it becomes more expensive to generate statistically

independent gauge configurations when going closer to the continuum limit. For full QCD simulations, where the generation of gauge configurations consumes the largest fraction of computer time, the dependence of the auto correlation length on the cutoff is not well known. An additional factor of 2 in computer time should be sufficient however for a moderate increase of a^{-1} .

Thus, one estimates that, without any further algorithmic improvement, a factor of $9 \times 5 \times 2 = 90$ in computer power would be sufficient to reduce the uncertainties on flavor singlet calculations to the 20% level.

According to the fact that the currently most advanced lattice calculations in this field, i.e. full QCD with $n_f = 2$ dynamical Wilson fermions, have been performed on (APE) computers with a sustained speed of 10 GigaFlops, one would need machines with a 1 TeraFlops performance to achieve this goal.

Since computers with a speed of a few hundred Gigaflops are already available [148,153], we would like to close this review with the optimistic view that a 20% uncertainty in full QCD flavor singlet calculations can be realized within the next 5 years. Quenched simulations with that accuracy could be done right now.

Acknowledgments I would like to thank Klaus Schilling, Apoorva Patel, Thomas Lipert, and Peer Ueberholz for many instructive and enlightening discussions on the subject of flavor singlet processes. I am also indebted to the Fachbereich Physik of the University of Wuppertal which made it possible to complete this review.

References

- [1] Y. Nambu, Phys. Rev. D10 (1974)4262; G. t'Hooft, Acta Phys. Austr. XXII (1980)531; G. t'Hooft, Nucl. Phys. B190 (1981)455.
- [2] Y. Nambu, Phys. Rev. Lett. 4 (1960)380; Y. Nambu, G. Jona-Lasinio, Phys. Rev. 122 (1961)345; Y. Nambu, G. Jona-Lasinio, Phys. Rev. 124 (1961)246.
- [3] J. Goldstone, Nuovo Cimento 19 (1961)154; J. Goldstone, A. Salam, and S. Weinberg, Phys. Rev. 127 (1962)965.
- [4] P.W. Higgs, Phys. Lett. 12 (1964)131, Phys. Rev. Lett. 13 (1964)508, and Phys. Rev. 145 (1966)1156.
- [5] F. Englert, R. Brout, Phys. Rev. Lett. 13 (1964)321.
- [6] G.S. Guralnik, C.R. Hagen, and T.W.B. Kibble, Phys. Rev. Lett. 13 (1964)585; T.W.B. Kibble, Phys. Rev. 155 (1967)1554.
- [7] J. Bernstein, Rev. Mod. Phys. 46 (1974)7.
- [8] S.L. Adler, W.A. Bardeen, Phys. Rev. 182 (1969)1517; J.S. Bell, R. Jackiw, Nuovo Cimento 51 (1969)47.
- [9] S.L. Adler, Phys. Rev 177 (1969)2426.
- [10] D. Gross, R. Jackiw, Phys. Rev. D6 (1972)477; H. Georgi, S.L. Glashow, Phys. Rev. D6 (1972)429; C. Bouchiat, J. Iliopoulos, and P. Meyer, Phys. Lett. 38B(1972)519.
- [11] G. t'Hooft, Phys. Rev. D14 (1976)3432.
- [12] E. Witten, Nucl. Phys. B156 (1979)269.
- [13] G. Veneziano, Nucl. Phys. B159 (1979)213.
- [14] G. Veneziano, Mod. Phys. Lett. A4 (1989)1605.
- [15] G.M. Shore, G. Veneziano, Phys. Lett.B244 (1990)75; Nucl. Phys. B381 (1992)23.
- [16] S. Narison, G.M. Shore, G. Veneziano, Nucl. Phys. B433 (1995)209.
- [17] U. Wiedner et al., Phys. Rev. D40 (1989)3568; P.Y. Bertin et al., Nucl. Phys. B106 (1976)341; E.G. Auld et al., Can. J. Phys. 57 (1979)73; J.T. Bragg et al., Phys. Rev. C34 (1986)1771; C38 (1988)2427; C41 (1990)2202; J.S. Frank et al., Phys. Rev. D28 (1983)1569; B.G. Ritchie et al., Phys. Lett. B125 (1983)128.
- [18] J. Gasser, H. Leutwyler, M.E. Sainio Phys. Lett. B253(1991)252; Phys. Lett. B253 (1991)260.
- [19] EMC,J. Ashman et al., Nucl. Phys. B328 (1989)1, Phys. Lett. B206 (1988)364.
- [20] SMC, B. Adeva et al., Phys. Lett. B302 (1993)533; D. Adams et al., Phys. Lett. B329 (1994)399; D. Adams et al., Phys. Lett. B339 (1994)332(E); D. Adams et al., Phys. Lett. B357 (1995)248; B. Adeva et al., Phys. Lett. B369 (1996)93.
- [21] SLAC-E142 Collab., P.L. Antony et al., Phys. Rev. Lett. 71 (1993)959;

- [22] SLAC-E143 Collab., K. Abe et al., Phys. Rev. Lett. 75 (1995)25; Phys. Rev. Lett. 74 (1995)346; Phys. Rev. Lett. 76 (1996)587.
- [23] SMC, D. Adams et al., Phys. Rev. D56, (1997)5330.
- [24] SLAC-E154 Collab., K. Abe et al., Phys. Lett. B405, (1997)180.
- [25] J. Ellis, R.L. Jaffe, Phys. Rev. D9. (1974)1444; Phys. Rev. D10 (1974)1669.
- [26] S. Aoki, M. Doui, and T. Hatsuda, Austr. J. Phys. 50 (1997)205.
- [27] For an introduction see for example
M. Creutz, Quarks, gluons and lattices, Cambridge University Press, 1983;
P. Hasenfratz, Lattice Quantum Chromodynamics, in Schladming 1983, Proceedings: Recent Developements in High Energy Physics, 283;
I. Montvay and G. Münster, Quantum Fields on a Lattice, Cambridge University Press, 1994;
M. Creutz, Quantum Fields on the Computer, World Scientific, 1992;
H.J. Rothe, Lattice Gauge Theories: An Introduction, World Scientific, 1992.
- [28] K. Wilson, "New Phenomena in Subnuclear Physics", Erice 1975, ed. A. Zichichi, New York 1977.
- [29] R.P. Feynman, A.R. Hibbs, Quantum Mechanics and Path Integrals, McGraw-Hill, New York 1965.
- [30] A. Chodos and J.B. Healy, Nucl. Phys. B127 (1977)426.
- [31] L.H. Karsten and J. Smit, Nucl. Phys. B183 (1981)103.
- [32] H.B. Nielsen and M. Ninomiya, Nucl. Phys. B185 (1981)20, erratum: B195 (1981)541; Nucl. Phys. B193 (1981)173; D. Friedan, Comm. Math. Phys. 85 (1982)481.
- [33] An nice introduction to functional methods has been given by
A.H. Zaidi, Fortschr. Phys. 31 (1983)403.
- [34] N. Metroprolis, A.W. Rosenbluth, M.N. Rosenbluth, A.H. Teller, and E. Teller, J. Chem. Phys. 21 (1953)1087; N. Cabibbo and E. Marinari, Phys. Lett. 199B (1982)387; K. Fabricius and O. Haan, Phys. Lett. B143 (1984)459; A. Kennedy and B. Pendleton, Phys. Lett. B156 (1985)393; M. Creutz, Phys. Rev. D36 (1987)51.
- [35] S. Duane, A.D. Kennedy, B.J. Pendleton, and D. Roweth, Phys. Lett. B 195 (1987)216; M. Lüscher, Nucl. Phys. B418 (1994) 637.
- [36] M. Creutz, Phys. Rev. D15 (1977)1128; M. Lüscher, Comm. Math. Phys. 54 (1977)283.
- [37] J. Kogut and L. Susskind, Phys. Rev. D11 (1975)395; T. Banks, J. Kogut, L Susskind, Phys. Rev. D13 (1976)1043; L. Susskind, Phys. Rev. D16 (1977)3031.
- [38] M. Lüscher et al., Nucl. Phys. B478 (1996)365; M. Lüscher and P. Weisz, Nucl. Phys. B479 (1996)429; M. Lüscher et al., Nucl. Phys. B491 (1997)323; K. Jansen and R. Sommer, Nucl. Phys. B (Proc. Suppl.)63 (1998)853

- [39] G.P. Lepage and P.B. Mackenzie, Phys. Rev. D48 (1993)2250; G.P. Lepage, proceedings of the 1996 Schladming School on *Perturbative and Nonperturbative Aspects of Quantum Field Theory*, hep-lat/9607076.
- [40] B. Sheikholeslami and R. Wohlert, Nucl. Phys. B259 (1985)572.
- [41] Y. Iwasaki, Nucl. Phys. B258 (1985)141; T. DeGrand et al., Nucl. Phys. B454 (1995)587; T. DeGrand et al., Nucl. Phys. B454 (1995)615; M. Lüscher and P. Weisz, Phys. Lett. 158B (1985)250.
- [42] T. Yoshié, Nucl. Phys. B (Proc. Suppl.)63A-C (1998)3.
- [43] J. Gasser and H. Leutwyler; Nucl. Phys. B250 (1985)465; H. Leutwyler, Nucl. Phys. B337 (1990)108.
- [44] J. Donoghue, B. Holstein, D. Wyler, Phys. Rev. Lett. 96 (1992)3444; E. Jenkins, A.V. Manohar, M.B. Wise, Phys. Rev. Lett 75 (1995)2272; C.W. Bernard and M.F.L. Golterman, Phys. Rev D49 (1994)486.
- [45] S.R. Sharpe, Phys. Rev. D41 (1990)3233; S.R. Sharpe, Phys. Rev. D46 (1992)3146; C. Bernard and M.F.L. Golterman, Phys. Rev. D46 (1992)853, J.N. Labrenz, S.R. Sharpe, Phys. Rev. D54 (1996)4595; R. Gupta Nucl. Phys. B (Proc.Suppl.) 42 (1995)85.
- [46] M. Gell-Mann, R.J. Oakes, and B. Renner, Phys. Rev. 175 (1968)2195.
- [47] S.L. Glashow, S. Weinberg, Phys. Rev. Lett. 20 (1968)224.
- [48] L.S. Brown, W.J. Pardee and R.D. Peccei, Phys. Rev. D4 (1971)2801.
- [49] G. Höhler, in: Landolt-Börnstein, Vol.9 b2, ed. H. Schopper (Springer, Berlin 1983).
- [50] B. Borasoy, U.G. Meißner, Phys. Lett. B365 (1996)285; V. Bernard, N. Kaiser, U.G. Meißner, Phys. Lett.B389 (1996) 144.
- [51] J. Gasser, Ann. Phys. (NY) 136 (1981)61.
- [52] J. Gasser and H. Leutwyler, Phys. Rep. 87(1982)77.
- [53] F. Fucito et al., Nucl. Phys. B210 (1982)407; B.L. Ioffe, Nucl. Phys. B188 (1981)317.
- [54] L. Maiani, G. Martinelli, M.L. Paciello, B. Taglienti, Nucl. Phys. B293 (1987)420.
- [55] L. Guisti, F. Rapuano, M. Talevi and A Vladikas, hep-lat/9807014.
- [56] H. Hellmann, Acta Physicochimica URSS I,6 (1935)913; IV,2 (1936)225; R.P. Feynman, Phys. Rev. 56 (1939)340; see also: C. Quigg, J.L. Rosner, Phys. Rep. 56 No.4 (1979)167.
- [57] R. Hestenes and E. Stiefel, J. Res. Nat. Bur. Standards 49 (1952)409; F.S. Beckmann, in "Mathematical Methods for Digital Computers", eds. A. Ralston, H.S. Wilf, New York 1960.
- [58] S.C. Eisenstat, H.C. Elman and M.H. Schultz, SIAM J. Number. Anal. Vol.20,2 (1983).

- [59] R. Freund, N. Nachtigal, Numer. Math. 60 (1991)315; H. van der Vorst, SIAM J. Sc. Stat. Comp. 13 (1992)631.
- [60] G. Martinelli, C.T. Sachrajda, Nucl. Phys. B316 (1989)355.
- [61] M. Fukugita et al., Phys. Rev. D51 (1995)5319.
- [62] K. Bitar et al., Nucl. Phys. B313 (1989)348.
- [63] S.J. Dong, K.F. Liu, Nucl. Phys. B(Proc. Suppl.)26 (1992)353.
- [64] S.J. Dong, K.F. Liu, Phys. Lett. B328 (1994)130;
- [65] S. Güsken, K. Schilling, R. Sommer, K.H. Mütter, A. Patel, Phys. Lett. B212 (1989)216.
- [66] M. Fukugita, Y. Kuramashi, M. Okawa and A. Ukawa, Phys. Rev. D51 (1995)5319.
- [67] S.J. Dong, J.F. Lagaë and K.F. Liu, Phys. Rev. D54 (1996)5496; S.J. Dong, K.F. Liu, Nucl. Phys. B (Proc. Suppl.)42 (1995)322.
- [68] CP-PACS Collaboration, S. Aoki et al., Nucl. Phys. B (Proc. Suppl.) 63A-C (1998)161.
- [69] J.F. Lagaë, K.F. Liu, Phys. Rev. D52 (1995)4042; Nucl. Phys. B (Proc. Suppl.)42 (1995)355.
- [70] SESAM Collaboration, N. Eicker et al., hep-lat 9896027, Phys. Rev. D.59, 014509 (1999).
- [71] B. Altmeyer, M. Göckeler, R. Horsley, E. Laermann and G. Schierholz, Nucl. Phys. B (Proc. Suppl.)34 (1994)376.
- [72] R. Gupta, C.F. Baillie, R.G. Brickner, G.W. Kilcup, A. Patel, S.R. Sharpe, Phys. Rev. D44 (1991)3272.
- [73] SESAM Collaboration, S. Güsken et al., hep-lat/9809066, Phys. Rev. D59, in print.
- [74] SESAM Collaboration, N. Eicker et al., Phys. Lett. B389 (1996)720.
- [75] SESAM Collaboration, N. Eicker et al., Phys. Lett. B407(1997)290.
- [76] T. Bhattacharya, R. Gupta, Nucl. Phys. B (Proc. Suppl.) 63A-C (1998)95.
- [77] CP-PACS Collaboration, R. Burkhalter et al., Nucl. Phys. B (Proc. Suppl.) (1999), to appear.
- [78] S. Capitani et al., Nucl. Phys. B (Proc. Suppl.)63 (1998)153.
- [79] V. Gimenez, L. Giusti, F. Rapuano, M. Talevi, *Non-perturbative Renormalization of Quark bilinears*, preprint Edinburgh 97/24, hep-lat 9806006; *Lattice quark masses: a non-perturbative measurement*, preprint Edinburgh 97/15, hep-lat 9801028.
- [80] S. Gottlieb, W. Liu, D. Toissaint, R.L. Renken, L. Sugar, Phys. Rev. D35 (1987)2531.
- [81] For recent reviews see:
 G.M. Shore, Nucl. Phys. Proc. Suppl. 64 (1998)167;
 H.-J. Cheng, Int. J. Mod. Phys. A11 (1996)5109;
 M. Anselmino, A. Efremov and E. Leader, Phys. Rep. 261 (1995)1.

- [82] K.G. Wilson, Phys. Rev. 179 (1969)1499.
- [83] S.A. Larin, T. van Ritbergen, J.A.M. Vermaseren, Phys. Lett. B404 (1997)153.
- [84] C. Caso et al., The European Physical Journal C3 (1998)1.
- [85] F.E. Close, R.G. Roberts, Phys. Lett. B316, (1993)165.
- [86] For a review see: R.D. Ball, Proceedings of the *Ettore Majorana International School of Nucleon Structure*, Erice 1995, hep-ph/9511330.
- [87] G. 'tHooft, Phys. Rev. Lett. 37 (1976)8, and G. 'tHooft, *Extended objects in gauge field theories*, in *Particles and Fields*, eds. D.H. Boal and A.N. Kamal, Plenum, New York, 1978, p.165.
- [88] R. Gupta and J.E. Mandula, Phys.Rev. D50 (1994)6931.
- [89] G.M. Shore, Nucl. Phys. B (Proc.Suppl.) 39B,C (1995)101.
- [90] A. Di Giacomo, hep-lat/9711034.
- [91] SESAM Collaboration, J. Viehoff et al., Nucl. Phys. B (Proc. Suppl.) 63A-C (1998)269.
- [92] SESAM Collaboration, J. Viehoff et al., Nucl. Phys. B (Proc. Suppl.) (1999), to appear.
- [93] S.L. Adler, it in 1970 Brandeis University Summer Ins. in Theoretical Physics, ed. S. Dreser, M. Grisaru and H. Pendleton, MIT Press, Cambridge, Mass. .
- [94] S.A. Larin, Phys. Lett. B303 (1993)113; K.G. Chetyrkin and J.H. Kühn, Z. Phys. C60 (1993)497; S.A. Larin, Phys. Lett. B334 (1994)192.
- [95] R. Groot, J. Hoek and J. Smit, Nucl. Phys. B237 (1984)111.
- [96] G. Parisi, in *High Energy Physics - 1980*, Proceedings of the XXth Int. Conf., Madison, Wisconsin, eds. L. Durand and L.G. Pondrom (American Institute of Physics, New York, 1981).
- [97] B. Bochiccio, L. Maiani, G. Martinelli, G. Rossi and M. Testa, Nucl. Phys. B262 (1985)331.
- [98] L. Maiani and G. Martinelli, Phys. Lett. B178 (1986)265.
- [99] G. Martinelli, C. Pittori, C.T. Sachrajda, M. Testa and A. Vladikas, Nucl. Phys. B445 (1995)81.
- [100] M. Lüscher, S. Sint, R. Sommer and H. Wittig, Nucl. Phys. B491 (1997)344; K. Jansen et al., Phys. Lett. B376 (1996)275.
- [101] M. Ciuchini, E. Franco, G. Martinelli and L.Reina, Phys. Lett. B301 (1993)263; Nucl. Phys. B415 (1994)403.
- [102] C. Parrinello, S. Petrarca and A. Vladikas, Phys. Lett. B341 (1994)187.
- [103] V. Gimenez, L. Giusti, F. Rapuano and M. Talevi, hep-lat/9806006, submitted to Elsevier preprint.

- [104] P. Di Vecchia, K. Fabricius, G.C. Rossi and G. Veneziano, Nucl. Phys. B192 (1981)392.
- [105] B. Allés, A. Di Giacomo, H. Panagopoulos and E. Vicari, Phys. Lett. B350 (1995)70.
- [106] M. Campostrini et al., Phys. Lett. B252 (1990)436, M. Campostrini, A. Di Giacomo and H. Panagopoulos, Phys. Lett. B212 (1988)206.
- [107] M. Teper, Phys. Lett. B232 (1989)227.
- [108] A. Di Giacomo and E. Vicari, Phys. Lett. B275 (1992)429.
- [109] C. Christou, A. Di Giacomo, H. Panagopoulos and E. Vicari, Phys. Rev. D53 (1996)2619.
- [110] M. Lüscher, Comm. Math. Phys. 85 (1982)39.
- [111] B. Allés, M. D'Elia, A. Di Giacomo, R. Kirchner, preprint IFUP-TH 51/97, hep-lat/9711026, submitted to Phys. Rev.D.
- [112] J. Smit and J.C. Vink, Nucl. Phys. B286 (1987)485.
- [113] SESAM Collab., J. Viehoff et al., hep-lat/9809073, to be published in Nucl. Phys. B (Proc. Suppl.)1999.
- [114] B. Allés, G. Boyd, M. D'Elia, A. Di Giacomo and E. Vicari, Phys. Lett B389 (1996)107.
- [115] B. Allés et al., Phys. Rev. D58 (Rapid Communication) 071503.
- [116] B. Allés et al., Phys. Lett. B336 (1994)248.
- [117] R. Altmeyer et al., Int. J. Mod. Phys. C5 (1994)331.
- [118] B. Allés, G. Boyd, M. D'Elia and A. Di Giacomo, Nucl. Phys. (Proc. Suppl.)63 (1998)239.
- [119] T χ L Collab., L. Conti et al., Nucl. Phys. B (Proc. Suppl.)53 (1997)222, SESAM, T χ L Collab., T. Lippert et al., Nucl. Phys. (Proc. Suppl.)63 (1998)946.
- [120] S. Güsken, U. Löw, K.H. Mütter, R. Sommer, A. Patel and K. Schilling, Phys. Lett. B227 (1989)266.
- [121] K.F. Liu, S.J. Dong, T. Draper, J.M. Wu and W. Wilcox, Phys. Rev. D49 (1994)4755.
- [122] S. Capitani et al., hep-lat/9809172, to be published in Nucl. Phys. B (Proc. Suppl.) 1999.
- [123] M. Fukugita, Y. Kuramashi, M. Okawa and A. Ukawa, Phys. Rev. Lett. 75 (1995)2092.
- [124] S.J. Dong, J.F. Lagaë and K.F. Liu, Phys. Rev. Lett. 75 (1995)2096.
- [125] SESAM Collab., S. Güsken et al., preprint WUB 98-44, HLRZ 1998-85, hep-lat/9801009, submitted to Phys. Rev. D. .
- [126] S.L. Glashow, in *Hadrons and their interactions*, Proc. 1967 Int. School of Subnuclear Physics, Erice 1967, ed. A. Zichichi, Academic Press, New York 1968, p.83.

- [127] M. Gell-Mann and Y. Ne'eman, *The eightfold way*, Benjamin, New York 1964.
- [128] S. Weinberg, Phys. Rev. D11 (1975)3583.
- [129] R. Jackiw and C. Rebbi, Phys. Rev. Lett. 37 (1976)172; C.G. Callan, R.F. Dashen and D.J. Gross, Phys. Lett. 63B (1976)334; Phys. Rev. D17 (1978)2717.
- [130] S. Coleman, in *The Whys of Subnuclear Physics*, Proc. 1977 Int. School of Subnuclear Physics, Erice 1977, ed. A. Zichichi, Plenum Press New York 1979, p.805.
- [131] F. Wilczek, in *How Far are We from the Gauge Forces*, Proc. 1983 Int. School of Subnuclear Physics, Erice 1983, ed. A. Zichichi, Plenum Press New York 1985, p.157.
- [132] G. 't Hooft, Phys. Rep. 142 (1986)357.
- [133] G.A. Christos, Phys. Rep. 116 (1984)251.
- [134] J.B. Kogut and L. Susskind, Phys. Rev. D11 (1975)1477.
- [135] C. Bernard and M. Golterman, Phys. Rev. D49 (1994)486; Phys. Rev. D46 (1992)853.
- [136] M. Atiyah and I. Singer, Ann. Math. 87, (1968)484.
- [137] S. Itoh, Y. Iwasaki and T. Yoshié, Phys. Rev D36 (1987)527.
- [138] I.M. Barbour, N.E. Behill, P.E. Gibbs, G. Schierholz and M. Teper, in *The Recursion Method and its Applications*, Springer Series in Solid-State Sciences 58, p.149, eds. D.G. Pettifor and D.L. Weaire, Springer, Berlin 1985.
- [139] B. Bunk, Nucl. Phys. (Proc. Suppl.) 53 (1997)987.
- [140] D.C. Sorensen, SIAM J. *Matrix Analysis and Applications* 13(1) (1992)357.
- [141] C. Gatttringer and I. Hip, Nucl.Phys. B536 (1998)363.
- [142] M. Fukugita, T. Kaneko and A. Ukawa, Phys. Lett. 145 B (1984)93.
- [143] Y. Kuramashi, M. Fukugita, H. Mino, A. Okawa and A. Okawa, Phys. Rev. Lett. 72 (1994)3448.
- [144] M. Fukugita, Y. Kuramashi, M. Okawa and A. Ukawa, Phys. Rev. D51 (1995)3952.
- [145] J. Hoek, M. Teper and J. Waterhouse, Nucl. Phys. B288 (1987)234.
- [146] L. Venkataraman and G. Kilcup, hep-lat/9711006.
- [147] R.D. Mawhinney, Nucl. Phys. (Proc. Suppl.)60A (1998)306.
- [148] QCDSF Collaboration: D. Chen et al., Nucl.Phys. (Proc.Suppl.) 63 (1998)997.
- [149] S. Güsken, Nucl. Phys. (Proc. Suppl.)17 (1990)361.
- [150] R. Petronzio, Nucl. Phys. B (Proc. Suppl.)42 (1995)952; G.M. de Divitiis, R. Frezotti, M. Guagnelli, M. Massetti and R. Petronzio, Nucl. Phys. B455 (1995)274.
- [151] R. Frezotti, M. Masetti, and R. Petronzio, Nucl. Phys. B480 (1996)381.
- [152] J.W. Negele, hep-lat/9810053, to be published in Phys. Rev. (Proc. Suppl.) (1999).
- [153] Y. Iwasaki, Nucl.Phys. (Proc.Suppl). 60A (1998)246.